Mechanics of distributed cracking

Zdeněk P Bažant

Professor of Civil Engineering and Director, Center for Concrete and Geomaterials, Northwestern University, Evanston IL 60201

This paper reviews some interesting recent results on mesh sensitivity and strain localization instability, nonlocal and micromechanics models, and the size effect in failure due to distributed cracking.

As we know, failure of many materials involves propagation of a large system of densely distributed cracks rather than a single, precisely defined fracture. This is typical of concrete and rock, as well as stiff clays, ice, especially sea ice, filled elastomers, wood, particle board, paper, two-phase ceramic composites, fiber-reinforced polymers, fiber-reinforced concrete, asphalt and polymer concretes, and refractory concretes. The number of cracks or microcracks is extremely large, and their locations and orientations are random. Therefore, it is inevitable to treat the densely cracked material as a continuum. The constitutive relation must then exhibit strain-softening, a phenomenon where the matrix of tangential elastic moduli ceases to be positive definite. Unreasonable though such an approach might seem (84.40), it has nevertheless been proven useful provided that certain mathematical difficulties inherent to it are properly tackled.

Some of these difficulties were already pointed out in 1903 by Hadamard (03.1) and others were further analyzed by Thomas, Maier, Mróz, Bažant, Burt and Dougill, Sandler and Wright, Bažant and Belytschko, Darvall, Read and Hegemier, Wu and Freund, and others (61.4, 76.2, 77.4, 84.40, 84.46, 84.58). Recently, due to large errors in finite element predictions of complete failures of concrete structures or rock masses subjected to blast, impact, earthquake, thermal loading, creep or shrinkage, the modeling of distributed cracking came to the center of attention. The literature has become so extensive that a complete coverage in one paper is impossible. Therefore, I will focus my review mainly on the work done at our Center at Northwestern University which was carried out jointly with T B Belytschko, L Cedolin, T P Chang, P Gambarova, J K Kim, F B Lin, B H Oh, P Pfeiffer, P Prat, and A Zubelewicz, under the sponsorship of the Air Force Office of Scientific Research (Grant No 85-0009) and the National Science Foundation (Grants Nos CEE800-3148 and CEE821-1642). If I fail to mention some important contributions, their authors should realize that they will be in a good company.

Let me begin by showing a micrograph of the fracture tip region in Portland cement mortar, obtained by means of scanning electron microscopy by Mindess and Diamond (80.22). Instead of a continuous crack we see many discontinuous microcracks which are not arranged along one line but are also spaced laterally (Fig. 1). On a much larger scale, Fig. 2 shows typical cracking patterns in reinforced concrete structures, as observed on punching shear specimens tested at Northwestern University (85.6). On a still much larger scale, Fig. 3 shows a typical map of cracking caused by advancing a stope through a bushveld norite rock formation in a very deep mine, as determined by drill sampling techniques by Brumer and Rorke (84.14).

How should we model such distributed and microscopically chaotic crack systems in finite element analysis?

1. STRAIN-SOFTENING CRACK BAND AND LINE CRACK MODELS

While mathematicians may prefer to seek good solutions to simplified problems, we engineers must seek simplified solutions to good problems. So, rather than limiting attention to problems with sharp line cracks, for which a good solution could be readily found, we must look for a simplified solution to the actual problem which takes the disperse nature of cracking into account. A useful simplifying idea, introduced by Rashid (68.9) 18 years ago, is to imagine continuously distributed or smeared cracks and describe them as strain-softening (81.24). This is easily taken into account by reducing the elastic modulus in the direction normal to the cracks and introducing an orthotropic matrix of elastic moduli along with an inelastic stress decrement. The stress decrease due to cracking was initially considered as a sudden, ie, vertical crack drop, but it is more correct to describe it as gradual strain-softening.

Strain-softening does not exist in the heterogeneous microstructure at sufficient resolution (84.40). It is merely an expedient macroscopic model accomplishing homogenization. Its mathematical formulation has recently been the subject of very interesting debates (84.40, 84.46). Some investigators, influenced by plasticity theory, have promulgated the view that strain-softening is a nonexistent and mathematically unacceptable property for a continuum. In my opinion they overstate, although they do describe certain difficulties correctly. Before I discuss them, I would like to point out some other branches of physics in which a similar problem arises. In the physics of gases, the liquid-vapor phase transition (83.1, 84.1) described by van der Waals' equation of state (64.1, 80.18) involves a region where pressure decreases at decreasing volume. This behavior, which we might classify as strain-softening, characterizes metastable superheated liquids or supersaturated vapors. In astrophysics, a continuum equation of state of stellar matter which

This paper is an expanded version of an invited Sectional Lecture given at the 2nd ASCE-ASME Joint Mechanics Conference, Albuquerque NM, Jun 1985. Transmitted by AMR Associate Editor George J Dvorak.

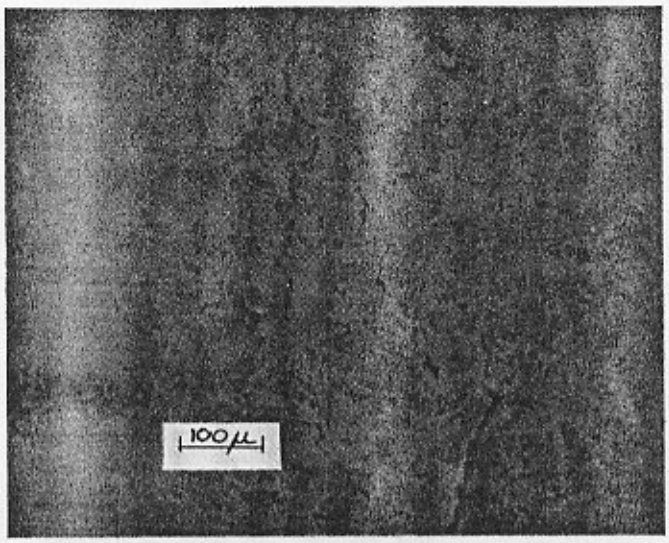

FIG. 1. Crack band in Portland cement mortar obtained by means of SEM by Mindess and Diamond (80.22).

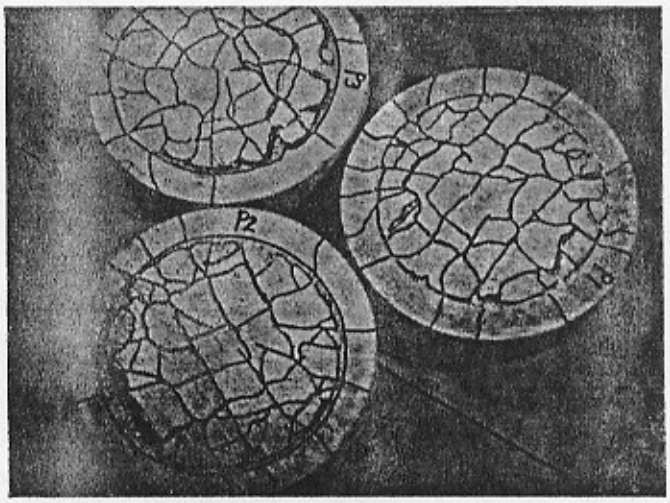

FIG. 2. Typical cracking patterns in reinforced concrete structures as observed on punching shear specimens tested at Northwestern Univ (85.6).

exhibits what we would call volumetric strain-softening is a well-established concept, treated by field quations which differ from those for the classical local continuum (58.2, 64.3, 65.2, 73.11, 82.29). This concept explains the gravitational collapse of stars (eg, the collapse of a white dwarf into a neutron star or the gravothermal collapse). It is, I think, more fruitful for us to accept the concept despite all its peculiar complications, and then attempt to deal with them.

One difficulty is that, in the strain-softening regime, the material can no longer propagate waves since, as Hadamard recognized (03.1), the wave speed ceases to be real and becomes imaginary (Fig. 4). However, this is not as problematic as thought until recently because the unloading tangential modulus remains positive even in the strain-softening range (76.2, 84.42, 84.41). By virtue of this fact, a solution to some wave propagation problems that involve strain-softening can be found, as I will show later.

First let me discuss the problems which arise in finite element analysis. Here the chief difficulty caused by strain-softening is the spurious mesh sensitivity. After large finite element programs with strain-softening models for distributed cracking had been written and widely applied, it was discovered that the convergence properties are incorrect and the calculation results are unobjective with regard to the analyst's choice of the mesh (76.2, 79.1, 80.2, 83.7, 85.19, 85.45). In Fig. 5 we see some numerical results for a rectangular panel in tension obtained with three different meshes the sizes of which are in the ratio

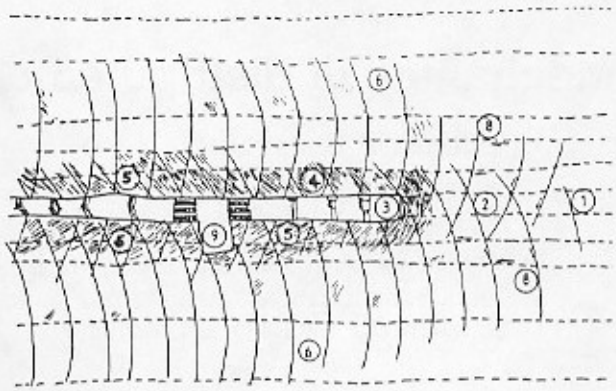

FIG. 3. Observed fracture distribution in bushveld norite rock ahead of an advancing stope face in a deep mine [after Bruner and Rorke (84.14)].

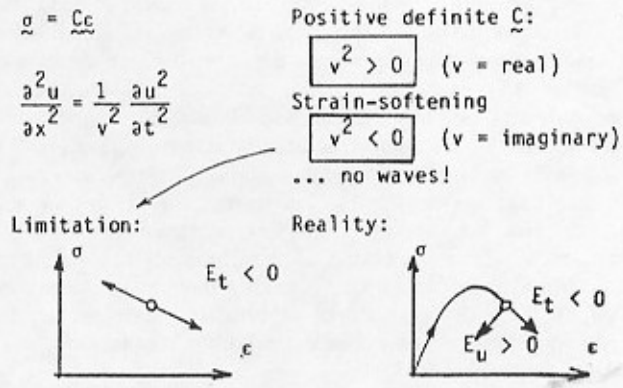

FIG. 4. Wave propagation: implication of Hadamard's (03.1) conclusion.

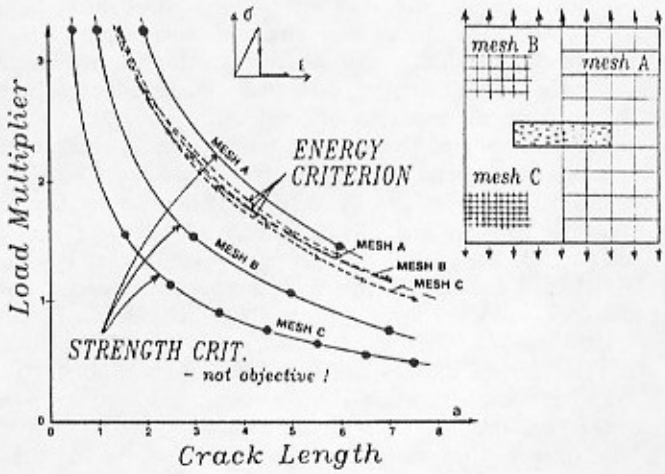

FIG. 5. Spurious mesh sensitivity and incorrect convergence, strain-softening local continuum (80.2, 79.1, 83.9).

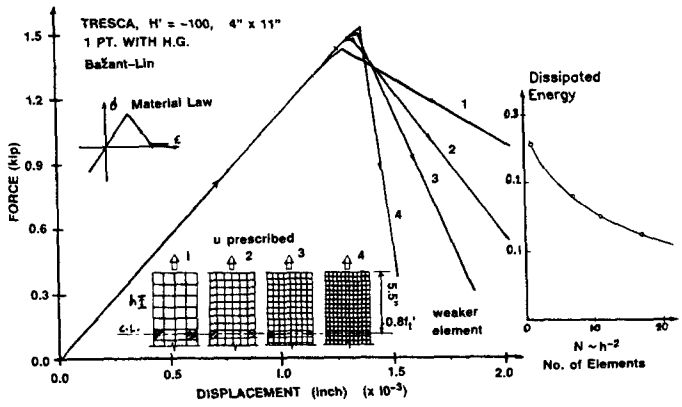

FIG. 6. Mesh sensitivity for strain-softening σ-ε law (calculated by F B Lin at Northwestern Univ).

4:2:1. We assume that a starter notch exists in the center of the panel, and we plot the value of the load necessary to further extend the crack band, as a function of the crack band length. If the strength criterion is used to decide whether the crack band extends into the next finite element, the results of the three meshes are as different as the solid curves in Fig. 5.

Pathological behavior of this kind, by now confirmed by many investigators, can be remedied by adopting for crack band propagation some form of an energy criterion, just as in classical fracture mechanics of sharp line cracks. With the energy criterion, we obtain in Fig. 5 the dashed curves (80.2) which differ from each other only by a small numerical error. Similarly (Fig. 6), the mesh size is found to affect incorrectly the load-deflection diagrams, for example, those for a rectangular panel (Fig. 6) in which symmetric crack bands start from the sides. Such spurious mesh sensitivity can occur not only for the post-peak response but also for the value of the maximum load,

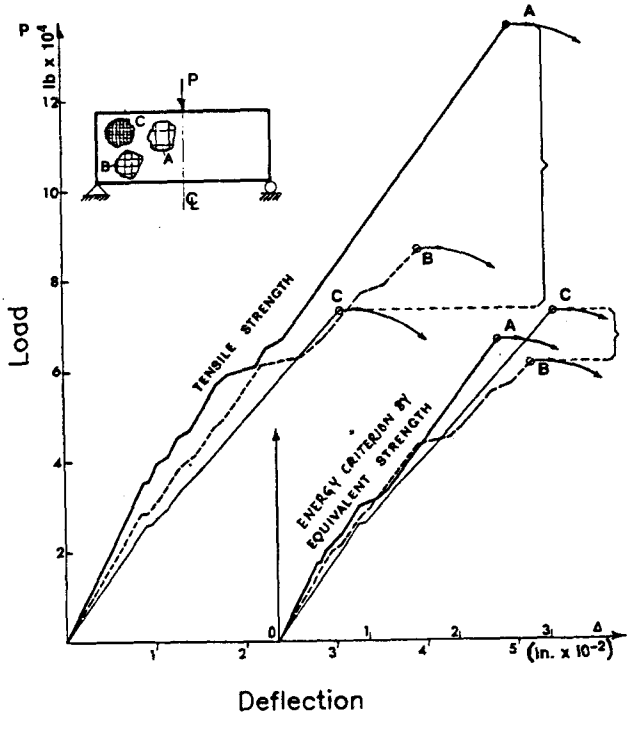

FIG. 7. Mesh sensitivity of diagonal shear prediction: (—) mesh A; (- - -) mesh B; (—) mesh C [after Bažant and Cedolin, 1981 (see 83.7, and discussion of Ref. 80.2)].

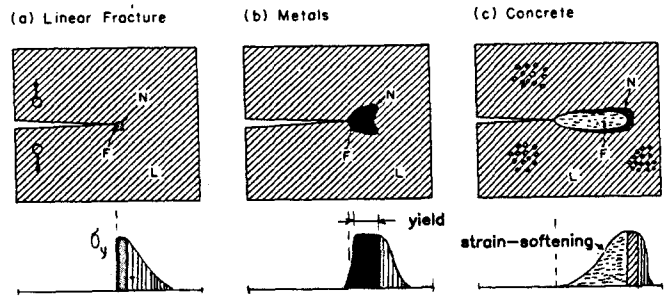

FIG. 8. Different extents of fracture process zone (82.3).

as documented, eg, for the finite element analysis of diagonal shear failure of beams (Fig. 7) (80.2, 83.7). The lack of objectivity or spurious mesh sensitivity is found both for the sudden (vertical) and the gradual stress drops (83.9).

The energy criterion, necessary to avoid the mathematical problem of inobjectivity or spurious mesh sensitivity, dictates that the energy dissipation due to localized cracking per unit length of fracture must be a material property which cannot depend on the chosen mesh size. The mesh-independence of energy dissipation can be achieved in finite element modeling in various ways, both for the sudden and the gradual stress drops. The essential physical aspect is that the distributed nature of cracking, which is in fact a consequence of material inhomogeneity (characterized by aggregate or grain size, reinforcement spacing, rock joint spacing, etc), blunts the front of localized fracture. This blunting, similar to that in ductile fracture of metals (Fig. 8), causes the fact that the stress decline along the line of fracture extension is gradual and occurs over a finite length which is approximately a certain constant multiple of the aggregate size. This length can approach the structure dimensions if the structure is not very large relative to the material inhomogeneity size.

One way to satisfy, for localized cracking, the mathematical requirement for a mesh-size independent energy dissipation, and capture at the same time the physical fact of fracture front blunting, is offered by the crack band model. As proposed in 1974, the cracking is assumed in this model to be uniformly smeared across a band having at its front a finite width w_c which is a material property (76.2). This is modeled by requiring the element size to be equal to w_c (Fig. 9). Fracture energy G_f is then given as w_c times the area under the uniaxial complete tensile stress–strain diagram, or more precisely the area under the loading and unloading diagrams emanating from the peak stress point (82.3). As the simplest form, the stress–strain diagram may be considered as bilinear, although a

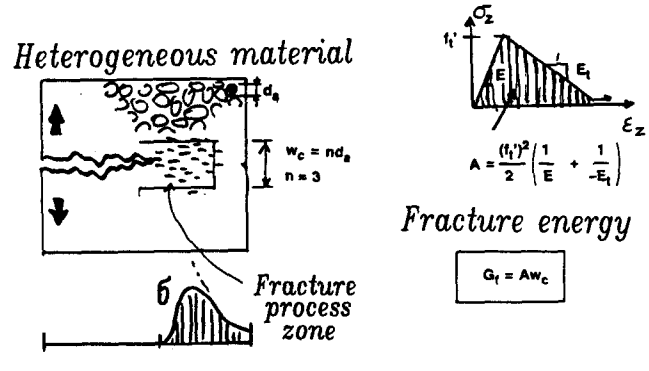

FIG. 9. Crack band theory (83.9).

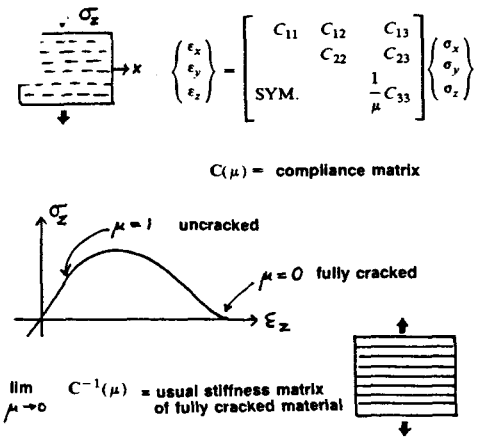

FIG. 10. Triaxial strain-softening law (83.9).

diagram with a curved convex strain-softening branch and a very long tail is usually more realistic (85.19).

The triaxial form of the strain-softening constitutive relation is most easily obtained by a secant compliance formulation referred to the crack axis, such that the secant diagonal stiffness term corresponding to the direction normal to the crack is divided by the cracked area fraction μ (a damage-type parameter) which decreases to zero as the transverse normal strain increases (Fig. 10). This model (82.3, 84.12) can closely describe essentially all known fracture test data for concrete as well as rock (67.3, 68.3, 69.2, 70.6, 71.3, 71.6, 71.11, 72.1, 73.3, 73.4, 75.3, 76.7, 76.10, 77.8, 78.9, 78.13, 79.16, 80.22, 80.27, 80.28, 81.4, 81.11, 81.17, 81.23, 82.9, 82.28, 82.31, 82.32, 83.29, 83.42, 83.46, 84.30, 84.52, 85.21, 85.30, 85.31, 85.39, 85.44); see, eg, Figs. 11 and 12 in which the optimum possible fits by linear elastic fracture mechanics are shown as the dashed lines and those for the crack band model as the solid lines. Figure 11 illustrates how the maximum load of fracture specimen depends on its size and notch length, while Fig. 12 shows how the specific energy required for crack growth depends on the length of the crack extension from the notch.

Aside from having to specify the shape of the strain-softening branch as well as the overall type of the strain-softening triaxial constitutive relation, we can characterize the crack band model by three material parameters: the tensile strength f_t', the fracture energy G_f, and the cracking front width w_c. The characteristic slope E_t (< 0) of the strain-softening diagram is a function of these parameters. f_t' and G_f being constant, the cracking front width w_c, which represents a characteristic length of the material, has an almost negligible influence on the capability to fit test data for localized fracture, and cannot be determined from them. It can be determined, however, if the strain-softening modulus E_t is specified independently, for example, on the basis of tests in which cracking does not localize. Such situations of nonlocalized cracking prevail for direct tension or bending of a bar or beam with sufficient reinforcement, or for cooling or shrinkage cracking near the surface of a massive specimen. Absence of localization of cracking can perhaps be also assumed for unreinforced tension specimens that are sufficiently short. Based on E_t, the cracking front width w_c is found to be approximately three times the maximum aggregate size for concrete (83.9). However, multiples from 1 to 10 make little practical difference if nonlocalized cracking is left out of consideration and only the data for localized cracking are analyzed.

For the majority of practical applications, an element size equal to several aggregate sizes is impracticably as well as unnecessarily small. Essentially identical results can be obtained with larger finite elements if the mesh is not too crude compared to the structure dimensions. For this purpose, it is necessary to adjust the average stress–strain relation for the

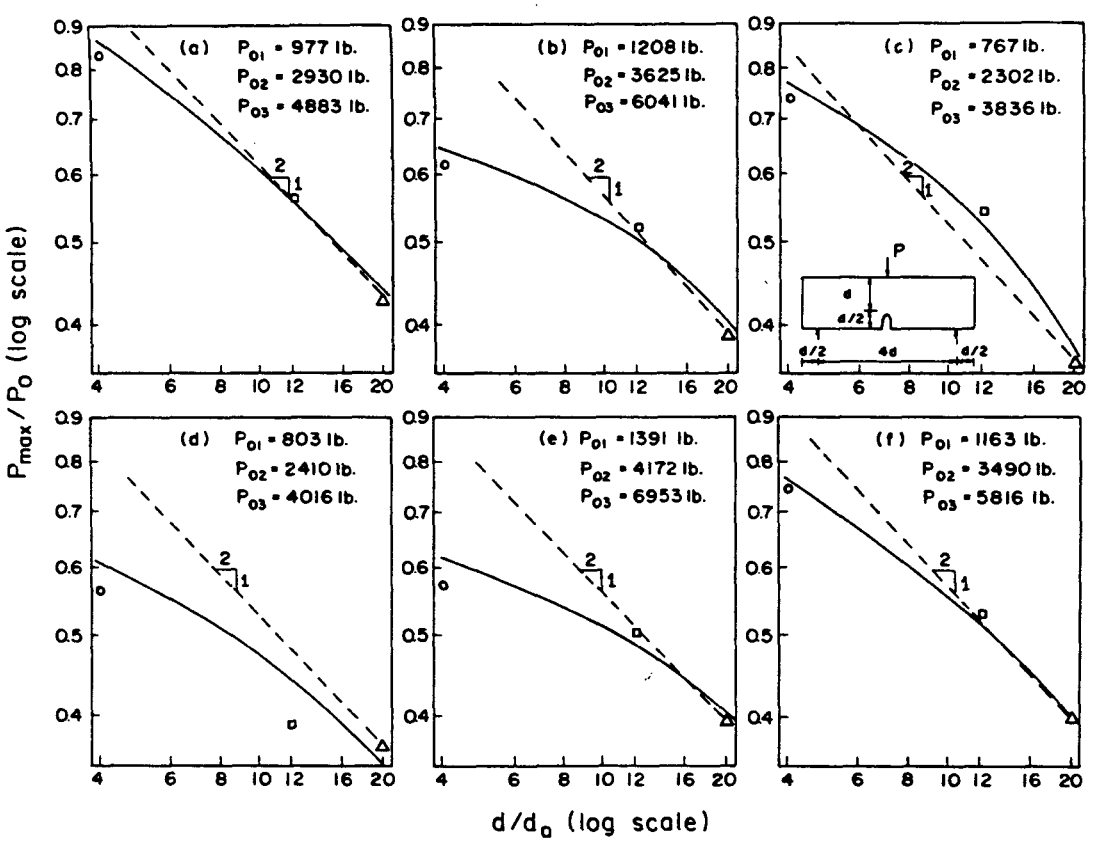

FIG. 11. Illustration of how the maximum load of fracture specimen depends on its size: (—) nonlinear theory; (- - -) linear theory; (○) $d = 2$ in.; (□) $d = 6$ in.; (△) $d = 10$ in. [test data by Walsh (72.9)].

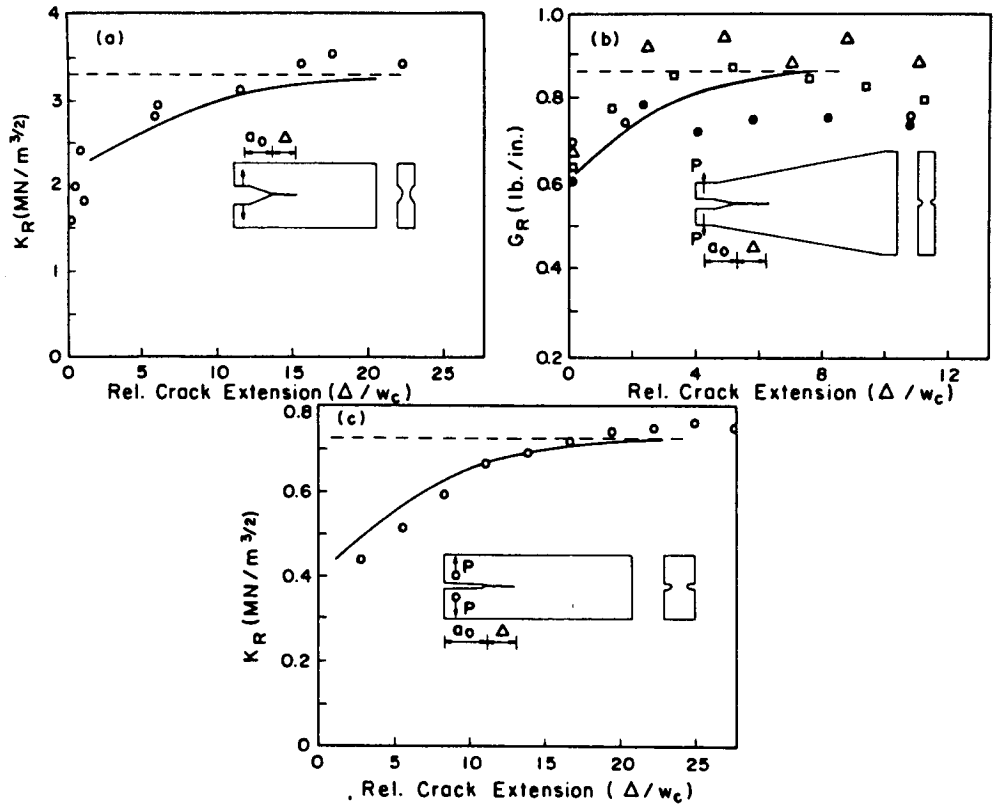

FIG. 12. Illustration of how the specific energy required for crack growth depends on the length of the crack extension from the notch: (—) nonlinear theory; (---) linear theory; (a) data points from Sok, Baron, and François (79.16); (b) data points from Wecharatana and Shah (80.27, 80.28); (c) data from Brown (72.1).

finite element so as to ensure the same energy dissipation, ie, the same fracture energy G_f, for any element size h. We may imagine a band of width $w_c = l$ to be embedded within the finite element (Fig. 13), and its relative normal displacement to be added to that corresponding to an elastic or elastoplastic (but nonsoftening) behavior. The average stress–displacement relations for the finite element then vary with the element size as shown in Fig. 13; the stress drop becomes progressively steeper until, for a certain characteristic element size l_{ch}, it becomes vertical (85.3, 85.13). With larger element sizes, which are often needed in practice for the analysis of large structures, the average stress–displacement diagram is of the snap-back type, which is unstable under displacement control. Such a situation requires dynamic analysis; however, an approximate static analysis becomes possible by replacing the snap-back diagram by a diagram with a vertical stress drop which dissipates the same amount of energy (85.3, 85.13). Under this restriction, the dynamic snap-through (ie, the vertical stress drop in Fig. 13) begins and ends with states of equal kinetic energy, thus permitting static analysis. It is found that for finite elements larger than l_{ch} the strength limit for the sudden vertical stress drop must be decreased as $h^{-1/2}$ (79.1, 80.1, 83.7, 85.3, 85.4, 85.12, 85.13). The finite element results are then essentially independent of the mesh size, unless the mesh is too crude.

The constancy of the crack front width w_c in the crack band model is certainly a simplifying assumption. While w_c cannot depend on the mesh size, it may vary depending on the stress and strain fields surrounding the fracture process zone. The

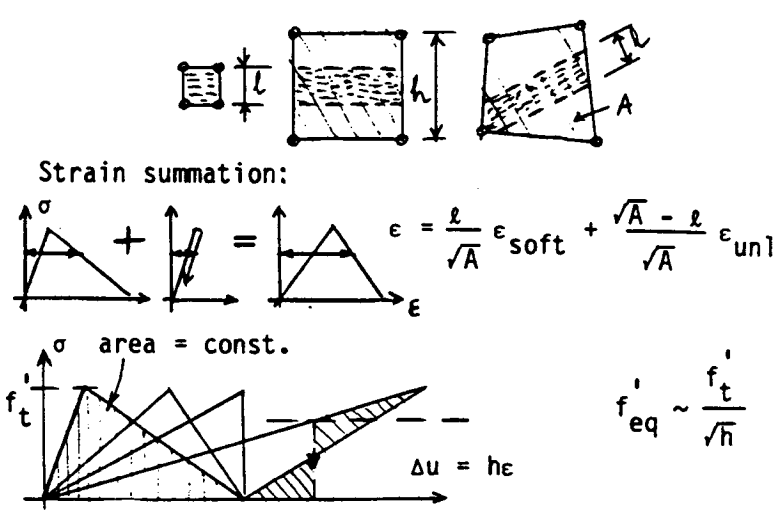

FIG. 13. Fully localized softening or distributed cracking (85.3, 85.13).

effective crack front width probably increases as fracture extends from a sharp notch. This behavior can be described by the crack layer model of Chudnovsky (83.16, 82.11), in which the width of the crack layer (synonymous to crack band) depends on three path-independent integrals around the cracking front: the J-integral giving the energy influx, and the M- and L-integrals giving the energy changes due to a rotation of the cracking front and a lateral expansion of the crack layer. Some applications of this approach and its systematic thermodynamic formulation have already been made in the area of polymer crazing. A general analysis of continuum damage based on these integrals was made by G Herrmann and J R Rice (84.44). No doubt, applications to concrete and geomaterials would be possible.

For the modeling of localized fracture, the essential property of the crack band model is not that its cracking front width w_c is finite, but that its finiteness forces the length of the fracture process zone in the direction of the crack axis (ie, the length of the strain-softening zone) to be finite and large. This same essential property may be alternatively obtained with various types of line crack models (Fig. 14), patterned after the original ideas of Barrenblatt (59.1, 62.1) and Dugdale (60.1), which were extensively applied to ductile fracture of metals (73.6, 74.5, 74.9, 77.10) and were adapted for concrete in the pioneering works of Hillerborg et al (76.8, 81.17, 81.21, 83.31, 84.27, 85.31).

In Hillerborg's model (as well as some similar preceding finite element models for metals), a sharp line crack is assumed to open up along the interelement boundary on which a stress–displacement relationship is specified as a material property. This is, nevertheless, approximately equivalent to the crack band model if the energy dissipation per unit length of fracture is the same, or if the transverse normal displacement on the line crack is equal to the accumulated transverse normal strain due to cracking over the width of the crack band. The equivalence of these two types of models can in fact be rigorously established by applying the J-integral, as Rice pointed out (85.41).

Another variant of the line crack approach, which was initially proposed for localization of strain-softening in shear (81.18), and is for concrete known as the composite damage (or composite fracture) model (84.53, 85.54), is to embed a line crack or a narrow crack strip inside the finite element (Fig. 14), superposing its relative displacement on the elastic deformation of the element. For the situations of localized fracture, eg, the fracture specimens, this approach yields again essentially the same results as the fictitious crack model of Hillerborg et al, as well as the crack band model.

The models based on the line crack idea, however, are not equivalent to the crack band model for situations of nonlocalized distributed cracking (85.3, 85.13). This is due to the fact that they are characterized by only two material parameters, strength f_t' and fracture energy G_f (if the shape of the strain-softening diagram is given in advance), while the crack band model involves a third material parameter, w_c, the characteristic length of the material. In this regard it is worthwhile to recall what has been learned in stability studies of crack systems.

2. STRAIN-LOCALIZATION INSTABILITY

An interesting parallel is provided by the propagation of a system of straight parallel equidistant cracks into a brittle elastic homogeneous half-space. Keer, Nemat-Nasser, and Ohtsubo worked with me at Northwestern on stability of this system, and our work has been extended by Cleary at MIT (77.2, 78.11, 79.3, 79.5, 80.30, 83.17). The cracks are driven by cooling or drying, and the cooling stress profile can be either gradual, as obtained from heat conduction, or may have an abrupt temperature drop, as obtained when water circulates through the cracks (the motivation for this research was a dry rock geothermal energy scheme involving rock fracturing). The stability condition may be reduced to the condition that the second-order variation of the free energy of the system as a function of the lengths of the individual cracks must be positive definite with the exclusion of certain instability modes that are inadmissible, such as crack shortening for a nonzero stress intensity factor (Fig. 15). From this condition it is found that the parallel crack system with equal crack lengths may be stable or unstable; stable if the cooling temperature profile is uniform for a certain length and then has a sufficiently rapid drop, and unstable if the cooling profile is gradual, such as the profile obtained from heat conduction without convection in the cracks.

If the system is unstable, every other crack during the cooling process stops growing when its length becomes approximately equal to the spacing of the leading cracks (77.2, 78.11, 79.3). In this manner the fracture permanently localizes into the leading cracks (Fig. 15). On the other hand, if the cracks are stable, they can be driven into the half-space at constant spacing as deep as desired, and remain stable with a spacing as close as desired (79.5). Thus, from the macroscopic sense, ie, over a volume involving many crack tips, the behavior at the cracking front is essentially the same as macroscopic

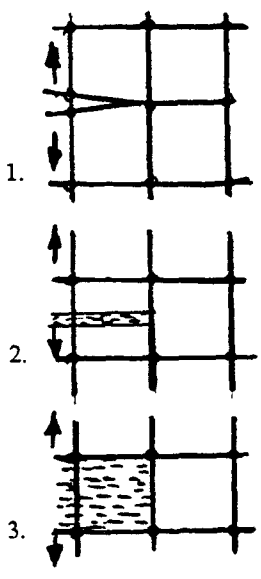

FIG. 14. Softening fracture models: (1) line crack between elements [Hillerborg et al (76.8, 81.17, 81.21, 83.31, 84.27, 85.31)]; (2) line crack embedded in elements [Pietruszczak, Mróz (81.18) and Willam et al (84.53, 84.54, 85.49)]; (3) blunt crack band (Bažant, Cedolin, Oh)— equivalent for fully localized fracture only (fracture tests).

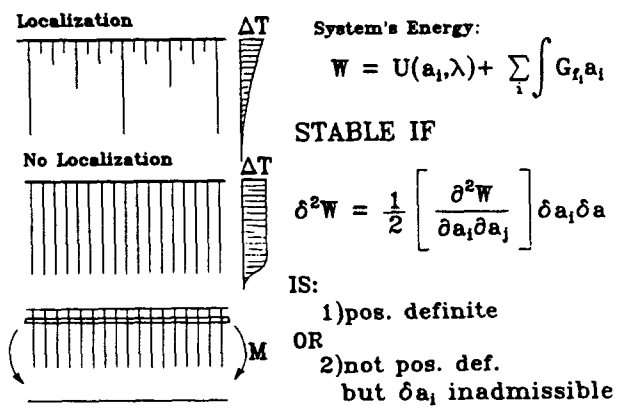

FIG. 15. Stability of crack system (77.2, 78.11, 79.3, 79.5, 80.1).

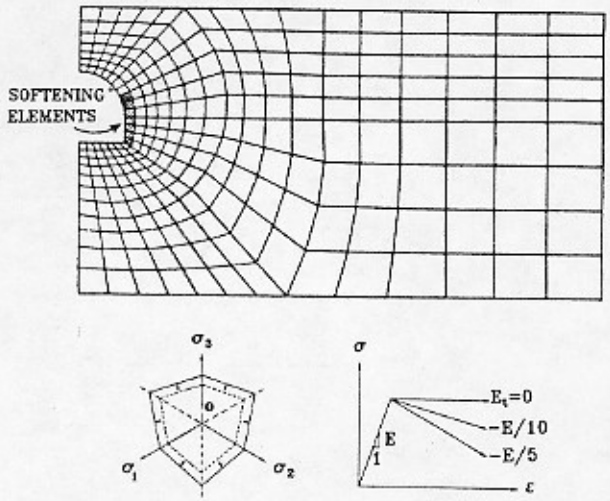

FIG. 16. Tunnel excavation in strain-softening, grouted soil (study in progress, by F B Lin, Northwestern Univ).

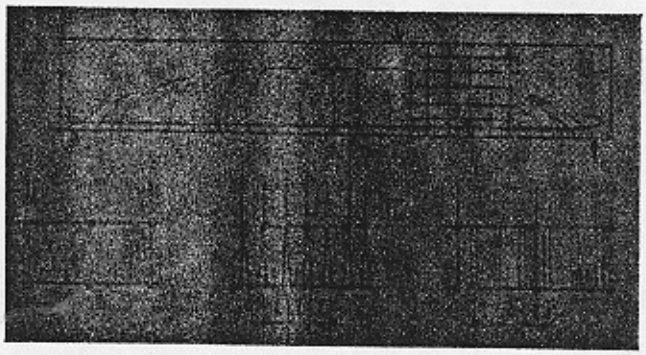

FIG. 17. Nonlocalized softening: models not equivalent; crack band preferable; characteristic length l required.

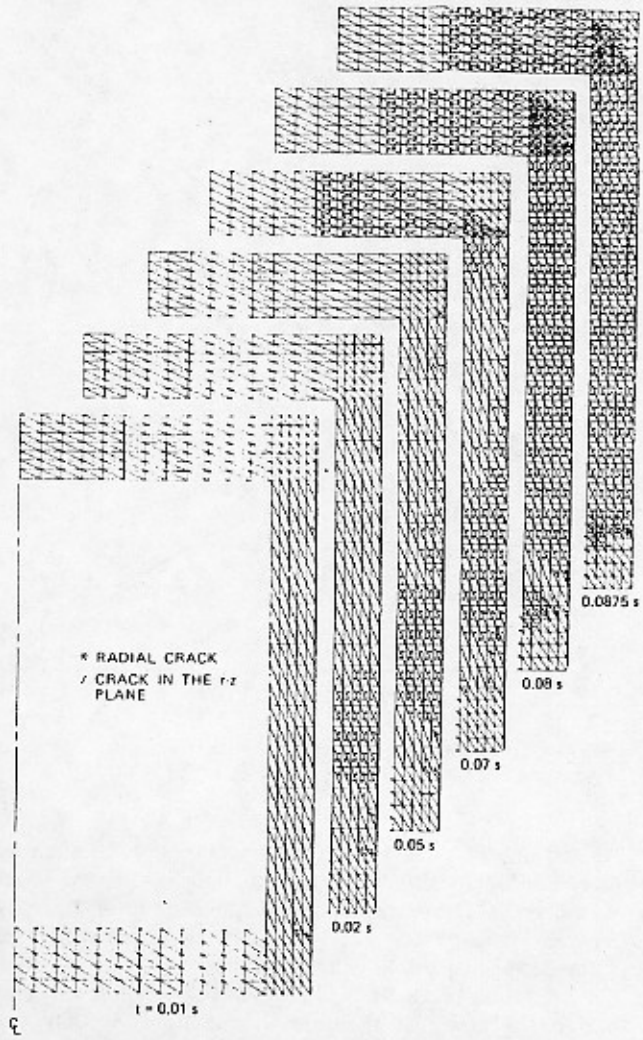

FIG. 18. Cracking sequence of PCRV under dynamic pressure loading [after Marchertas, Belytschko, and Bažant (79.13)].

strain-softening. This softening, or distributed cracking, is stable over a cracking front which can be arbitrarily wide.

Similarly, and not surprisingly in view of the observations of reinforced concrete beams, a system of densely distributed parallel cracks in an elastic homogeneous brittle solid may be stable if there is a compression zone closely ahead of the crack tips, as found for instance for the cracking caused by tunnel excavation in a grouted soil (Fig. 16) or the cracking caused by bending in a beam, which contains sufficient reinforcement (80.8) (Fig. 17). (For bending cracks, the sufficient reinforcement percentage calculated from stability conditions is surprisingly small and roughly equal to the empirical minimum reinforcement prescribed in building codes.) The stabilizing influence of reinforcing bars provides an *a posteriori* justification to many of the finite element analyses of reinforced concrete structures in which the questions of possible localization instability of cracking and the associated spurious mesh sensitivity were ignored. It is the reason why many practical structures are fracture-insensitive and can be analyzed without paying attention to the problems we are now discussing.

In dynamics, another influence which tends to temporarily stabilize a nonlocalized cracking front is the inertia force. In dynamic finite element analysis, especially for loads of extremely short durations such as blast or impact, the times of response are not long enough for the cracking localization to take place, and nonlocalized distributed cracking is then the correct solution for many problems; see, eg, Fig. 18 which shows the cracking sequence for a prestressed concrete reactor vessel subjected to an explosive loading in the cavity, as calculated by Marchertas, Belytschko, and Bažant (79.13).

The crack band model has the advantage that it can deal with both localized and nonlocalized cracking, and it is no doubt for this reason that it is being widely applied in general finite element programs (Rots, de Borst, Kusters, Darwin, Pan, Marchertas, et al., 84.45, 84.18, 84.21, 84.20, 84.19, 84.41, 85.19, 85.45, 85.46, 85.20, 86.6, 85.44, 84.47, 84.15, 83.44, 83.30). In the case of nonlocalized cracking, a zone of many neighboring finite elements is simply allowed to exhibit smeared cracking, as practiced since the inception of this approach. However, if the models based on the line crack idea, eg, those of Hillerborg (76.8) or Willam and Sture (84.54), are used in a situation of nonlocalized cracking, the results are found to strongly depend on the element size, ie, are unobjective with regard to the analyst's choice of the mesh. This is illustrated by the example (84.15, 85.3, 85.13) of a concrete bar (Fig. 19) with 5% reinforcement, in which smeared cracking is stable without localizing. The finite element results obtained for three different mesh sizes differ from each other intolerably (Fig. 19) for the models based on a line crack (ie, the fictitious crack model, or the composite damage or composite fracture models), but are identical for the crack band model, which is in this case equivalent to the classical smeared cracking approach.

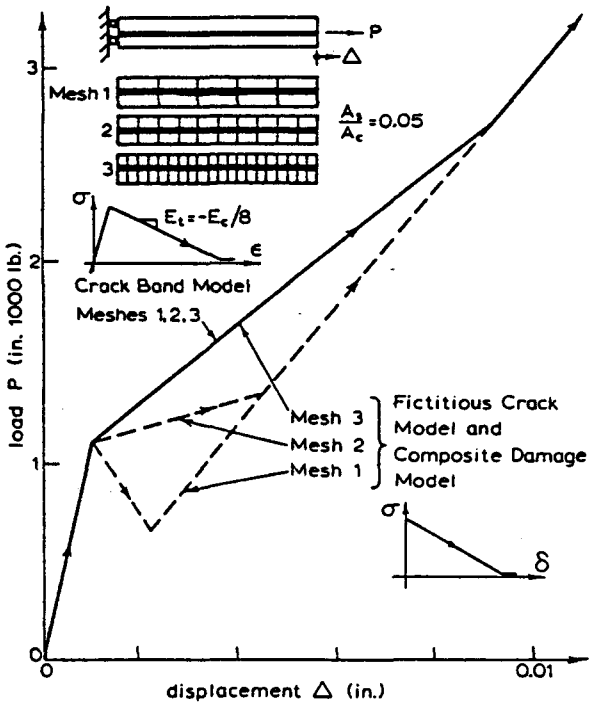

FIG. 19. Example of a concrete bar with 5% reinforcement, in which smeared cracking is stable without localizing (84.15, 85.3, 85.13).

To sum up, the picture of objectivity at mesh refinement for localized and nonlocalized cracking situations is as shown in the table in Fig. 20. The crack band model appears to be objective in general, ie, when one does not know in advance whether distributed cracking will or will not localize.

The limitation of the line crack models to localized cracking is due to the fact that they are characterized by only two material parameters f_t' and G_f, whereas the crack band model has three parameters, f_t', G_f, and the characteristic length $l = w_c$. For parallel cracking, the line crack models can, of course, be easily modified so as to be applicable for both localized and nonlocalized cracking; in the fictitious crack model (ie, interelement sharp cracks), it suffices to treat the element size h as a fixed material property so as to enforce the required crack spacing, $h = w_c$, and in the composite damage or composite fracture models, to imagine that there is not just a single line crack or crack strip embedded within each finite element, but that there are as many line cracks or strips as needed, spaced at distance w_c which is a material property (Fig. 17). Plausible though this generalization of the existing line crack models might be, it nevertheless runs into trouble for nonparallel cracking, simply because nonparallel straight-line cracks cannot have a constant spacing. On the other hand, if cracking is characterized by a multiaxial strain-softening constitutive law, there is no particular difficulty when the cracking direction

Model	Localized cracking	Nonlocalized cracking
1. Classical smeared cracking	no	yes
2. Fictitious crack model	yes	no
3. Composite damage model	yes	no
4. Crack band model	yes	yes

FIG. 20. Attainment of objectivity with respect to element size (85.3, 85.13).

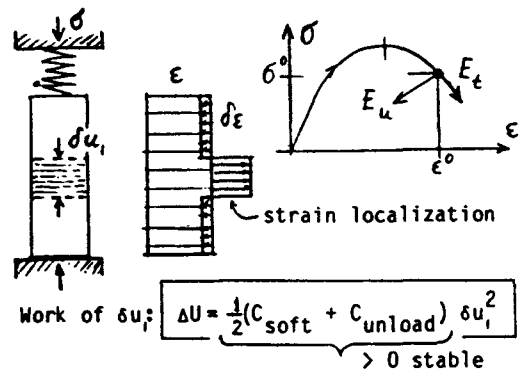

FIG. 21. Stability criterion for strain-softening: a simple example (76.2, 78.2).

varies over the space, or even when multidirectional cracking takes place, or when the direction of cracking rotates during the loading process.

Thus far we have seen how both the localized and the nonlocalized distributed cracking can be modeled. However, we have not yet addressed the question whether the cracking will or will not localize. This is a difficult problem whose handling in large finite elements programs has not yet been developed. Aside from the stability analysis of the regular parallel crack system mentioned before (Fig. 15), an exact analytical solution is possible for uniaxial tensile or compression strain-softening in a bar loaded under displacement control through a spring (76.2, 82.3) (Fig. 21). This simulates a compression or tensile specimen in a testing machine, whose flexibility is represented by the spring.

Stability requires that strain increments that are positive over some portion of the specimen length and negative over another portion (Fig. 21) lead to a positive second variation of the system's energy at fixed supports. If strain-softening is assumed to occur only over a negligible portion of the length, which would be correct for a perfectly homogeneous continuum (without inhomogeneous microstructure), it is found that instability always occurs at the peak stress point. Thus, the strain-softening could never be realized. The fact that it can be realized and measured proves that the existence of strain-softening within only a negligible portion of the length is an incorrect assumption. Correctly, the length of the strain-softening region must be assumed to be a material property, or else objectivity could not be achieved, and then the strain-localization instability occurs at a finite distance behind the peak rather than at the peak. The shorter the specimen, or the stiffer the machine, the farther is the instability point pushed beyond the peak stress point. The stability condition can be reduced to the requirement that, for an axial load applied at the boundary of the strain-softening region, the sum of the spring constant of the strain-softening region and the spring constant of the rest of the system including the unloading portion of the specimen and the supports must be positive. This appears to be a special case of the general requirement that the incremental stiffness matrix of the system be positive definite.

This type of stability condition must be met for all admissible (ie, compatible) deformation increments of the system at which the prescribed boundary displacements are fixed and the prescribed loads are constant. Checking it, however, may be difficult. For a larger finite element system, the number of all possible deformation increments is extremely large. In theory, all possible combinations of loading and unloading in various elements that have so far entered the strain-softening regime must be checked for the positive definiteness of the associated

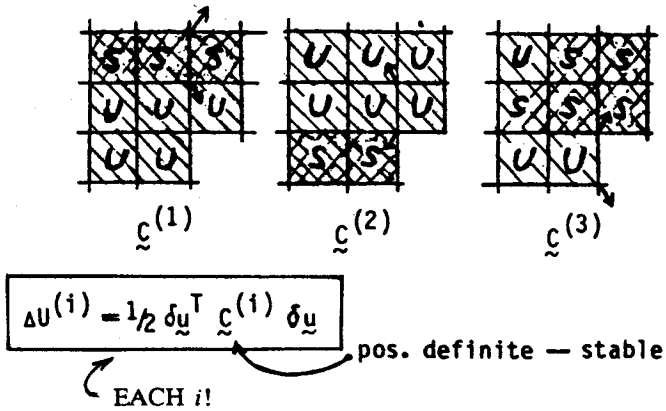

FIG. 22. Stability of strain-softening zones. All combinations of S (softening) and U (unloading).

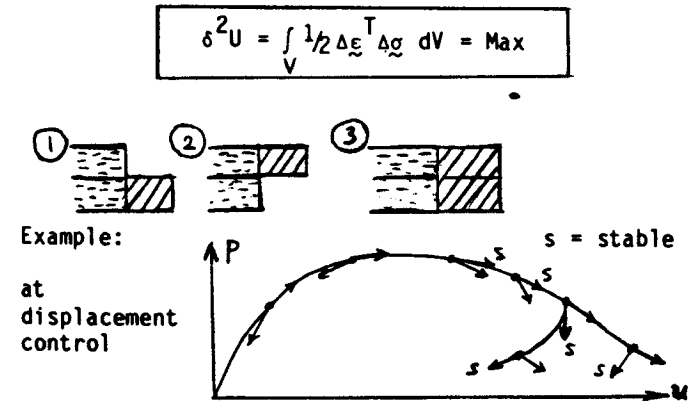

FIG. 24. Principle of maximum second-order energy release (85.3).

incremental stiffness matrix. Such checks are not normally carried out in the present finite element practice. If the instability for a certain mode is not checked, a possible instability may remain undetected. The iterations of the loading steps in the finite element program may converge and leave the unsuspecting analyst happy that he has obtained the solution, while in fact his solution cannot exist in reality since another solution releases more energy. The situation is not the same as in buckling of elastic systems in which the energy is compared only for infinitely close adjacent equilibrium configurations. Due to loading–unloading transitions in which the tangential stiffness changes discontinuously, there is no continuity between various deformation increments with various combinations of loading and unloading, ie, the unstable path is not infinitely close to another stable path. For this reason, no trouble is encountered in computations unless the right instability mode is actually tried.

As an illustration, Fig. 22 shows various possible combinations of unloading and softening in various elements which ought to be checked. Figure 23 shows an example of a doubly symmetric rectangular panel in which two symmetrically located elements at each side have a slightly smaller strength and start softening simultaneously. One possible equilibrium extension of the cracking (or softening) zone is a band of two cracking elements next to each other. If one does not deliberately perturb the system, one remains unaware that another possible equilibrium solution is an asymmetric crack band of a single-element width. For each of these two loading paths the computer program works well and iterations in each loading step converge. However, only one of these two equilibrium solutions is correct; it is the asymmetric solution with the band of a single element width.

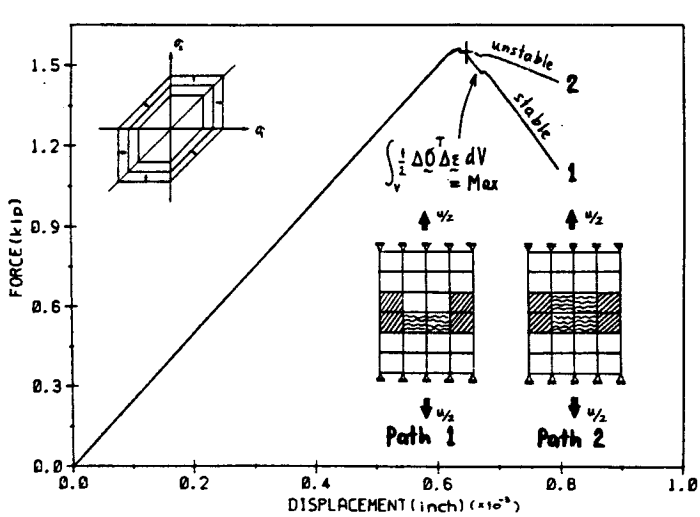

FIG. 23. Bifurcation of equilibrium path (calculation by F B Lin at Northwestern Univ, 1985). Tresca criterion, 4 × 5 in., mesh 4 × 6.

A somewhat simpler criterion for detecting localization instability may be stated by comparing all the possible equilibrium paths for the same loading step, characterized by the prescribed displacement increments and load increments. These paths are much less numerous than all the equilibrium and nonequilibrium kinematically admissible increments at fixed loading. It appears that among all possible equilibrium paths of the system, with various combinations of loading and unloading in the strain-softening elements, the actual path is that for which the second-order free energy release of the system, as indicated in Fig. 24, is maximized.

In general, stability checks with the foregoing criteria are too numerous to be feasible. It will no doubt be necessary to develop some practical ways to correctly select only a few equilibrium paths for which the stability checks are to be made.

A remark is in order on the recently popular theory of continuous damage mechanics, which originated with the work of Kachanov (58.3). Numerous papers have been written on stress–strain relations for damage resulting in failure of the material; yet the stability problems inherent to these formulations have been ignored, as if by calling strain-softening the damage the stability problems would go away. They do not. If the damage stress–strain relation results in an incremental material stiffness matrix that is not positive definite, the problems with unstable strain localization and spurious mesh sensitivity are again encountered. These problems went mostly undetected since little finite element computation has so far been done with the continuous damage mechanics formulation, and when it was done mesh sensitivity has not normally been checked. It has been also thought that stability problems are avoided by rate-dependent damage laws (84.46). However, if the matrix of the effective stiffnesses for the time interval under consideration is not positive definite, the stability problems must still be tackled (86.5). Valuable though many continuous damage theory developments were, the systematic lack of attention to the material instabilities due to damage—a more important problem in my opinion—has been a flaw of this school of thought.

3. IMBRICATE NONLOCAL CONTINUUM

From the purely mathematical viewpoint, the fracture models based on a line crack permit that the mesh size be reduced to zero. From the physical viewpoint, though, it makes no sense to reduce the mesh to sizes that are smaller than a certain limit, say, the aggregate size. In the same sense, the mesh size can be arbitrarily reduced also for the crack band approach, provided that the mean downward slope of the strain-softening diagram is made appropriately milder to ensure the same fracture energy for fully localized crack band. From the physical viewpoint, though, the finite elements in the crack band approach should not be made smaller than a certain characteristic length, l, which may be assumed to be about three times the aggregate size for concrete.

Nevertheless, mesh refinement is needed for three reasons: (1) to have a convergent discretization, the limit of which must be a continuum, (2) to accurately determine the energy dissipation due to cracking, and (3) to capture variations of the effective width of the crack band. It is obvious that the density of cracks or microcracks will not be uniform across the fracture process zone but will increase gradually towards its center. The crack band model assumes a uniform distribution of the cracking strain, with a sudden jump at the boundary of the band, but no doubt the correct picture is a smooth, nonuniform variation of the cracking strain across a crack band whose width depends on the problem. These objectives may be achieved by adopting the concept of nonlocal continuum.

The nonlocal continuum is a classical concept introduced in the late 1960's by Kröner, Krumhansl, Kunin, Levin, Eringen, Edelen, and others (68.5, 68.6, 68.7, 71.8, 72.3, 83.24). The central hypothesis is that the stress at a point is not a function of the smoothed (homogenized) stress at the same point but a function of the (smoothed) strain distribution over a certain characteristic volume centered at that point (Fig. 25), the size of

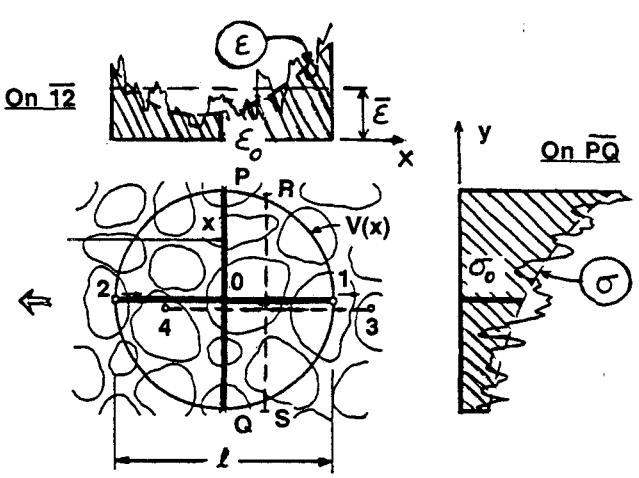

Hypothesis:

$$\sigma_{PQ} = \boxed{\sigma(x) = f[\bar{\varepsilon}(x)]} \neq \sigma_{RS}, \quad \neq f[\varepsilon(x)]$$

$$\bar{\varepsilon}(x) = \frac{1}{l}\left[u\left(x+\frac{l}{2}\right) - u\left(x-\frac{l}{2}\right)\right] = \frac{\Delta l_{12}}{l_{12}}, \quad \neq \frac{\Delta l_{34}}{l_{34}}$$

$$= \frac{1}{l}\int_{-l/2}^{l/2} \varepsilon(x+s)\, ds,$$

possibly add weight $\alpha(s)$

FIG. 25. Nonlocal continuum; l = characteristic length.

Mean Strain: $\bar{\varepsilon} = \frac{1}{V}\int_V \varepsilon(x')\alpha(x')\, dV = H\varepsilon$

Broad-range stress: $\sigma = F(\bar{\varepsilon})$

Eq. of motion: $(1-c)\underline{\underline{(H\sigma_{ij})_{,j}}} + c\tau_{ij,j} = \rho\ddot{u}_i$

Stability: $\underline{\underline{c > 0}}$

Work: $(1-c)\sigma_{ij}\delta\bar{\varepsilon}_{ij} + c\tau_{ij}\delta\varepsilon_{ij}$

Differential approximation: $H \simeq 1 + \lambda^2\nabla^2$

FIG. 26. Imbricate nonlocal continuum (84.6).

which is the characteristic length l. Thus, one defines the mean strain, $\bar{\varepsilon}$, as a certain averaging integral over the characteristic volume V with a suitable empirical weighting function $\alpha(\mathbf{x})$ (Fig. 26). The constitutive relation then defines a broad-range stress σ as a function of the mean strain $\bar{\varepsilon}$ (Fig. 26).

In the classical theory of nonlocal continuum, the continuum equation of motion (or of equilibrium) has been written in terms of the gradient of σ. With regard to finite element analysis, however, this form of the continuum equation of motion is objectionable, because of two shortcomings: (1) The differential operator in the continuum equation of motion is not self-adjoint, with the result that the stiffness matrix of the finite element system is nonsymmetric even if the material stiffness matrix is symmetric (84.6, 86.5), and (2) for certain reasonable weighting functions α in the averaging integral (and especially for the most useful uniform weighting function) the finite element formulation admits periodic zero energy solutions, with a wavelength equal to the characteristic length of the material (84.6, 85.12).

The latter shortcoming may be avoided by imagining an overlay of nonlocal and local continua, characterized by empirical coefficient c in Fig. 26. If $c = 1$, we have the usual or local continuum equation of motion, and, if $c = 0$, we have a purely nonlocal formulation. With $c = 0$, however, the aforementioned instability with a zero energy mode takes place. For a uniform weighting function this instability is avoided if $c > 0$. In theory, this would mean that an extremely small local component, eg, $c = 0.001$, would suffice to avoid this instability; however, in practice one obtains excessive noise when c is close to the stability limit. Experience shows that $c = 0.1$ is usually the minimum needed to suppress this noise (84.6).

The problem with nonsymmetry of the operators and matrices may be avoided by applying the averaging operator H once more to the broad-range stress σ before σ is substituted into the equation of motion (84.6, 86.5, 84.3) (see Fig. 26). It has been in fact rigorously demonstrated that the second application of the averaging operator H is required by a consistent use of the variational calculus (84.3).

For the purpose of some analytical solutions it is of interest to note that the integral averaging operator may be approximated by a differential operator involving a Laplacian ∇^2 with a characteristic length λ (Fig. 26) related to the cross section l of the representative volume V (84.3).

When a uniform weighting function α is used, a very simple discrete approximation is possible. This approximation consists of an imbricate (or regularly overlapping) finite element system as illustrated in Figs. 27 and 28 (84.3, 84.6, 85.12). When the finite elements are larger than the characteristic length l, the imbricate and the usual finite element models are identical. For smaller finite elements, the element size must be kept constant, equal to l, so that each finite element would automatically implement strain averaging over the length l. Thus, the finite

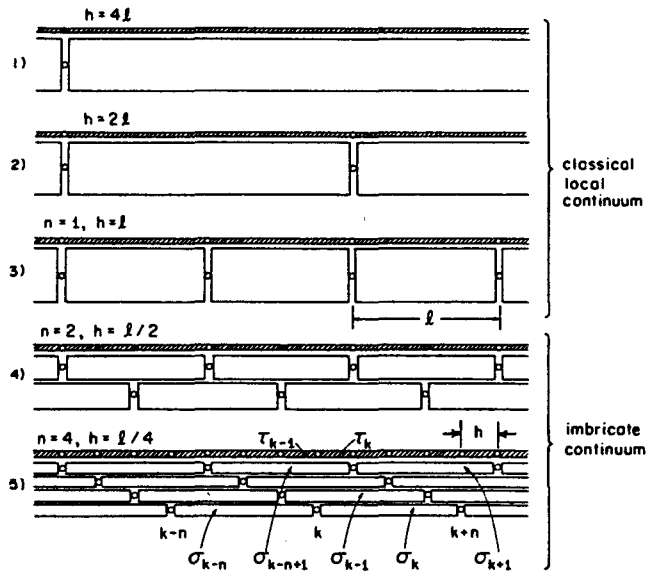

FIG. 27. Mesh refinement for imbricate nonlocal continuum (84.6).

elements must be regularly overlapping, or imbricated, and their thickness or cross section must be reduced so that the combined thickness of all overlapping finite elements remain 1. The discrete equations of motion for this finite element system represent difference equations, and it is easy to show that their continuum limit is exactly the continuum equation of motion in Fig. 26.

The imbricate finite element system is relatively easy to program. The only change that needs to be made in a usual, local finite element code is to redefine the integer matrix of nodal connectivity, which specifies the node numbers for each element number, and to program another integer matrix which gives the numbers of all finite elements that overlap each square of the mesh.

To validate a finite element program for strain softening, it is important to make a comparison with some exact solutions for strain-softening. An exact solution has been found to a wave propagation problem for a uniaxially stressed bar (85.5). The bar is subjected at its ends to sudden tensile stress jumps producing strains just below the strain-softening limit. As the inward elastic waves meet at the center of the bar, strain-softening is produced in the central cross section (Fig. 29). It is found that the strain-softening region remains subsequently localized

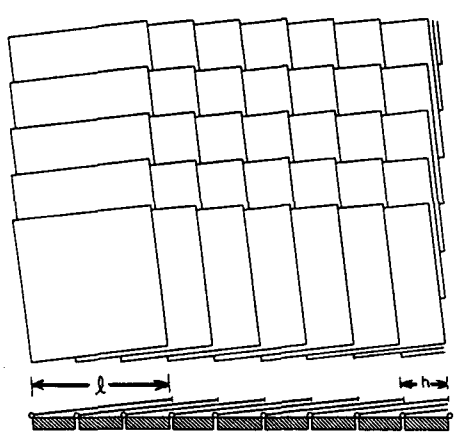

FIG. 28. Multidimensional discretization: imbricated system of ordinary elements (84.6).

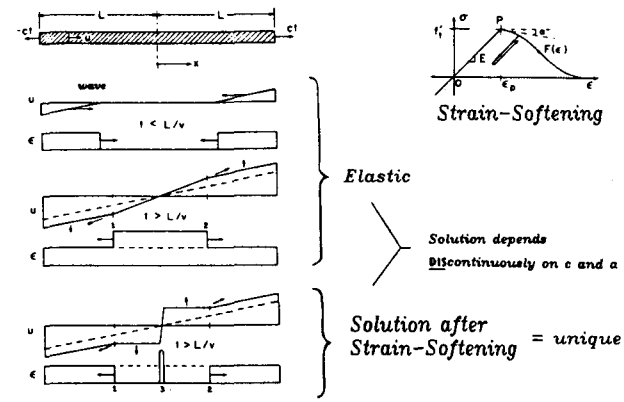

FIG. 29. Exact solution for a wave in strain-softening bar, local continuum (85.5).

in this cross section, and unloading waves of strain emanate toward the ends of the bar as if the bar split in the middle. As the magnitude of the stress applied at the boundary is increased, the solution changes discontinuously when the limit of strain-softening is attained. Thus, the solution depends discontinuously on the boundary conditions. This means that the problem does not belong to the class of the so-called well-posed problems (as pointed out by Sandler, 84.46).

Nevertheless, a solution exists and is apparently unique (85.5). Moreover, a numerical finite element solution obtained with the standard explicit step-by-step algorithm is found to converge to the exact solution (Fig. 29), and to do so in fact quadratically (84.6). Clearly, the idea of strain-softening in a local continuum is not mathematically meaningless. However, it is physically unrealistic. According to the exact solution, the energy dissipation due to strain-softening which leads to breakage of the bar in the middle is zero (84.6, 76.2, 80.1). This cannot be true for any real material. We thus have another indication that a nonlocal continuum concept is required if the mesh is refined.

Figure 30 shows the profiles of the mean strain at various times obtained for progressively finer element subdivisions. The first subdivision has only five elements over the bar length, in which case the solution is local because the characteristic length is assumed to be 1/5 of the bar length. As the mesh is refined the width of the strain-softening region decreases, apparently converging to the Dirac delta function.

By contrast, for the imbricate finite element formulation (Fig. 31), the solution converges to strain distributions in which many elements next to each other undergo strain-softening (84.6). For the finest mesh, there are 195 elements over the bar, and about one-half of them are in the strain-softening regime. The energy consumed by failure of the bar is plotted in Fig. 32 as a function of the number of elements. While for the local finite element model the energy strongly depends on the mesh subdivision and apparently converges to zero, for the imbricate finite element solution, the energy consumed by failure of the bar remains approximately constant for various element subdivisions (Fig. 32). This behavior seems typical of all comparisons between local and imbricate finite element solutions for strain-softening.

In the foregoing solution, the strain softening is limited to an immobile point. However, as Belytschko et al just discovered, for problems with partial softening followed by hardening, strain-softening can develop in a finite region whose front can travel with a finite wave speed.

Another strain-softening problem, suggested by Belytschko as a one-dimensional problem which involves triaxial stresses, is

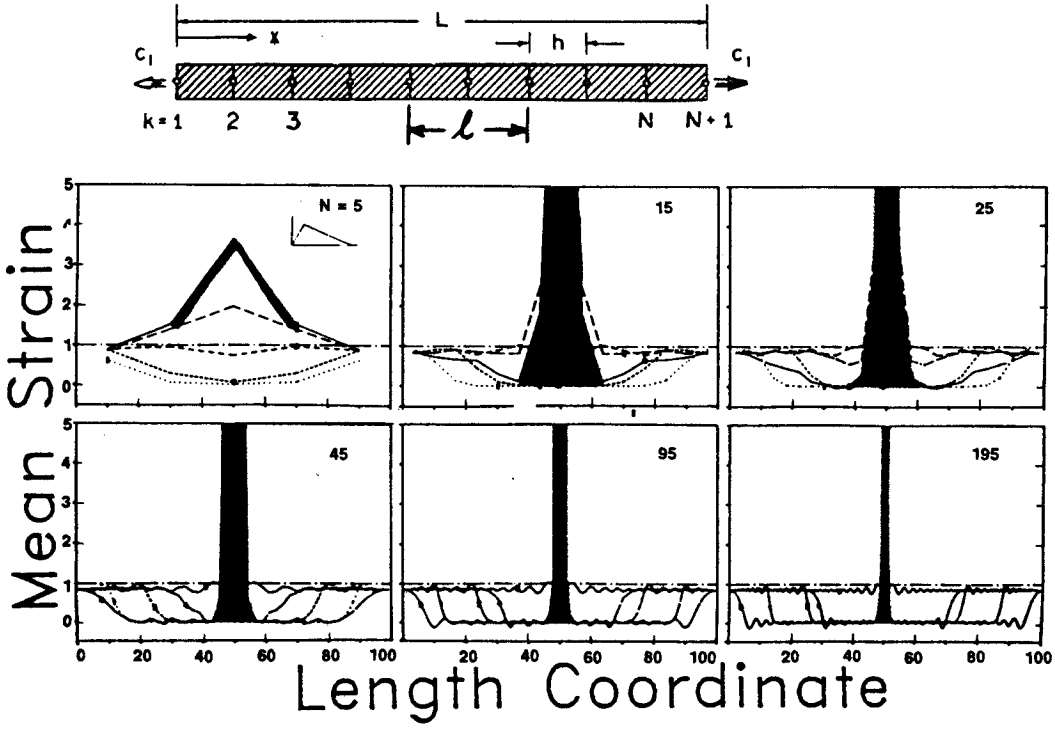

FIG. 30. Finite element solution of wave propagation in one-dimensional strain-softening bar, local continuum (84.6).

the imploding spherical wave (86.5). Figure 33 shows a hollow sphere whose volumetric stress–strain relation exhibits strain-softening. A stress jump applied at the sphere's surface produces an inward radial wave. An exact solution exists for elastic behavior, and it shows that the wave front grows. At a certain distance from the surface, depending on the magnitude of the suddenly applied stress, the strain-softening limit is inevitably reached. For elastic behavior, the explicit time-step finite element solution is found to converge to the exact solution. For strain-softening behavior, the local and imbricate nonlocal finite element solutions are shown in Fig. 33 for various element subdivisions, involving 10, 40, and 160 elements over the thickness. The characteristic length of the material is considered such that the local and nonlocal solutions are identical for a subdivision with 10 line elements of equal length. From the volumetric strain profiles at various times shown in the left column of Fig. 33, we see that the local solution does not converge. An interesting feature is that strain-softening does not arise merely at one point. The wave is able to penetrate beyond the point of first strain-softening and create further strain-softening points

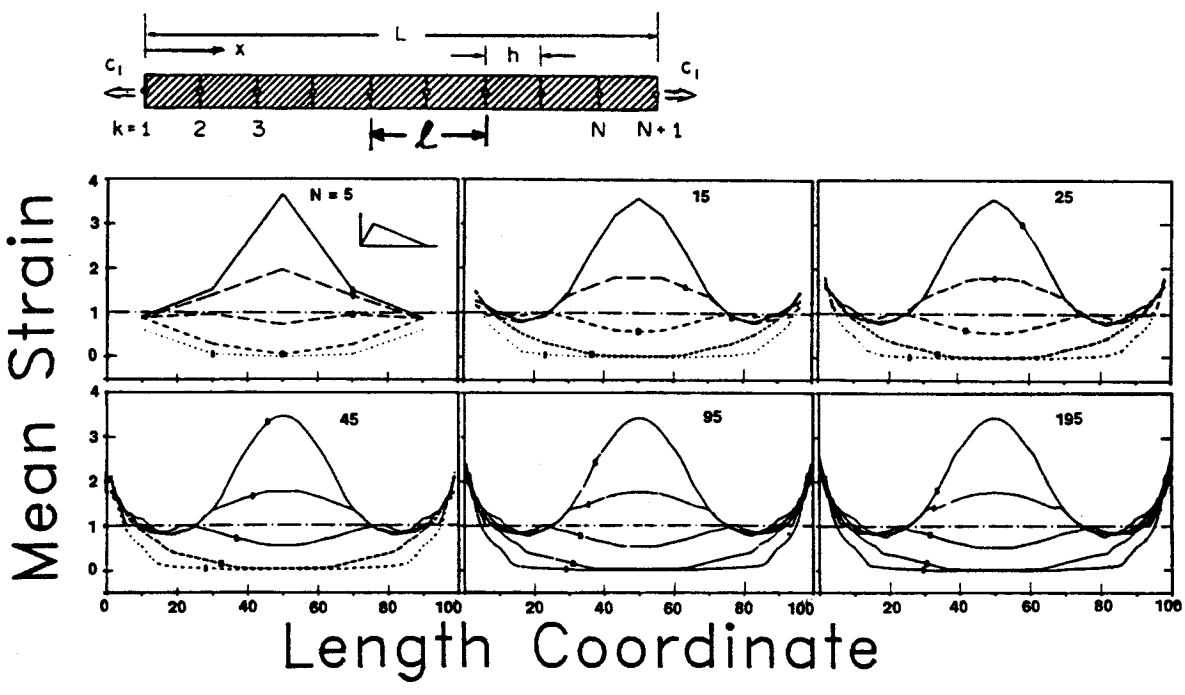

FIG. 31. Same as Fig. 30 but, imbricate continuum (84.6).

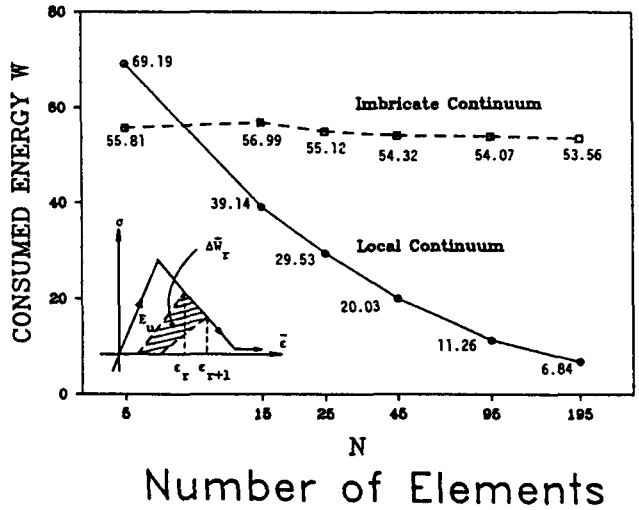

FIG. 32. Energy consumed by failure of strain-softening bar (85.6).

at apparently random locations which vary chaotically from one element subdivision to another. By contrast, the imbricate nonlocal solution, shown in the right column, appears to converge. Similar results are obtained for a cylindrical wave.

Figure 34 shows application of the imbricate analysis to a rectangular panel pulled vertically, with prescribed displacements of the boundary nodes on top and bottom (85.7). The properties of all finite elements are the same, except that in two elements at the centers of the sides the strength limit is assumed to be 2% smaller than in the other elements. Three meshes, with sizes in the ratio 1:1/3:1/5, are considered. The problem is static and an implicit step-by-step algorithm is used. Figure 35 shows the solutions obtained for various meshes, the local ones in the left column and the imbricate nonlocal ones in the right column. The load-displacement diagrams (top), as well as the transverse normal strain profiles across a strain-softening band growing horizontally across the panel, are rather different for the three meshes and the strain is seen to localize. By contrast, the imbricate nonlocal solutions are almost the same for the three meshes, and no strain localization in the middle of the panel occurs. The dependence of the energy consumed by strain-softening on the number of elements (middle) is similar as before; for the local solution, the dissipated energy value depends strongly on the number of elements and apparently converges to zero for an infinite mesh refinement, while for the imbricate nonlocal solution the dissipated energy is about the same for all mesh subdivisions.

4. MICROMECHANICS MODELING

Although a realistic stress–strain relation with strain-softening is not all that is required for finite element analysis of distributed cracking by the crack band approach, it is an essential ingredient. Numerous researchers, including Dougill, Bažant, Prat, Kim, Darwin, Pecknold, Murray, Darve, Zienkiewicz, Dafalias, Mroz, Hueckel, Maier, Dragon, Zubelewicz, and others have tackled this question from the macroscopic phenomenologic viewpoint and produced various sophisticated constitutive models with strain-softening (endochronic, plastic, fracturing, plastic-fracturing, bounding surface, etc) (71.10, 76.3, 76.5, 76.6, 76.9, 76.12, 77.1, 77.6, 77.11, 78.5, 78.7, 78.12, 79.8, 79.9, 79.12, 79.14, 79.18, 80.4, 80.6, 80.13, 80.14, 80.26, 81.10, 82.10, 82.16, 82.21, 82.22, 83.2, 83.18, 83.23, 83.25, 83.35, 84.35, 84.38, 84.40, 85.16, 85.47, 85.52). One promising approach is a damage constitutive law based on an idea of Kachanov (58.3),

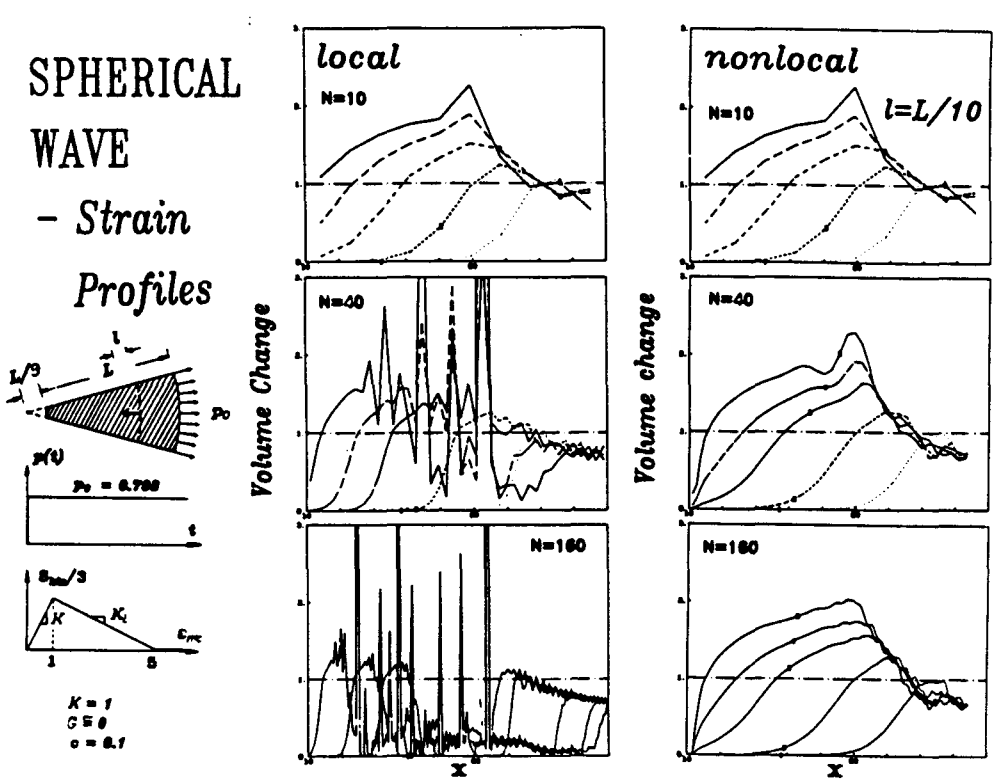

FIG. 33. Spherical wave, in strain-softening material,strain profiles (86.5).

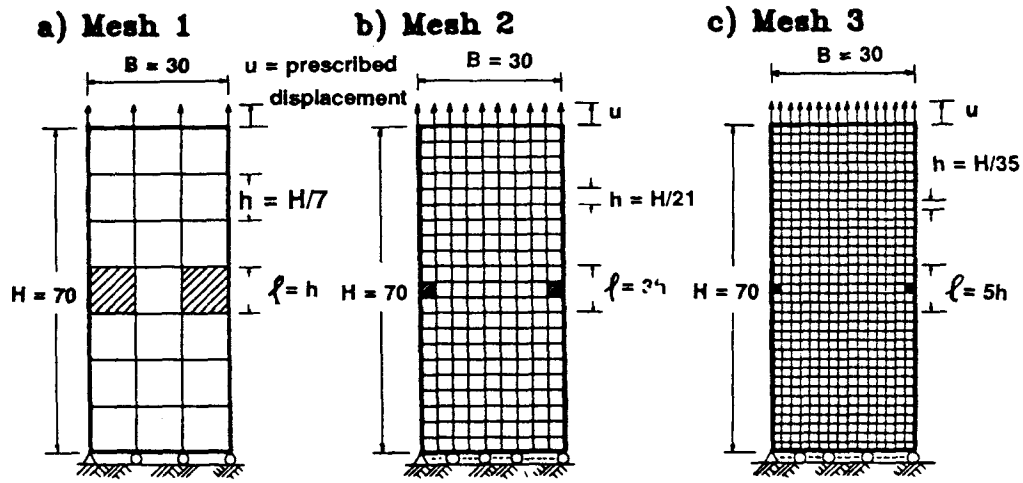

FIG. 34. Mesh refinement strain-softening zones for refined meshes (85.7).

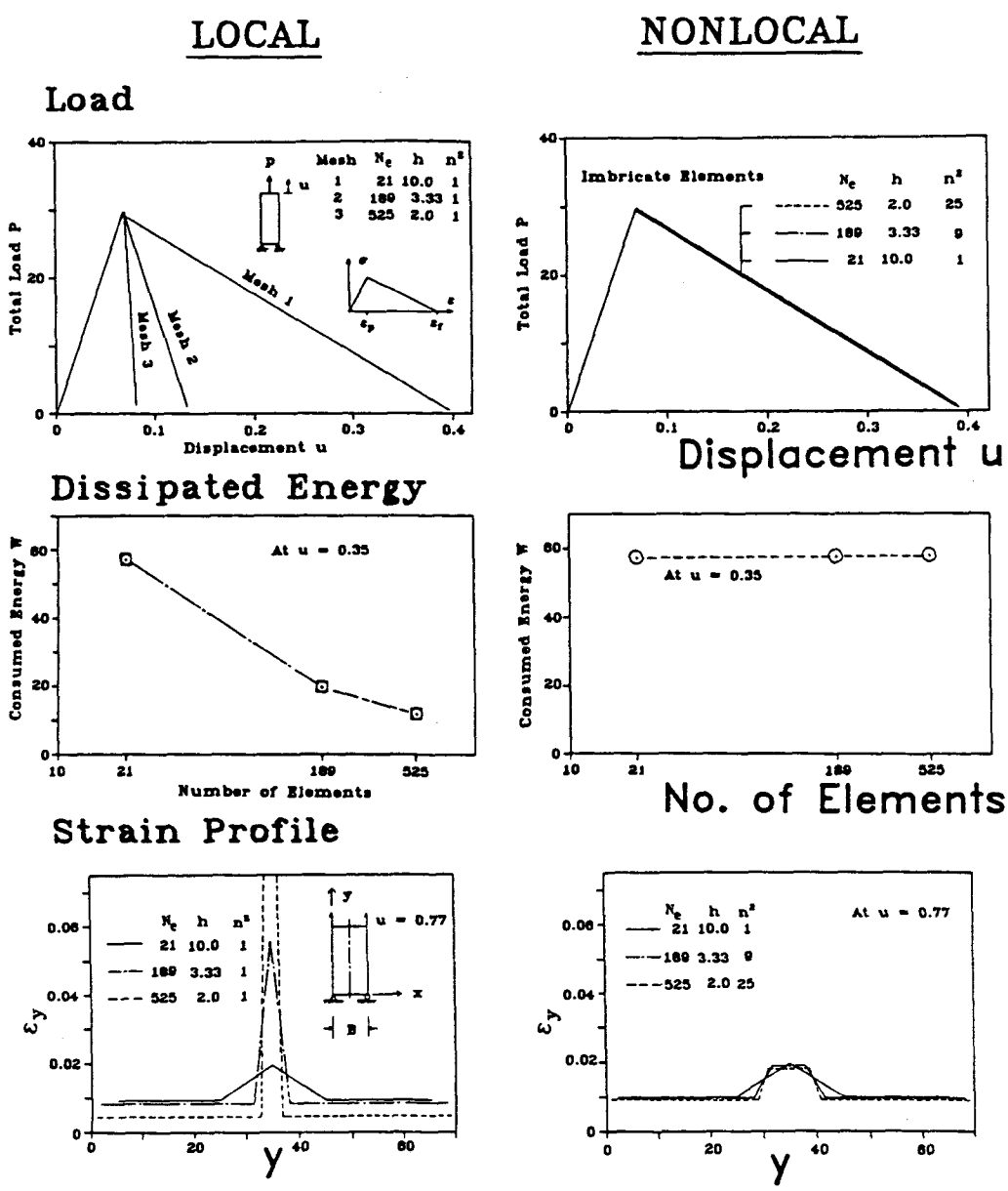

FIG. 35. Convergence at mesh refinement for Fig. 34 (85.7).

at first used extensively for metals. In this approach the constitutive properties depend on a certain damage variable (scalar, or vector, or tensor) which is specified by an evolution law. For materials that exhibit distributed cracking, such damage formulations were developed by Mazars, Løland, Resende and Martin, Krajcinovic, Fonseka, Popov, Ortiz, and others (77.9, 78.8, 80.19, 81.9, 81.12, 81.14, 82.21, 83.36, 84.33, 84.50, 82.17, 84.43, 84.34, 85.42, 83.39, 84.37). The latest Ortiz's formulation (84.37), in which the damage measure coincides with the fourth-order tensor of elastic moduli of the material, appears particularly realistic and promising.

Many of the damage constitutive laws involve some form of rate dependence, in which case the strain-softening may be disguised as stress relaxation. It is unclear, though, whether the modeling of strain-softening as stress relaxation is more than a simplifying device suitable merely for a limited range of applications. As it seems, this type of formulation does not permit that strain-softening be obtained for various loading rates differing by orders of magnitude, as observed in testing of concrete. On the other hand, the strain rate in most materials affects the response as a parameter, and in this form the damage constitutive laws are no doubt useful for modeling strain-softening failures.

After less than complete satisfaction with macroscopic phenomenologic modeling, intensive efforts are now being made to deduce the constitutive relation from physics and micromechanics analysis. Such formulations, involving statistics of crack distributions, their sizes and openings, statistics of slips, thermodynamics of material cracking, etc., have been formulated by Kachanov, Vakulenko, Zaitsev, Wittmann, Roelfstra, Seamann, Shockey, Bui, Ehrlacher, Stout, Dienes, Horii, Nemat-Nasser, Davison, Chudnovsky, Ortiz, Margolin, Costin, and others (73.3, 75.8, 76.4, 78.6, 79.11, 79.17, 80.17, 80.21, 81.27, 82.15, 82.27, 83.19, 83.20, 83.21, 83.40, 83.49, 84.56, 85.28, 85.33, 85.48, 85.53, 86.8).

One simple and effective micromechanics approach to the stress–strain relation is the microplane model. It is based on G I Taylor's basic idea (38.1), developed long ago in the slip theory of plasticity for polycrystalline metals by Batdorf and Budianski (49.1). To rocks and soils, these ideas were applied by Zienkiewicz and Pande (77.18, 82.16, 82.23, 82.24) in what they called the overlay model, and more recently to concrete by Bažant, Oh, and Gambarova (85.9, 84.8). The basic idea of these formulations is to characterize the inelastic behavior by a relation between the stress and strain components on a plane of an arbitrary inclination in the material, for which recently the general term "microplane" has been introduced. The stresses or strains from the microplanes of all orientations are suitably superimposed to obtain the macroscopic stress or strain tensor.

The macroscopic stiffness matrix is obtained from the condition that the rate of energy dissipation expressed in terms of the macroscopic and microscopic stresses and strains must be the same for any specified strain rate tensor. In formulations of this type it was normally assumed that the microstructure is statically constrained, which means that the stresses on each microplane are assumed to be the resolved components of the macroscopic stress tensor (49.1). Another equally simple possibility is to assume a kinematically constrained microstructure, in which the strains rather than the stresses on a microplane of any orientation are the resolved components of the macroscopic strain tensor. The latter, recent approach appears to be more realistic for concrete (85.9), for which the microplanes may be imagined to represent the thin contact layers between rigid aggregate particles. The deformation of these layers is essentially determined by the relative displacements of the aggregate particles, ie, is kinematically constrained. Aside from that, it is found that the kinematic rather than static constraint is necessary to obtain a stable model for the case of strain-softening, and in the practical sense this is the overriding reason for introducing this approach.

The basic relations for a simple kinematically constrained microplane model in which only normal strains on the microplanes are permitted are written in Fig. 36; n_i are the direction cosines of the normal to each microplane, ε_n is the normal component, ε_{ij} is the macroscopic strain tensor, and $\mathbf{D}$ is the macroscopic stiffness matrix obtained by integration over a unit hemisphere. Function $f(\vec{n})$ indicates the frequency of the microplanes for various orientations and is able to introduce anisotropic characteristics of the material. [For isotropy, $f(\vec{n})$ = const.] A more sophisticated model which takes into account not only the normal but also the shear components on each microplane has been formulated (84.13), but it is not clear at the present whether consideration of the shear strains is necessary since a shear strain on one plane is equivalent to normal strains on certain inclined planes. If the normal stress–strain relation for each microplane exhibits strain-softening, one obtains strain-softening also macroscopically, and it is easy to fit various tensile strain-softening data for concrete. It seems that the microplane model should be also capable of modeling compression splitting as well as the inelastic behavior of concrete under compression and shear in general, but work on this problem is still in progress (P C Prat, Northwestern University).

Conceptually, the attractiveness of the microplane approach rests on the fact that we do not need to deal with relations between the tensors of stress and strain, worrying about their proper invariance. Rather, we need to describe only a simple relation between the components of stress and strain on one plane, and the tensorial invariance restrictions are then automatically satisfied by integration over all spatial directions.

With regard to application in finite element programs, it is important to integrate over a unit hemisphere (Fig. 36) as efficiently as possible, since this integration must be repeated at each integration point of each finite element, at each loading step. Various efficient Gaussian-type numerical integration formulas for the spherical surface are available in the literature (71.12, 85.9), and one of the most efficient ones is illustrated by the point arrangement on an icosahedron in Fig. 37, in which the points indicate the discrete spatial orientations used in approximating the integral over a unit hemisphere by a finite sum, with certain suitable weights for each direction (86.3). The

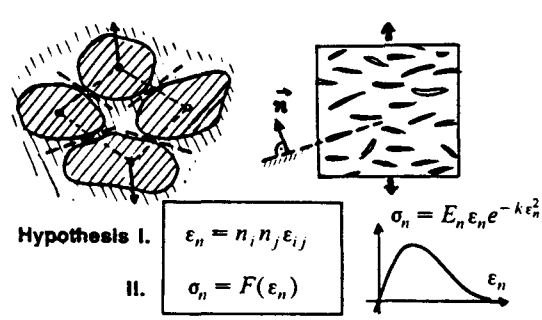

Hypothesis I. $\varepsilon_n = n_i n_j \varepsilon_{ij}$

II. $\sigma_n = F(\varepsilon_n)$

Result:

$$\mathbf{D}\sigma = \mathbf{D}\, d\varepsilon$$

where

$$\mathbf{D} = \int_S n_i n_j n_k n_m \underbrace{f(\vec{n})}_{\text{anisotropy}} F'(\varepsilon_n)\, dS$$

FIG. 36. Microplane model for tensile microcracking: analog of Batdorf and Budianski's slip theory (49.1).

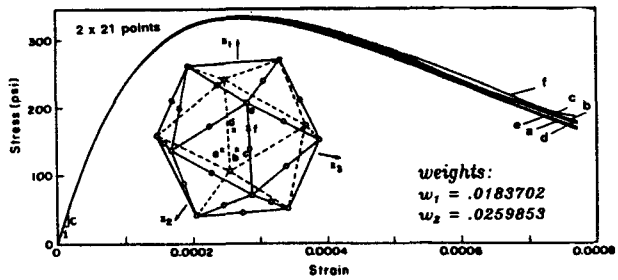

FIG. 37. Points of a numerical integration formula for a spherical surface: icosahedron vertices and midedges (degree 9) (86.3, 85.9).

error of the integration formula may be estimated by assuming a certain type of loading, eg, uniaxial tension, and applying it at various orientations with regard to the set of integration points. If the integration formula were exact, identical response curves of stress versus strain would be obtained. Due to the approximate nature of the numerical formula, the response curves have a certain spread which must be acceptable, both in the hardening and softening ranges (Fig. 37). Achieving a narrow spread of the response curves for the softening range is much harder than for the hardening range, and it necessitates in three dimensions the use of at least 21 integration points (85.9) (ie, discrete spatial directions). For two-dimensional problems, the number of discrete directions may be reduced to about eight (84.8).

In the microplane approach, we trade conceptual simplicity for a penalty in computer time. Compared to the phenomenologic macroscopic constitutive models, the basic relations are simpler and involve fewer material parameters. Aside from that, the microplane approach is more realistic, especially when complicated loading paths in the stress or strain space are considered (eg, shear and normal extension applied either proportionally or in sequence). The microplane model can capture the development of cracking in various directions at the same point of the structure during the loading sequence.

The macroscopic constitutive law does not provide complete information on the material properties. It is equally important to use micromechanics to determine material parameters that limit strain localization, such as the characteristic length l in the imbricate formulation or the cracking front width w_c in the crack band model. To obtain these parameters, the micromechanics model cannot be restricted to a single idealized point of the macroscopic homogenized (smoothed) continuum, but the spatial fields themselves must be directly modeled in terms of an idealized microstructure.

An example of this approach is the rigid particle contact model introduced for concrete by Zubelewicz (83.49) and subsequently developed in detail by Zubelewicz and Bažant (see Fig. 38). In this model, which is patterned after Cundall's distinct element method for frictional interaction of the grains of sand, gravel, and other bulk solids, one assumes that all inelastic deformation is concentrated into contact layers between rigid particles. In Fig. 39 this interaction is described simply as a sudden (vertical) stress drop when the specified strength limit is reached. The computer program generates a random system of rigid particles and their contact planes, and solves the problem in an incremental manner considering in each loading step the force and moment equilibrium conditions for each particle loaded by the interparticle contact forces. Figure 39 shows the calculated load-displacement curve and the curve of dissipated energy obtained for the example in Fig. 38, in which the top and bottom boundaries are subjected to prescribed uniform displacement. Evidently, the calculated tensile load displacement diagram seen in Fig. 39, with its very long tail of the strain-softening response, looks quite realistic.

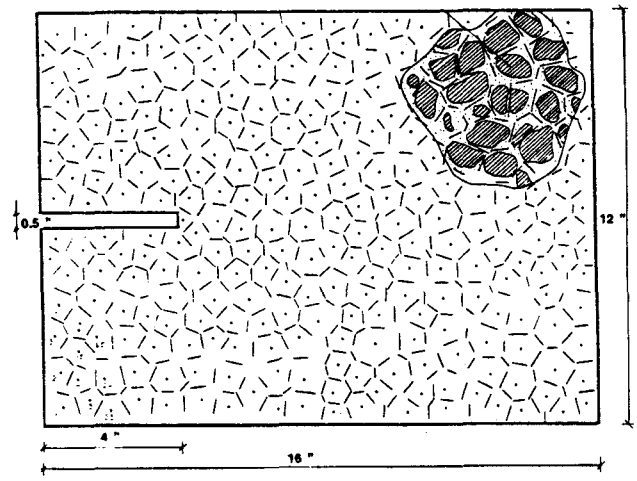

FIG. 38. Rigid particle contact model simulating microstructure of concrete (85.56).

Figures 40–42 illustrate the interparticle contact forces and the development of cracks. The heavy solid, dashed, and light solid lines indicate the lines of interparticle forces exceeding 0.8, 0.6 and 0.4 of the strength limit. Note the concentration of interparticle forces in the vicinity of the notch tip and the general disappearance of heavily loaded contacts at subsequent stages of softening, as the material outside the fracture process zone is getting unloaded. The cracks obviously propagate discontinuously, and not along the line of the symmetry of the panel. This is due partly to the randomness of the microstructure, and probably also to instability of the straight crack direction in double cantilever fracture specimens (cf. Cotterell and Rice, 80.11).

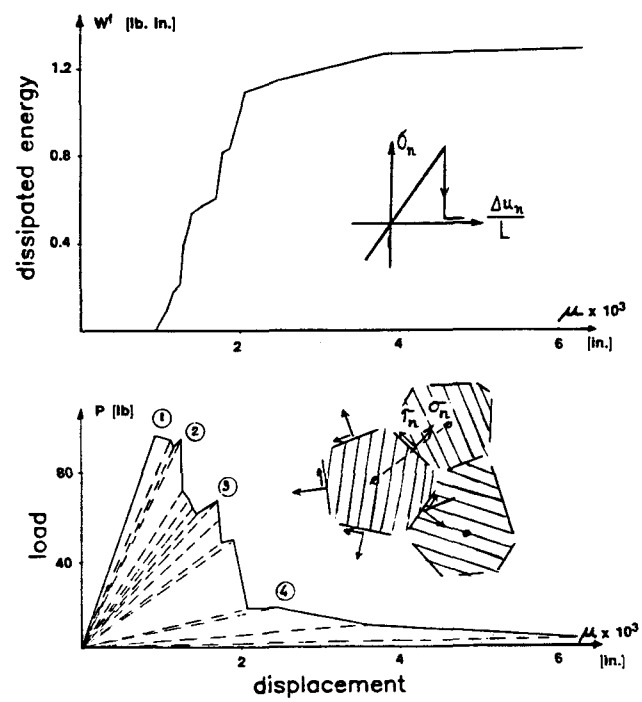

FIG. 39. Curves of dissipated energy and of load VS displacement for rigid particle contact model (85.56).

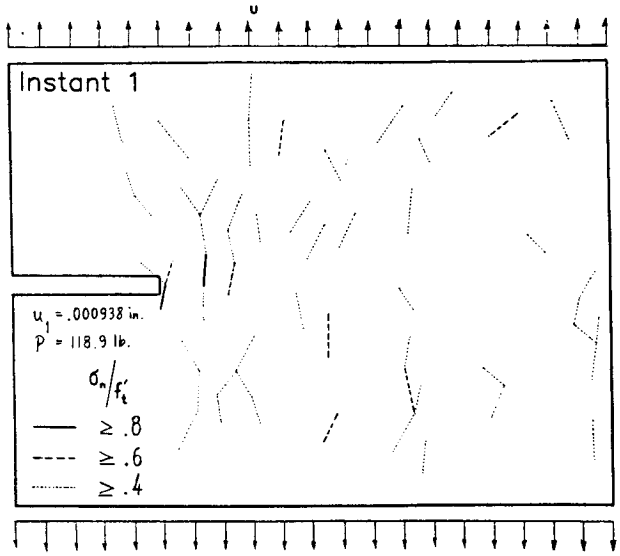

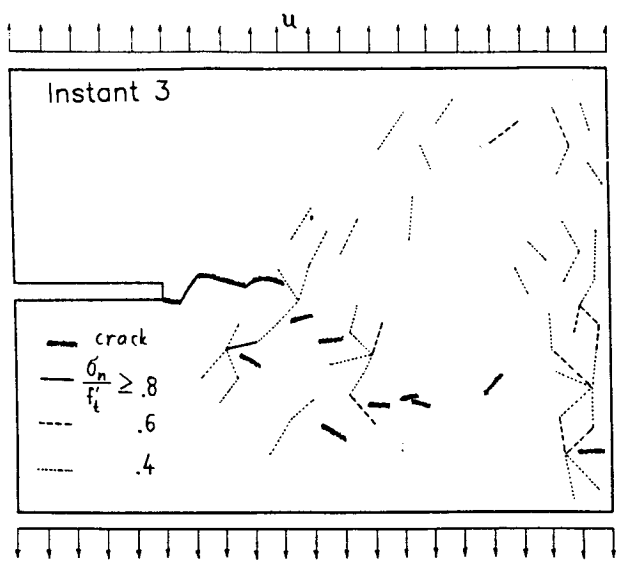

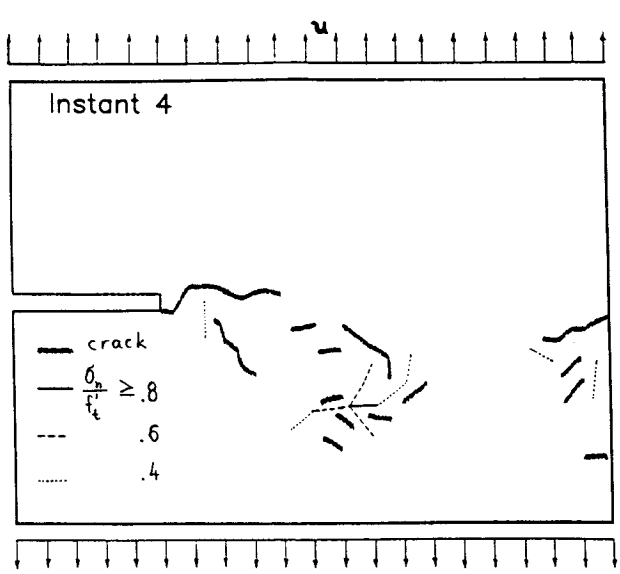

FIGS. 40–42. Interparticle contact forces and the development of cracks: instants 1, 3, and 4, respectively (after Zubelewicz and Bažant, 1985).

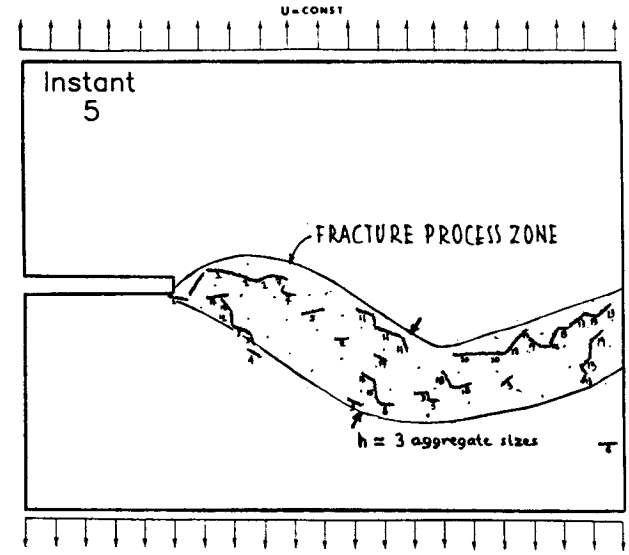

FIG. 43. Latest stage of crack evolution (after Zubelewicz and Bažant, 1985).

The latest stage of crack evolution is shown in Fig. 43, in which the approximate range on the cracked area is shaded. With regard to the crack band model, it is of interest to note that the mean width of the fracture process zone in this simulation is roughly three times the particle size. Hence, this model reveals the length restriction on the extent of localization of cracking, a characteristic which is impossible to obtain with pointwise micromechanics models, such as the microplane model. There is no doubt much further potential in the rigid particle contact approach. However, it would be difficult to apply this approach to real large structures because an increase in particle size would change the fracture energy, same as an increase in mesh size.

Other very valuable studies of the propagation of microcracks in a random microstructure of concrete have been made by Wittmann and Zaitsev (85.50, 85.53, 83.47, 82.33, 81.27, 81.26, 77.17). Finite elements have been applied to model the microstructure in the concrete–mortar system by Darwin (80.20), and recently Roelfstra and Wittmann use them in detailed modeling of the microscopic process of fracture as well as creep, water diffusion, and shrinkage in concrete (82.33, 85.11, 85.50).

The most important aspect of the micromechanics approach I wish to emphasize is that it is not enough to use micromechanics to obtain the macroscopic stress–strain relation, which has been the exclusive objective of nearly all the studies up to now. As Belytschko and I have been emphasizing, it is equally important to use micromechanics to determine the macroscopic parameters and laws which prevent complete localization of damage into a region of zero volume. Examples are the minimum crack band width w_c in the blunt crack band model, the characteristic length, the weighting function, and the form of the averaging law in the imbricate nonlocal model. The stress–strain relation suffices to describe the macroscopic material properties of a statistically heterogeneous material only if the body is in the state of uniform stress and strain, but not if the state is nonuniform. Likewise, it is insufficient to test material properties on specimens which are designed to be as nearly as possible in a state of homogeneous strain, and incorrect to interpret the test results by assuming a homogeneous strain distribution.

If the properties of the particle system in Fig. 38 were described merely by a macroscopic stress–strain relation, the

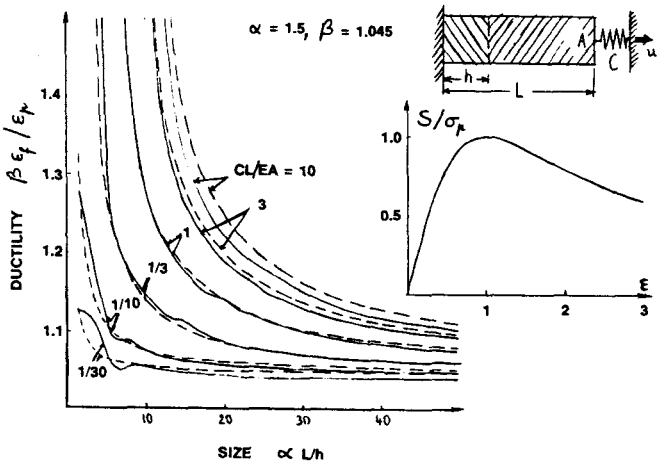

FIG. 44. Ductility by local and nonlocal theory; exact nonlocal solution from $[(1-c)E_t(1+\lambda^2\delta_{xx})^2+cE]u_{,xx}=0$: (—) nonlocal theory, $\alpha=\beta=1$; (- - -) local theory with $h=l/a$ (Bažant and Zubelewicz, 1986, in preparation).

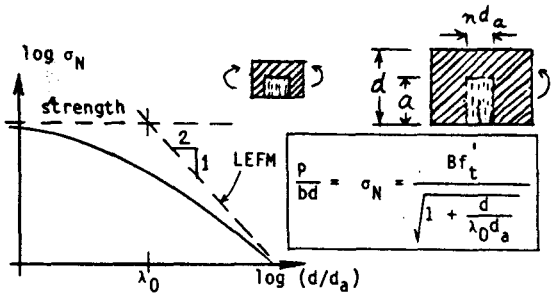

FIG. 45. Structural size effect. Hypothesis: Energy release depends on (1) crack length a and (2) cracking area $nd_a a$, where nd_a = const (84.5).

cracking zone would localize into a line. The fact that it does not can be captured only by properties other than the stress–strain relation, properties that serve to restrict the localization. It is time to realize that the thrust of micromechanics studies should be redirected towards the localization restricting characteristics of damage models.

5. SIZE EFFECT

As Willard Gibbs once remarked, the principal objective of science is to find the viewpoint from which a given problem appears the simplest. What is such a viewpoint for distributed cracking? In my opinion, it is the size effect. It must be taken into account in extrapolating from reduced-size laboratory tests to full-size real structures. We may distinguish size effects of different kinds and sources.

One kind of size effect is manifested in ductility, ie, the ratio of the deformation at the failure load to the deformation at the maximum load. The simplest example is a uniaxially stressed bar loaded in a displacement controlled manner through a spring (Fig. 44). The strain along the bar remains uniform until a certain critical point at which two different equilibrium increments become possible (76.2, 82.3, 85.4). For one of them the strain remains uniform, and for the other the strain becomes nonuniform at uniform stress—it increases (and is uniform) over a segment h of specimen length L and decreases (while remaining uniform) over the remaining segment of length $L-h$, ie, segment h undergoes loading and segment $L-h$ unloading. The latter nonuniform deformation increment can occur at fixed load-point displacement, and represents an instability of failure. If $h\to 0$, the failure occurs at the peak stress point, ie, no strain-softening can be realized. The fact that strain-softening can be observed in tests means that the strain-localization length h must be finite. As proposed in 1974 (76.2), this length represents the band width in the crack band theory ($h=w_c$), which is assumed to be a material constant.

Assuming a certain realistic stress–strain diagram for the material (Fig. 44), we obtain the diagrams in Fig. 44 showing the ductility, ie, the ratio of the failure strain to the strain at peak stress, as a function of the relative size L/h. The diagrams are plotted for various ratios of the spring constant to the equivalent spring constant for unloading of the bar. The dashed curves represent the simplified original solution (76.2) based on the crack band theory and the usual local continuum, and the solid curves represent the exact solution obtained by Bažant and Zubelewicz (1985) according to the imbricate nonlocal formulation in which the averaging operator is approximated as a differential operator with the Laplacian, as mentioned before (Fig. 26). An exact solution is possible in terms of trigonometric and hyperbolic functions. We see that, for a certain ratio α of the characteristic length of the imbricate continuum to the crack band width imposed for a local continuum discretization, the ductility diagrams are nearly identical.

Another kind of size effect, usually the most important one, is the effect of the structure size on the nominal stress at failure, σ_N, when geometrically similar structures are compared. In a two-dimensional problem, σ_N, defined as the maximum load P divided by structure thickness b and the characteristic structure dimension d, is independent of the structure size if the solutions based on plastic limit design or elastic allowable stress design (as well as hardening plasticity, viscoplasticity, or viscoelasticity) are considered. For fracture mechanics, however, there is a cardinal difference: σ_N decreases as the structure size increases.

The structural size effect was observed in fracture testing by Walsh (72.9) and others (84.30, 84.31, 85.6, 85.10). It was found that the size effect of linear elastic fracture mechanics is too severe. This size effect is of the type $\sigma_N\approx d^{-1/2}$ (82.9, 84.26, 81.4, 81.3, 81.16, 73.14, 74.3, 73.7) or $\log\sigma_N=-\frac{1}{2})\log d+$ const, which means that the plot of $\log\sigma_N$ versus $\log d$ for geometrically similar structures of different sizes is a straight line of downward inclination $-\frac{1}{2}$ (Fig. 45). The test results, however, point to a milder size effect, somewhat like that shown by the solid curve.

An approximate formula for the size effect law, shown in Fig. 45, was obtained by means of simplified solutions of certain simple problems by crack band theory. The same size effect law was also shown to ensue from the approximate, but apparently quite realistic, hypothesis (Fig. 45) that the energy release rate at failure depends on: (1) the length a of the fracture or the crack band, and (2) the area of the cracking zone $nd_a a$, where nd_a is the cracking front width which is assumed to be a constant multiple of the aggregate size d_a (84.5).

If only the second part of the hypothesis were made, one would obtain the size effect law of limit analysis or elastic allowable stress design, according to which σ_N is independent of the structure size, as shown by the horizontal dashed line in Fig. 45. This is the classical strength (or yield) criterion of failure. If only the first part of the hypothesis were made, one would obtain the size effect of linear elastic fracture mechanics, given by the straight line of slope $-\frac{1}{2}$, as already mentioned.

It has been shown by dimensional analysis and similitude arguments (84.5, 85.13) that the complete hypothesis leads, with

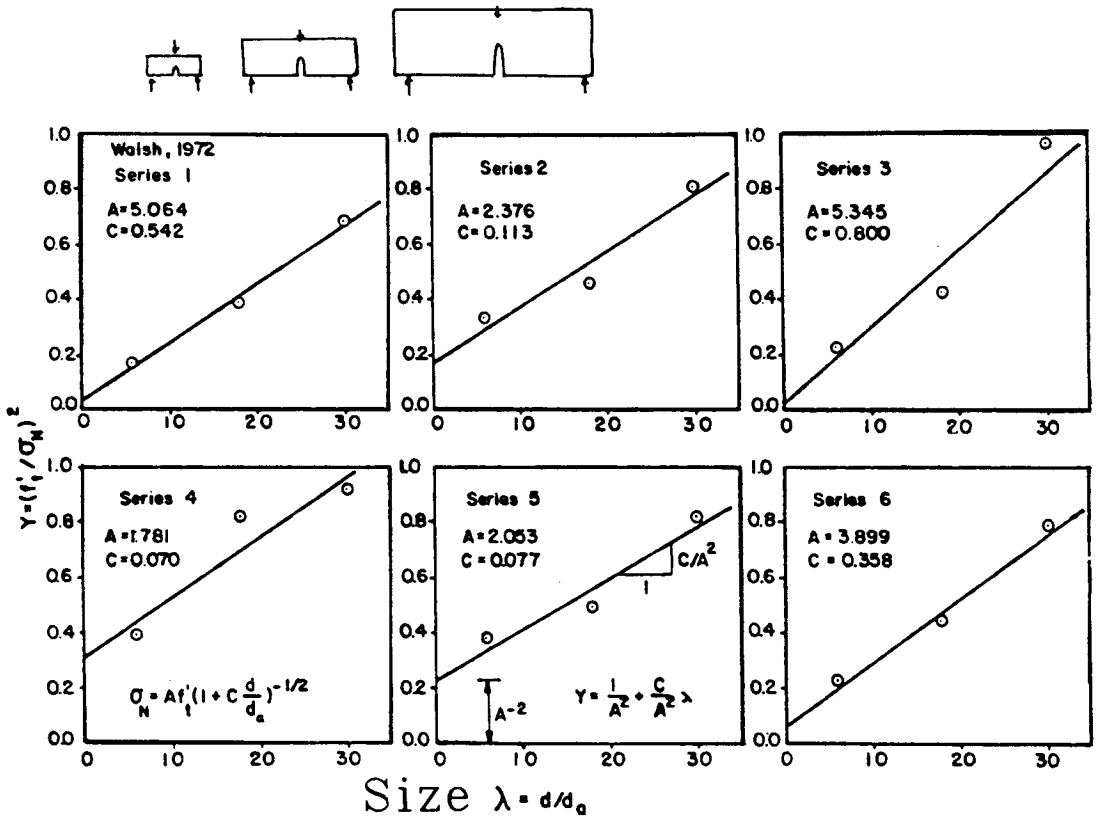

FIG. 46. Regression of Walsh's fracture data by size effect law (72.9).

a certain reasonable approximation, to the size effect law given and plotted in Fig. 45; B and λ_0 are two empirical constants characterizing the shape of the structure. Zaitsev and Kovler (85.54) confirmed this formula (Fig. 45) by analyzing notch sensitivity with a force approach. Intuitively, the key point is that in a small structure the area of the crack band occupies a large portion of the whole structure, and in a large structure it occupies a relatively small portion. For a relatively small structure, for which $d/\lambda_0 d_a$ is negligible compared to 1, the size effect reduces to $\sigma_N = Bf_t'$, which is the strength criterion of plastic limit analysis or elastic allowable stress design. For a very large structure, for which 1 may be neglected as it is much smaller than $d/\lambda_0 d_a$, we obtain $\sigma_N \approx d^{-1/2}$. Thus, we see that the size effect law represents a gradual transition from the strength or yield criterion to the linear elastic fracture mechanics criterion (84.5, 85.13).

Most available laboratory tests of structures are conducted on reduced size models, which are made, according to the conventional wisdom, as small as possible for a given aggregate size. The results then lie on the left, ie, near the strength-criterion end of the size effect curve (Fig. 45). Extrapolation of such test results into real structure sizes is at present done according to the strength criterion. This is obviously questionable. In fact, the existing codes for the design of concrete structures (77.3, 78.3) do not take fracture mechanics into account and their formulas exhibit no size effect, ie, always correspond to a horizontal line in the size effect plot. Nevertheless, the size effect should be observed for all failures that are of a brittle type, for which there exists no yield plateau after the maximum load is reached but the load declines at increasing displacement. Such brittle failures must exhibit size effect. In the case of concrete, they include the diagonal shear failure and the torsional failure of beams, the punching shear failure of slabs, the torsional-punching shear failure, the bending failure of plain concrete, the failure of pavement under wheel load, the beam and ring failures of unreinforced pipes, etc.

The size effect law agrees reasonably well with the results of laboratory fracture tests; see, eg, Fig. 46 in which the classical test results of Walsh (72.9) for three-point loaded beams at three different beam sizes are plotted in a straight-line regression plot with the coordinate d/d_a and ordinate $(f_t'/\sigma_N)^2$. In this plot, the size effect law appears as a straight line. Many subsequent results for different types of fracture tests provided similar results (85.6, 85.10). For brittle failures of real structures the data are much more limited; however, some information exists in the literature on the diagonal shear failure of beams (61.3, 62.2, 66.3, 68.1, 71.13, 72.8, 68.1, 75.5, 78.14, 81.19, 81.20); see the data points in Fig. 47, where the size effect plot is on the right and its linear regression on the left (84.9, 86.2). The scatter of the data is large, due to the fact that test results from different laboratories on different concretes and different types of beams are combined in one diagram. Nevertheless, the downward trend with increasing beam depth is clearly apparent and contrasts with the present codes (77.3, 78.3) which imply no size effect (a horizontal line). It is also clearly apparent that the size effect is considerably milder than that for linear elastic fracture mechanics (the straight line of downward slope $-\frac{1}{2}$). Similar results, which are highly scattered but clearly confirm the downward trend, have been obtained at Northwestern University for other types of failure (85.6, 86.1).

The nonlinear fracture parameters have usually been determined on the basis of the so-called R-curves (resistance curves) which plot the energy required for crack growth as a function of the crack length c from the notch tip (60.3, 61.2, 73.14, 74.3, 82.32, 84.7, 84.26, 84.49). These curves are normally determined by measuring crack opening displacements and unloading compliance associated with various crack lengths in the same specimen. Such measurements are rather difficult,

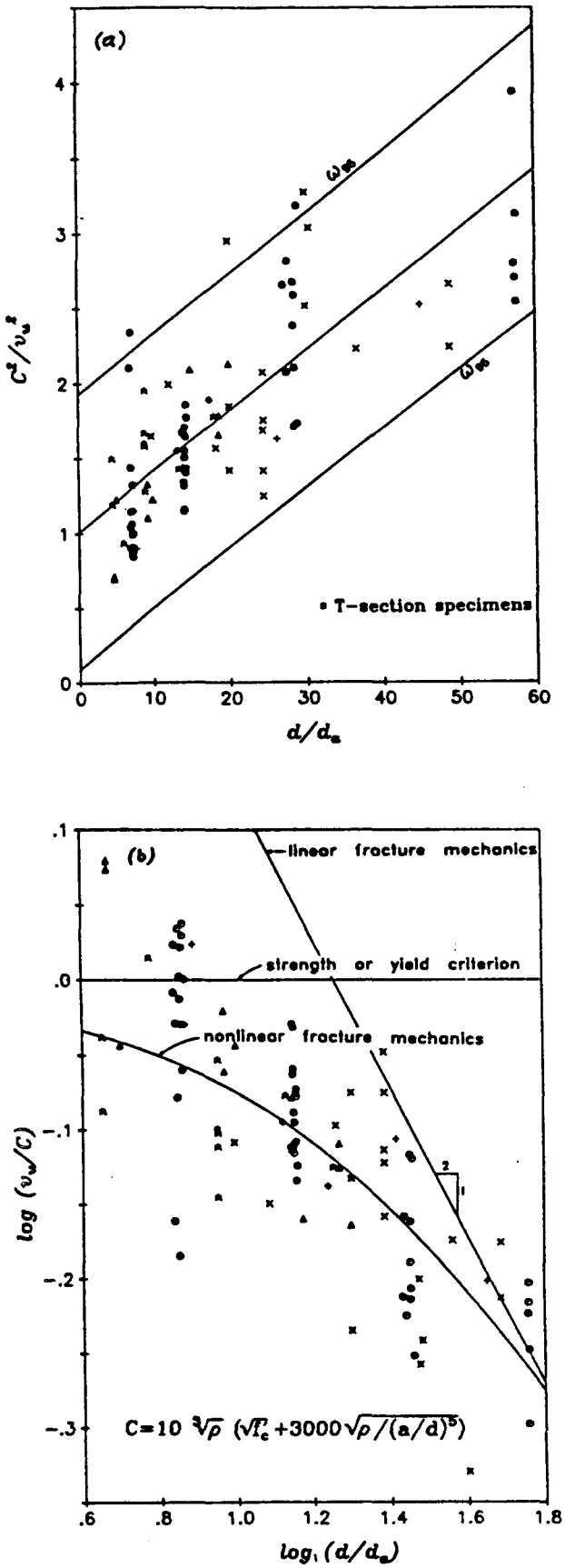

FIG. 47. Fit of existing diagonal shear test data by size effect law (84.9), different beam sizes: (●) Kani (1967); (▲) Leonhardt (1962); (+) Walraven (78.14); (×) Taylor (72.8); (◆) Rüsch (62.2); (×) Bhal (68.1); (*) Swamy (71.13).

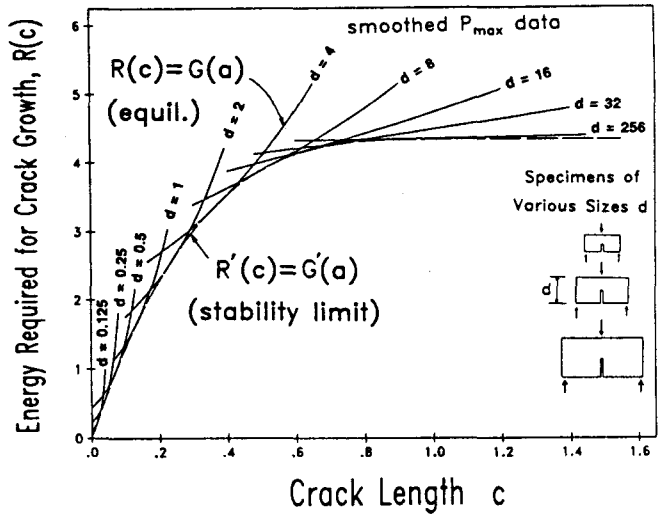

FIG. 48. R-curve as an envelope (86.4): $Bf_t' = 302$, $d_a = 4.436$, $E_a = 4.08 \times 10^5$, $b = 1$, $a_0/d = \frac{1}{3}$, $l/d = 4$; (---) $k'c = G_r[1-(1-c/c_m)^n]$, $G_r = 4.34$, $n = 3.6$, $c_m = 1.07$.

chiefly because of the ambiguity in the location of the crack tip. A considerably simpler measurement of nonlinear fracture parameters is made possible by the size effect law (84.10); it necessitates only the maximum load values for geometrically similar specimens of different sizes, which are easy to measure even with the most rudimentary equipment. The slope of the regression line as exemplified in Fig. 46 yields the fracture energy, and the Y-intercept of this line provides the remaining nonlinear fracture parameters. For each specimen size, it is possible to plot from these data one of the fracture equilibrium curves in Fig. 48. The R-curve then results as the envelope of these curves (84.10). A simple formula to obtain the approximate envelope from the parameters of the linear regression plot also exists. Furthermore, if the R-curve is given, it is possible to construct from it the size effect plot. So there is a one–two–one correspondence between these different characteristics of nonlinear fracture (84.10).

The size effect law in Fig. 45 is a simple approximation which is probably sufficient for most practical applications but is not likely to be valid for a very broad range of sizes. The most general size effect law can be expressed similarly to the formula in Fig. 45 if the expression in the denominator is replaced by a certain infinite series;

$$\sigma_N = Bf_t'\left(a_0\xi^{-1} + 1 + a_1\xi + a_2\xi^2 + a_3\xi^3 + \cdots\right)^{1/2r},$$

where $\xi = (d_a/d)^r$ and $B, f_t', r, a_0, a_1, \cdots$ are constants (85.13). This yields a general asymptotic approximation which still has the same limits: the strength criterion and the linear elastic fracture mechanics. A special case, $\sigma_N = Bf_t'[1 + (d/\lambda_0 d_a)^r]^{-1/2r}$, is probably sufficient for most applications (85.2).

Another generalization of the size effect law in Fig. 45 is needed when concretes of greatly different aggregate sizes d_a are considered. In that case the size effect law must be generalized as shown in Fig. 49, in which c_0 is an additional, third empirical material parameter (discussion closure of Ref. 84.9). This generalization is obvious if we realize that propagation of the cracking front cannot be continuous in the microscopic sense. The cracks must first form in the thin contact layers between the aggregate pieces, and only later they can join

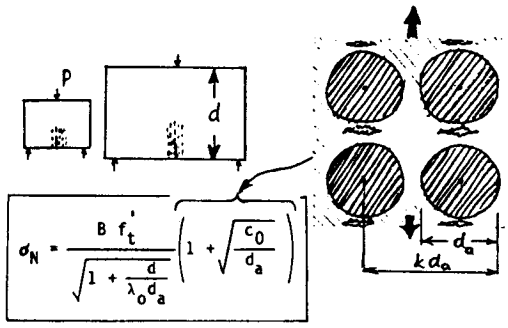

FIG. 49. Structural size effect law at variable aggregate size (see discussions of Ref. 84.9).

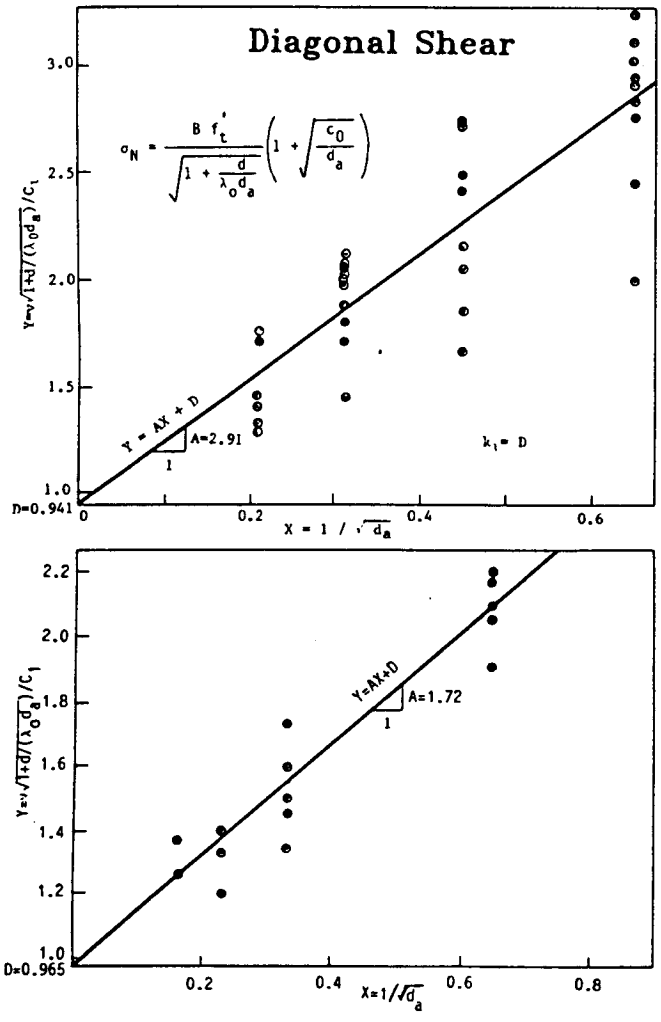

FIG. 50. Effect of aggregate size d_a. Top: Chana, 1981 (85.13); $r = 0.843$, $w = 0.126$, $\bar{Y} = 2.15$, $\lambda_0 = 8.34$; $k_1 = D = 0.941$, $c_0 = 9$ mm. Bottom: Taylor (72.8); $r = 0.947$, $w = 0.065$, $\bar{Y} = 1.64$, $\lambda_0 = 45.1$, $k_1 = 0.965$, $c_0 = 4$ mm (fits by S Sener and Z P Bažant).

through the soft matrix of mortar. The formula in Fig. 49 results theoretically from the condition that a discontinuous microcrack must be produced in the next contact layer ahead of the microcracking front. Although fracture mechanics is used in this argument, the derivation is mathematically similar to that of the well-known Petch formula for the yield stress of polycrystalline metals, which was derived from dislocation theory.

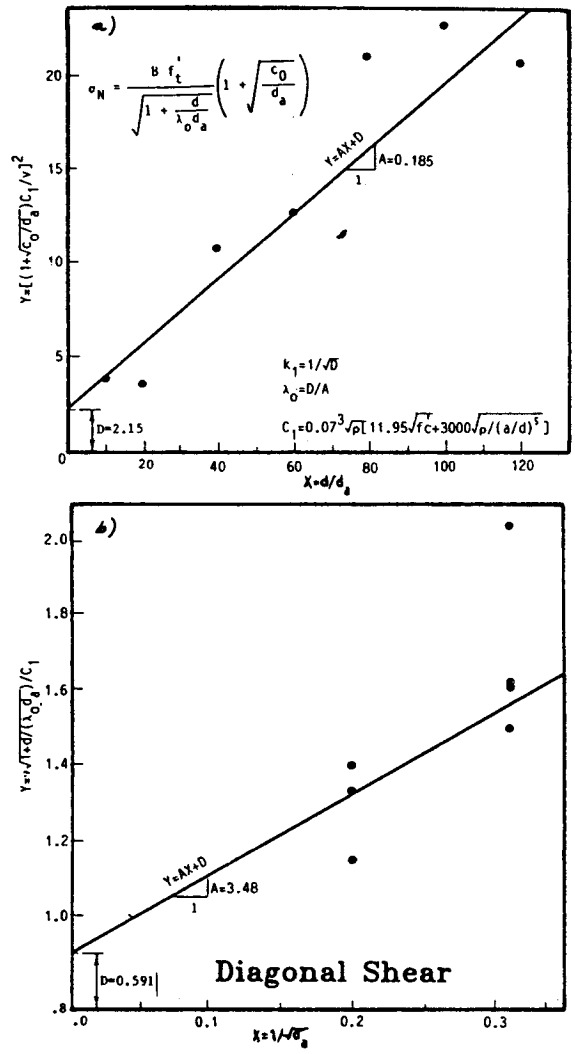

FIG. 51. Top: Effect of beam size (Iguro et al, 1984). $r = 0.942$, $w = 0.170$, $\bar{Y} = 13.5$, $\lambda_0 = D/A = 11.6$, $k_1 = 1/\sqrt{D} = 0.683$, $c_0 = 15$ mm, $c_1 = 0.07\sqrt[3]{\rho}[11.95\sqrt{f'c} + 3000\sqrt{\rho}/(a/d)^5]$. Bottom: Effect of aggregate size d_a. $r = 0.759$, $w = 0.103$, $\bar{Y} = 1.52$, $\lambda_0 = 11.6$, $k_1 = 0.591$, $c_0 = 15$ mm (fits by S Sener and Z P Bažant).

The effect of the aggretate size is shown in the linear regression plots in Fig. 50 and the bottom of Fig. 51, in which the data of Chana, Taylor, and Iguro, Shioya et al, are used (85.13). Figure 51 shows the size effect regression plot of these data.

The effect of aggregate size, presents an interesting question: given the structure size, should the maximum aggregate size be large or small? The answer depends on where the structure is located on the size effect curve (Fig. 52). While in the plot of σ_N vs the relative structure size d/d_a, a smaller aggregate always yields a larger strength at equal d/d_a, in the plots of σ_N vs the structure size d, a smaller aggregate may yield either a larger or a smaller strength. If the structure is smaller than a certain critical size, it is better to use a small aggregate, and, if the structure is larger than this critical size, it is better to use a larger aggregate. This observation justifies, eg, the practice of using very large aggregate pieces in concrete dams.

Apart from the foregoing, deterministic sources of size effect, another source is statistical. In the past, the size effects observed in concrete structures have usually been explained by Weibull's statistical theory (39.1, 59.3, 68.4, 74.1, 77.13, 78.1, 83.41, 84.36).

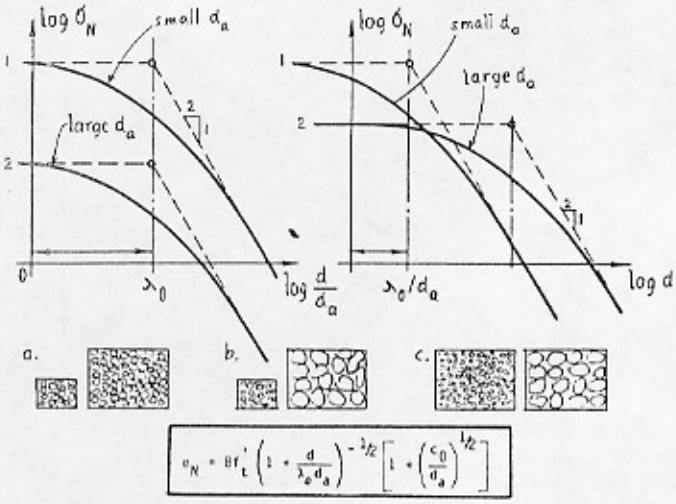

FIG. 52. Size effect law, variable aggregate size d_a (see discussions of Ref. 84.9).

Recognizing that material strength is a random variable, and introducing for it a certain suitable extreme value distribution, Weibull showed that the strength of a chain of elements decreases as the number of elements increases. It seems, however, that indiscriminate applications of this theory to all kinds of concrete structures have been misguided. For example, in the case of diagonal shear failure (Fig. 53), the range of locations at which the cracking front propagation can take place is very limited and is far smaller than the overall structure size. Furthermore, the condition of a series coupling of elements, implied in Weibull's theory, is obviously not met, even as an approximation. Thus, the statistical effect due to spatial random variation of strength should be relatively small. The major size effect is due to energy flow. It consists in the fact that in a larger structure there is much more energy available for being supplied to the cracking front. When test data of a limited size range are available, the size effect might seem to be in a reasonable agreement with the statistical theory; however, extrapolation to very large sizes is different. The reduction of structure strength is more severe for the fracture mechanics type of size effect. To be sure, a statistical aspect is always present in the failure of heterogeneous materials such as concrete or rock, but does not seem to be dominant for failures in which, by contrast to the failure of a chain, the failure occurs by propagation of a localized cracking band.

The size effect is not limited to tensile fracture. This effect, as well as the spurious mesh size sensitivity, is to be expected

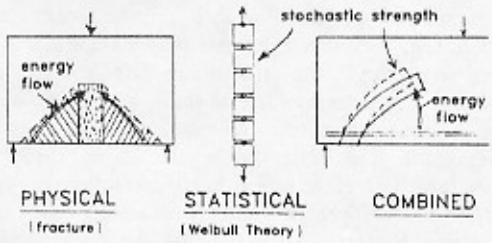

FIG. 53. Types of size effect. (Note that for limit analysis or plasticity, elastic σ_{all} design, and elastic buckling: no size effect; P/bd = const.)

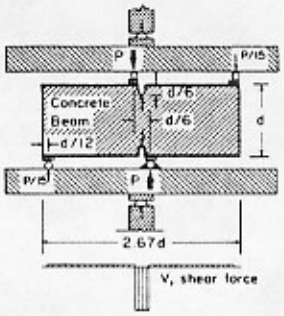

FIG. 54. Shear-loaded specimens (85.10).

for all structures whose failure is due to strain-softening. This includes concrete failures due to compression or shear.

Tests of the shear-loaded specimens shown in Figs. 54 and 55, carried out at Northwestern University under displacement control in an MTS testing machine (Fig. 56), yielded the results shown in Fig. 57 (85.10). A strong size effect is evident. Furthermore, these tests verified that shear fracture is possible, despite previous claims that "shear fracture is sheer nonsense," heard in some recent debates. If the cracks in Fig. 54 extended from the notch in a direction normal to the maximum principal tensile stress, they would not run vertically but deviate to the sides. Such cracks were observed by Arrea and Ingraffea (82.2) for a different loading in which the zone of high shear stress in the beam was relatively wide. In the present test, the zone of high shear stress is rather narrow. The fact that the cracks run vertically appears to be consistent with the criterion of the maximum energy release rate, the fundamental criterion for the fracture direction.

It must be also admitted that the specimen in Fig. 54 is not an ideal one for shear (Mode II) fracture, because, according to linear elastic fracture mechanics, the stress intensity factors K_I and K_{II} are both nonzero (85.35). However, K_I is small and has a negative value since the stresses are compressive, and so it should have a negligible effect. Pure Mode II situation could be generated by a slightly different loading system, which would, however, require additional tensile loads and would be much more difficult to realize (Bažant's discussion of Ref. 85.35).

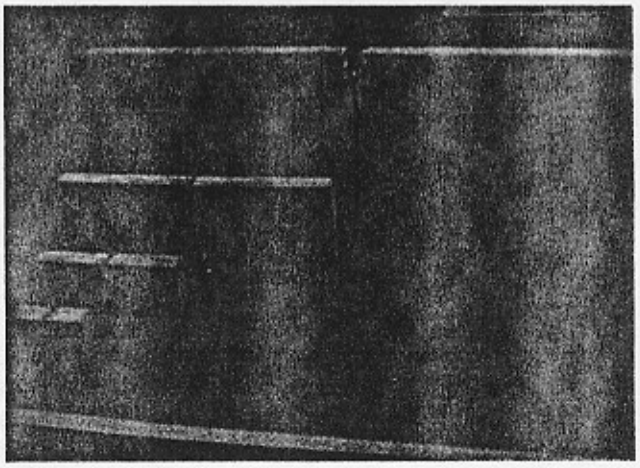

FIG. 55. Specimens of sizes 1:2:4:8 after shear fracture (85.10, and *Matériaux et constructions*, RILEM, 1986, to appear).

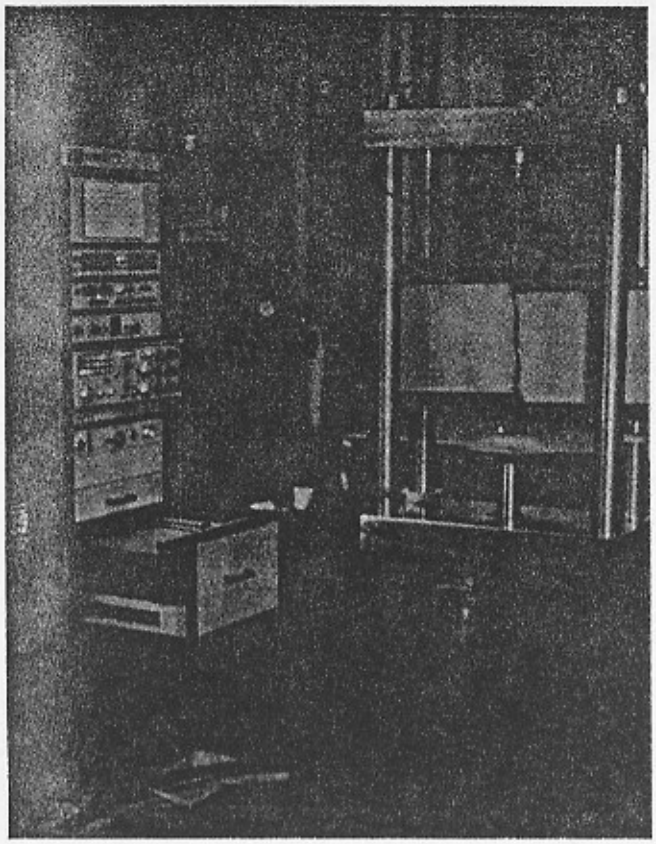

FIG. 56. Size effect fracture tests in MTS testing machine (at Northwestern Univ).

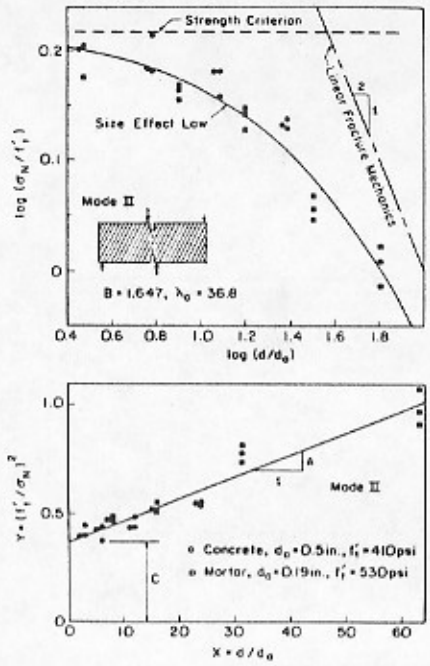

FIG. 57. Results of shear-loaded specimen tests (Figs. 54 and 55) carried out at Northwestern Univ under displacement control in an MTS testing machine (Fig. 56) [after Bažant and Pfeiffer (85.10)]. Top: (●) concrete; (■) mortar. Bottom: (○) concrete, $d_a = 0.5$ in., $f_t' = 410$ psi; (□) morta $d_a = 0.19$ in., $f_t' = 530$ psi; $Y = AX + C$, $A = 0.01002$, $C = 0.3688$, $r = 0.9522$, $\omega_{Y|X} = 0.0911$.

The regression plot for the shear fracture tests of geometrically similar specimens (Fig. 57, bottom) yields for the shear fracture energy a value which is much higher than that for Mode I (tensile) fracture—approximately 25 times higher. We can explain it (Fig. 58) by realizing that the shear stress is equivalent to tensions and compressions in diagonally inclined directions. The inclined tensile stresses produce a row of inclined microcracks; however, for the shear fracture to be complete, it is also necessary that the inclined compression stresses parallel to these microcracks would crush the material between the cracks, and the work of this crushing must be counted in calculating the fracture energy. Such an analysis yields shear fracture energy values which reasonably agree with those determined on the basis of the size effect regression plot.

The picture of the crack band with inclined microcracks in Fig. 59 further suggests a means of simulating shear friction and dilatancy on rough cracks in concrete and rock. If a shear stress is applied on a previously formed tensile crack, compression stresses are generated in the inclined directions across the rough crack modeled as a crack band. These inclined compression stresses have a horizontal component which represents the shear friction, as well as a normal stress component which either opposes dilatancy or leads to crack dilatancy if the normal stress component is not balanced. This type of mechanism of shear on cracks was analyzed using the microplane model (84.8), and it was found capable of closely representing various test data for aggregate interlock due to the shearing of cracks in concrete; see, eg, the comparisons of the results of the microplane model with the test data by Walraven and Reinhardt (81.25).

A particularly attractive aspect of the crack band simulation of shear fracture and aggregate interlock by the microplane model is that it makes it possible to analyze shear on tensile cracks which are only partially formed (84.8). Such discontinuous cracking is more typical of concrete structures than the presently used assumption of continuous cracks subjected to shear.

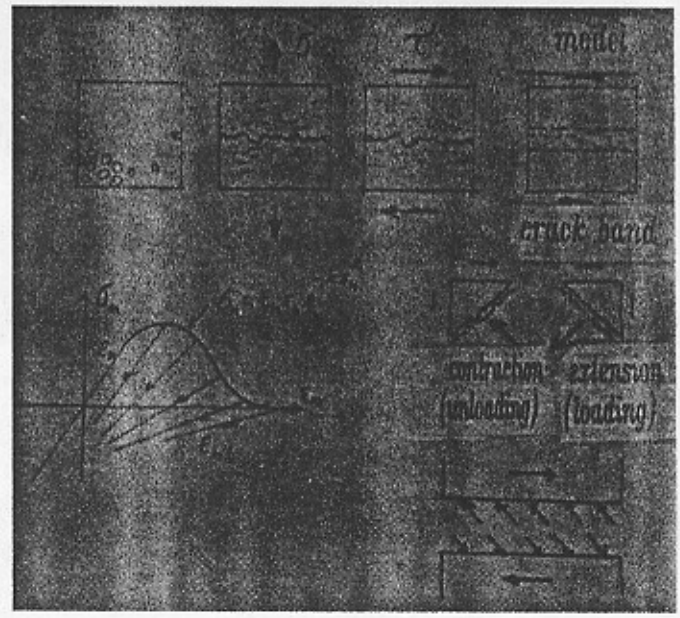

FIG. 58. Shear after total or partial tensile fracture and aggregate interlock tests.

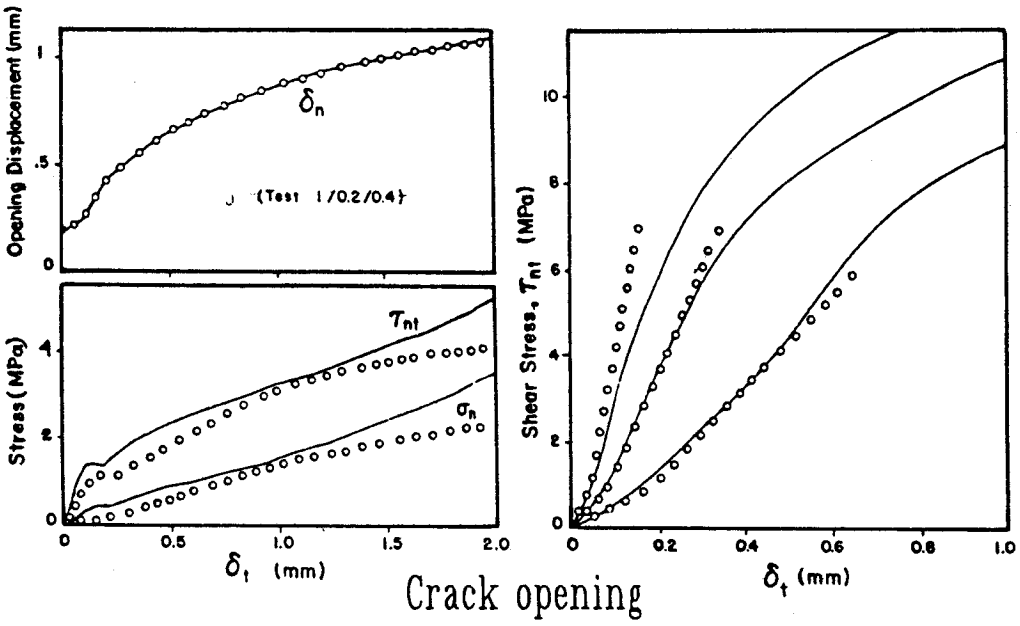

FIG. 59. Fits of existing crack shear test data. Left: (O) Walraven and Reinhardt (Test 1/0.2/0.4) (81.25); (—) theory; $f'_{cc} = 36.7$ MPa, $d_a = 16$ mm. Right: (—) theory, $w_c = d_a$ (2×25 points); (O) Park and Paulay (75.5), $f'_{cc} = 19$ MPa [Bažant and Gambarova (84.8)].

CONCLUSION

To sum up, distributed cracking in brittle heterogeneous materials may be modeled as strain-softening, but strain-localization instabilities must then be carefully analyzed and a complete localization into a line prevented. As a device to prevent such localization, the concept of imbricate nonlocal continuum may be used. The nonlocal concept introduces a new challenge to micromechanics: micromechanics should be used to predict not only the constitutive relation between homogenized stress and strain, but also the properties that prevent localization, such as the characteristic length and the averaging operator.

Finally, what is the salient aspect of the mechanics of distributed cracking? In my opinion it is the size effect. As Einstein once remarked, a good theory should be as simple as possible but no simpler than that. In our case, the theory of distributed cracking must not be as simple as to miss the size effect. This is the principal issue.

ACKNOWLEDGMENTS

Partial financial support under AFOSR Grant No 83-0009 to Northwestern University is gratefully acknowledged. Mary Hill deserves thanks for her invaluable secretarial assistance.

BIBLIOGRAPHY

1903–1960

03.1 Hadamard, J (1903). *Leçons sur la propagation des ondes*, Hermann, Paris, chap VI.

34.1 Taylor, G I (1934). The mechanisms of plastic deformation of crystals, *Proc Roy Soc* **A145**, 362–404.

38.1 Taylor, G I (1938). Plastic strain in metals, *J Inst Metals, London*, **62**, 307–324.

39.1 Weibull, W (1939). *Phenomenon of rupture in solids, Ingenioersvetenskapsakad Handl* (153), 1–55.

49.1 Batdorf, S B, and Budianski, B (1949). A mathematical theory of plasticity based on the concept of slip, NACA Tech Note TN 1871, Apr.

58.1 Chandrasekhar, S (1958). *An introduction to the study of stellar structure*, Dover, New York.

58.2 Hill, R (1958). A general theory of uniqueness and stability in elastic plastic solids, *J Mech Phys Solids* **6**, 236–249.

58.3 Kachanov, L M (1958). Time of rupture process under creep conditions, *Izv Akad Nauk SSR, Otd Tekh Nauk No* 8, 26–31.

59.1 Barrenblatt, G I (1959). The formation of equilibrium cracks during brittle fracture, general ideas and hypothesis, axially symmetric cracks, *Prikl Mat Mekh* **23**(3), 434–444.

59.2 Hori, M (1959). Statistical aspects of fracture in concrete, *Int J Phys Soc Japan* **14**(10), 1444–1452.

59.3 Watstein, D, and Mathey, R G (1959). Width of cracks in concrete at the surface of reinforcing steel evaluated by means of tensile bond specimens, *J Am Concr Inst, Proc* **56**(1), 47–56.

60.1 Dugdale, D S (1960). Yielding of steel sheets containing slits, *J Mech Phys Solids* **8**, 100–108.

60.2 Bristow, J R (1960). Mirocracks and the static and dynamic elastic constants of annealed and heavily cold-worked metals, *Br J Appl Phys* **11**, 81–85.

60.3 Irwin, G R (1960). Fracture testing of high strength sheet materials, Report of a Special Committee, ASTM Bull, p 29 (also Irwin, G R, Fracture testing of high strength sheet materials under conditions appropriate for stress analysis, Rep No 5486, Naval Res Lab).

1961

61.1 Kaplan, M F. Crack propagation and the fracture of concrete, *J Am Concr Inst* **58**(5), 591–610.

61.2 Krafft, J M, Sullivan, A M, and Boyle, R W. Effect of dimensions on fast fracture instability of notched sheets, in *Cranfield Symposium*, vol 1, pp 8–28.

61.3 Leonhardt, F, and Walther, R. *Beiträge zur Behandlung der Schubprobleme im Stahlbetonbau*, Beton-u Stahlbetonbau, vol 56, no 12 (1961), vol 57, no 2, 3, 6, 7, 8 (1962), vol 58, no. 8, 9 (1963).

61.4 Thomas, T Y. *Plastic flow and fracture in solids*, Academic, New York.

1962

62.1 Barenblatt, G I. The mathematical theory of equilibrium cracks in brittle fracture, *Adv Appl Mech* **7**, 55–129.

62.2 Rüsch, M, Haugli, F R, and Mayer, M. *Schubversuche an Stahlbeton Rechteckbalken mit Gleichmässig verteilter Belastung*, Deutscher Ausschuss für Stahlbeton, 145, W Ernst und Sohn, Berlin, W Germany.

1963

63.1 Hsu, T T, Slate, F O, Sturman, G M, and Winter, G. Microcracking of plain concrete and the shape of the stress-strain curve, *J Am Concr Inst* **60**(2), 209.

63.2 Rüsch, H, and Hilsdorf, H. *Deformation characteristics of concrete under axial tension*, Vorunterschungen, Bericht 44, Munich.

63.3 Slate, F O, and Olsefski, S. X-rays for study of internal structure and microcracking of concrete, title no 60-31, *J Am Concr Inst* (May), 575–588.

1964

64.1 Cottrell, A H (1964). *The mechanical properties of matter*, Wiley, New York, pp 40–41.

64.2 Lott, J L, and Kesler, C E. *Crack propagation in plain concrete*, T&A M, Rep No 648, Univ of Illinois at Urbana-Champaign.

64.3 Misner, C W, and Zapolsky, H S, High density behavior and dynamical stability of neutron star models, *Phys Rev Lett*, **12**, 635.

64.4 Saenz, L P. Discussion of "Equation for stress-strain curve of concrete," by P Desayi and S Krishnan, *J Am Concr Inst* **61**, 1229–1235.

64.5 Sinha, B P, Gerstle, K H, and Tulin, L G. Stress-strain relations for concrete under cyclic loading, *J Am Concr Inst* **61**(2), 195–210.

1965

65.1 Budianski, B. On the elastic moduli of some heterogeneous materials, *J Mech Phys Solids* **13**, 223–227.

65.2 Harrison, B K, Thorne, K S, Wakano, M, and Wheeler, J A. *Gravitation theory and gravitational collapse*, Univ Press, Chicago, 1965.

65.3 Rice, J R. An examination of the fracture mechanics energy balance from the point of view of continuum mechanics, in *Proceedings first*

international conference on fracture, Sandia, T Yokohori et al, Eds, Japanese Soc for Strength and Fracture of Mat, Tokyo, Japan, vol 1, pp 309–340.
65.4 Sturman, G M, Shah, S P, and Winter, G. Effects of flexural strain gradients on micro-cracking and stress-strain behaviour of concrete, title no 62-50, *J Am Concr Inst*, 805–822.

1966

66.1 Hughes, B P, and Chapmann, B P. The complete stress-strain curve for concrete in direct tension, RILEM (Paris) Bull No 30, pp 95–97.
66.2 Hughes, B P, and Chapman, G P. The deformation of concrete and microconcrete in compression and tension with particular reference to aggregate size, *Mag Concr Res* **18**(54), 19–24.
66.3 Kani, G N J. Basic facts concerning shear failure, Parts I and II, *J Am Concr Inst* **63**(6), 675–692.
66.4 Mróz, Z. On forms of constitutive laws for elastic plastic solids, *Arch Mech Stos* **18**, 3–35.

1967

67.1 Bažant, Z P. Instability of a continuum and compression strength (in French), RILEM (Paris) Bull No. 35, pp 99–112, 1967; see also *Stavebnicky Casopis SAV (Czech)* **16**(1), 48–64 (1966).
67.2 Bieniawski, Z I. Mechanism of brittle fracture of rock, Parts I, II, III, *Int J Rock Mech, Min Sci* **4**, 395–430.
67.3 Higgins, D D, and Bailey, J E. Fracture measurements on cement paste, *J Mat Sci* **11**, 1995–2003.
67.4 Kröner, E. Elasticity theory of materials with long-range cohesive forces, *Int J Solids Struct* **3**, 731–742.
67.5 Ngo, D, and Scordelis, A C. Finite element analysis of reinforced concrete beams, *J Am Concr Inst* **64**(3), 152–163.

1968

68.1 Bhal, N S. Über den Einfluss der Balkenhöhe auf Schubtragfähihkeit von einfeldrigen Stahlbetonbalken mit und ohne Schubbewehrung, dissertation, Universität Stuttgärt.
68.2 Branson, D E. Design procedures for computing deflection, *J Am Concr Inst* **65**(9), 730–742.
68.3 Evans, R H, and Marathe, M S. Microcracking and stress-strain curves for concrete in tension, *Mat Struct (RILEM, Paris)* **1**, 61–64.
68.4 Freundenthal, A M. Statistical approach to brittle fracture, in *Fracture*, H Liebowitz, Ed, Academic, New York, vol 2, pp 592–619.
68.5 Kröner, E. Interrelations between various branches of continuum mechanics, in *Mechanics of generalized continua*, E Kröner, Ed, Springer-Verlag, W Berlin, W Germany, pp 330–340.
68.6 Krumhansl, J A. Some considerations of the relation between solid state physics and generalized continuum mechanics, in *Mechanics of generalized continua*, E Kröner, Ed, Springer-Verlag, W Berlin, W Germany, pp 298–331.
68.7 Kunin, I A. The theory of elastic media with microstructure and the theory of dislocations, in *Mechanics of generalized continua*, E Kröner, Ed, Springer-Verlag, W Berlin, W Germany, pp 321–328.
68.8 Nilson, A H. Nonlinear analysis of reinforced concrete by finite element method, *J Am Concr Inst* **65**(9), pp 757–766.
68.9 Rashid, Y R. Analysis of prestressed concrete pressure vessels, *Nucl Eng Des* **7**(4), 334–355.
68.10 Rice, J R. Mathematical analysis in the mechanics of fracture, in *Fracture, an advanced treatise*, H Liebowitz, Ed, Academic, New York, vol 2, pp 191–250.
68.11 Shah, S P, and Chandra, S. Critical stress, volume change, and microcracking of concrete, title 65-57, *J Am Concr Inst* **65**, 770–781.
68.12 Shah, S P, and Slate, F O. Internal microcracking, mortar-aggregate bond and the stress-strain curve of concrete, in *Proceedings, international conference on the structure of concrete*, Cement and Concr Assoc, London, pp 82–92.
68.13 Zienkiewicz, O C, Valliappan, and King, I P. Stress analysis of rock as a "no-tension" material, *Geotechnique* **18**, 56–66.

1969

69.1 Bieniawski, Z I, Denkhaus, H G, and Vogler, U W. Failure of fractured rock, *Int J Rock Mech Min Sci* **6**, 323–341.
69.2 Heilmann, H G, Hilsdorf, H K, and Finsterwalder, K. *Festigkeit und Verformung von Beton unter Zugspannungen*, Deutscher Ausschuss für Stahlbeton, Heft 203, W Ernst und Sohn, Berlin, W Germany.
69.3 Karstan, I D, and Jirsa, J O. Behaviour of concrete under compressive loadings, *J Struct Eng ASCE* **95**(12), 2543–2563.
69.4 Kupfer, H, Hilsdorf, H K, and Rüsch, H. Behaviour of concrete under biaxial stresses, *J Am Concr Inst* **66**(8), 656–666.
69.5 Moavenzadeh, F, and Kuguel, R. Fracture of concrete, *J Mat JMLSA* **4**(3), 497–519.
69.6 Naus, D J, and Lott, J L. Fracture toughness of Portland cement concretes, *J Am Concr Inst* **66**(Jun), 481–489.
69.7 Walsh, J B. New analysis of attenuation in partially melted rocks, *J Geophys Res* **74**, 433–437.

1970

70.1 Červenka, V. Inelastic finite element analysis of reinforced concrete panels under in-plane loads, PhD thesis, Univ of Colorado, Boulder CO.
70.2 Hughes, B P, and Ash, J E. Anisotropy and failure criteria for concrete, *Mat Struct (RILEM)* **3**(18), 371–374.
70.3 Launay, P, Gachon, H, and Poitevin, P. Déformation et résistance ultime du béton sous contrainte triaxiale, *Ann Inst Tech Bâtiment Travaux Publics*, no 269, 23–48.
70.4 Mills, L L, and Zimmermann, R M. Compressive strength of plain concrete under multiaxial loading conditions, *J Am Concr Inst* **67** (Oct), 802–807.
70.5 Rosenthal, I, and Glucklich, J. Strength of plain concrete under biaxial stress, *J Am Concr Inst* **67**, 903–914.
70.6 Shah, S P, and Chandra, S. Fracture of concrete subjected to cyclic and sustained loading, *J Am Concr Inst* **67**(Oct), 816–825.
70.7 Wawersik, W R, and Fairhurst, C. A study of brittle rock fracture in laboratory compression experiments, *Int J Rock Mech Min Sci* **7**, 561.

1971

71.1 Buyukozturk, O, Nilson, A H, and Slate, F O. Stress-strain response and fracture of a concrete model in biaxial loading, *J Am Concr Inst* **68**(8), 590–599.
71.2 Cervenka, V, and Gerstle, K H. *Inelastic analysis of reinforced concrete panels*, Int Assoc for Bridge and Struct Eng, Zurich, Switzerland, vol 31, pp 31–45 and vol 32, pp 25–79 (1972).
71.3 Hillemier, B, and Hilsdorf, H M. Fracture mechanics on concrete composites, *Cement Concr Res* **7**, 523–536.
71.4 Hudson, J A, Brown, E T, and Fairhurst, C. Shape of the complete stress-strain curve for rock, in *Proceedings, 13th symposium rock mechanics*, Univ of Illinois, Urbana IL.
71.5 Jofriet, J C, and McNeice, G M. Finite element analysis of reinforced concrete slabs, *J Struc Eng ASCE* **97**(3), 785–806.
71.6 Kesler, C E, Naus, D J, and Lott, J L. *Fracture mechanics—its applicability to concrete*, Int conf on the mech behaviour of mat, Kyoto, Aug 1971.
71.7 Launay, P, and Gachon, H. Strain and ultimate strength of concrete under triaxial stress, in *Proceedings of the first international conference on structural mechanics in reactor technology*, Berlin, paper H 1/3, pp 23–34.
71.8 Levin, V M. The relation between mathematical expectation of stress and strain tensors in elastic microheterogeneous media, *Prikl Mat Mekh* **35**, 694–701 (in Russian).
71.9 Naus, D J. Applicability of linear-elastic fracture mechanics to Portland cement concretes, PhD thesis, Univ of Illinois, Urbana-Champaign IL.
71.10 Scanlon, A. Time dependent deflections of reinforced concrete slabs, PhD thesis, Univ of Alberta, Edmonton, Canada.
71.11 Shah, S P, and McGarry, F J. Griffith fracture criterion and concrete, *J Eng Mech ASCE* **EM6**, 1663–1676.
71.12 Stroud, A H. *Approximate calculation of multiple integrals*, Prentice-Hall, Englewood Cliffs NJ, pp 296–302.
71.13 Swamy, R N, and Qureshi, S A. Strength, cracking and deformation similitude in reinforced T-beams under bending and shear, Parts I and II, *J Am Concr Inst* **68**(3), 187–195.
71.14 Swanson, S R, and Brown, W S. An observation of loading path independence of fracture of rock, *Int J Rock Mech Min Sci* **8**, 277–281.
71.15 Wawersik, W R, and Brace, W F. Post-failure behavior of a granite and diabase, *Rock Mech* **3**, 61.

1972

72.1 Brown, J H. Measuring the fracture toughness of cement paste and mortar, *Mag Concr Res* **24**(81), 185–196.
72.2 Coon, M D, and Evans, R J. Incremental constitutive laws and their associate failure criteria with application to plain concrete, *Int J Solids Struct* **8**(9), 1169–1187.
72.3 Eringen, A C, and Edelen, D G B. On nonlocal elasticity, *Int J Eng Sci* **10**, 233–248.
72.4 Liu, T C Y, Nilson A H, and Slate, F O. Biaxial stress-strain relations for concrete, *J Struct Eng ASCE* **98**(5), 1025–1034.
72.5 Liu, T C Y, Nilson, A H, and Slate, F O. Stress-strain response and fracture of concrete in uniaxial and biaxial compression, *J Am Concr Inst* **69**, 291–295.
72.6 Nayak, G, and Zienkiewicz, O C. Elasto-plastic stress analysis. A generalization of various constitutive relations including strain softening, *Int J Numer Methods Eng* **5**, 113.
72.7 Nelissen, L J M. Biaxial testing of normal concrete, *Heron* **18**(1).
72.8 Taylor, H P J. The shear strength of large beams, *J Struct Eng ASCE* **98**, 2473–2490.
72.9 Walsh, P F. Fracture of plain concrete, *Indian Concr J* **46**(11), 469–476.

1973

73.1 Aveston, J, and Kelly, A. Theory of multiple fracture in fibrous composites, *J Mat Sci* **8**, 352–362.
73.2 Brady, B T, Duvall, W I, and Horino, F G. An experimental determination of the true uniaxial stress-strain behavior of brittle rock, *Rock Mech* **5**, 107.
73.3 Davison, L, and Stevens, L. Thermodynamic constitution of spalling elastic bodies, *J Appl Phys* **44**, 667–674.
73.4 Diaz, S, and Hilsdorf, H K. Fracture mechanisms of concrete under compressive loads, *Cement Concr Res* **3**, 363–388.
73.5 Hallbauer, D K, Wagner, H, and Cook, N G W. Some observations concerning the microscopic and mechanical behavior of quartzite specimens in stiff, triaxial compression tests, *Int J Rock Mech Min Sci* **10**, 713.
73.6 Knauss, W C. On the steady propagation of a crack in a viscoelastic sheet; experiments and analysis, in *The deformation in fracture of high polymers*, H H Kausch, Ed, Plenum, New York, pp 501–541.
73.7 Knott, J F. *Fundamentals of fracture mechanics*, Butterworths, London.
73.8 Kupfer, H B, and Gerstle, K H. Behavior of concrete under biaxial stress, *J Eng Mech ASCE* **99**(4), 853–866.
73.9 Liebowitz, H, and Jones, D L. *On test methods for nonlinear fracture*

mechanics, Proc 10th annual meeting, Soc of Eng Sci, Raleigh NC.
73.10 Lin, C S. Nonlinear analysis of reinforced concrete slabs and shells, PhD thesis, UC-SESM 73-7, Univ of California, Berkeley.
73.11 Misner, C W, Thorne, K S, and Wheeler, J A. *Gravitation*, Freeman, San Francisco.
73.12 Palmer, A C, and Rice, J R. The growth of slip surfaces in the progressive failure of overconsolidated clay, *Proc Roy Soc* **A332**, 527–543.
73.13 Suidan, M, and Schnobrich, W C. Finite element analysis of reinforced concrete, *J Struct Eng ASCE* **99**(10), 2109–2122.
73.14 Tada, H, Paris, P C, and Irwin, G R. *The stress analysis of cracks handbook*, Del Res Corp, Hellertown PA (also 2nd ed, 1986).
1974
74.1 Batdorf, S B, and Crose, J G. A statistical theory for the fracture of brittle structures subjected to polyaxial stress states, *J Appl Mech ASME* **41**, 459–465.
74.2 Bažant, Z P. A new approach to inelasticity and failure of concrete, sand and rock: endochronic theory, in *Proceedings of the Society of Engineering Science 11th Annual Meeting*, G J Dvorak, Ed, Duke Univ, Durham NC, Nov 1974, pp 158–159.
74.3 Broek, D. *Elementary engineering fracture mechanics*, Noordhoff, Leyden, Netherlands.
74.4 Kfouri, A P, and Miller, K J. Stress displacement, line integral and closure energy determinations of crack tip stress intensity factors, *Int J Pressure Vessel Piping* **2**(3), 179–191.
74.5 Knauss, W C. On the steady propagation of a crack in a viscoelastic plastic solid, *J Appl Mech ASME* **41**(1), 234–248.
74.6 Knauss, W C. On the steady propagation of a crack in a viscoelastic sheet; experiments and analysis, in *The deformation in fracture of high polymers*, H H Kausch, Ed, Plenum, New York, pp 501–541.
74.7 Romstad, K M, Taylor, M A, and Herman, L R. Numerical biaxial characterization for concrete, *J Eng Mech ASCE* **100**(5), 935–948.
74.8 Willam, K J, and Warnke, E P. Constitutive model for the triaxial behaviour of concrete, in *Seminar on concrete structures subjected to triaxial stresses*, Int Assoc of Bridge and Struct Eng, Bergamo, Italy, May.
74.9 Wnuk, M P. Quasi-static extension of a tensile crack contained in viscoelastic plastic solid, *J Appl Mech ASME* **41**(1), 234–248.
1975
75.1 Chen, A C T, and Chen, W F. Constitutive relations for concrete, *J Eng Mech ASCE* **101**(4), 465–481.
75.2 Delameter, W R, Herrmann, G, and Barnett, D M. Weakening of elastic solids by a rectangular array of cracks, *J Appl Mech ASME* **42**, 74–80 (erratum **44**, 190).
75.3 Entov, V M, and Yagust, V I. Experimental investigation of laws governing quasi-static development of macrocracks in concrete, *Mech Solids* (transl from Russian) **10**(4), 87–95.
75.4 Lin, C S, and Scordelis, A. Nonlinear analysis of RC shells of general forms, *J Struct Eng ASCE* **101**(3), 523–538.
75.5 Park, R, and Paulay, T. *Reinforced concrete structures*, Wiley, New York.
75.6 Prevost, J H, and Hoeg, K. Soil mechanics and plasticity analysis of strain softening, *Geotechnique* **25**, 279.
75.7 Rudnicki, J W, and Rice, J R. Conditions for the localization of deformation in pressure-sensitive dilatant materials, *J Mech Phys Solids* **23**, 371–394.
75.8 Spooner, D C, and Dougill, J W. A quantitative assessment of damage sustained in concrete during compressive loading, *Mag Concr Res* **27**(92), 151–160.
1976
76.1 Argyris, J H, Faust, G, and Willam, K J. Limit load analysis of thick-walled concrete structures, a finite element approach to fracture, *Comput Methods Appl Mech Eng* **8**, 215–243.
76.2 Bažant, Z P. Instability, ductility and size effect in strain-softening concrete, *J Eng Mech ASCE* **102**, 331–344; discussions, **103**, 357–358, 775–777, **104**, 501–502, based on Struct Eng Rep No 74-8/640, Northwestern Univ, Aug 1974, and private communication to K Gerstle, S Sture, and A Ingraffea in Boulder CO, Jun 1974.
76.3 Bažant, Z P, and Bhat, P D. Endochronic theory of inelasticity and failure of concrete, *J Eng Mech ASCE* **102**(4), 701–722.
76.4 Budianski, B, and O'Connell, R J. Elastic moduli of a cracked solid, *Int J Solids Struct* **12**, 81–97.
76.5 Darwin, D, and Pecknold, D A. Analysis of R/C shear panels under cyclic loading, *J Struct Eng ASCE* **102**(2), 355–369.
76.6 Dougill, J W. On stable progressively fracturing solids, *J Appl Math Phys (ZAMP)* **27**, 423–436.
76.7 Higgins, D D, and Bailey, J E. Fracture measurements on cement paste, *J Mat Sci* **11**, 1995–2003.
76.8 Hillerborg, A, Modéer, M, and Petersson, P E. Analysis of crack formation and crack growth in concrete by means of fracture mechanics and finite elements, *Cement Concr Res* **6**(6), 773–782.
76.9 Kabir, A F. Nonlinear analysis of reinforced concrete panels, slabs and shells for time dependent effects, PhD thesis, UC-SESM 76-6, Univ of California, Berkeley.
76.10 Mindess, S, and Nadeau, J S. Effect of notch width on K_{Ic} for mortar and concrete, *Cement Concr Res* **6**, 529–534.
76.11 Naaman, A E, and Shah, S P. Pull-out mechanism in steel fiber-reinforced concrete, *J Struct Eng ASCE* **102**(8), 1532–1547.
76.12 Phillips, D V, and Zienkiewicz, O C. Finite element nonlinear analysis of concrete structures, *Proc Inst Civ Eng, Part 2* **61**, 59–88.
76.13 Rice, J R. The localization of plastic deformation, in *Theoretical and applied mechanics*, preprints, IUTAM Congress held in Delft, W T Koiter, Ed, North-Holland, Amsterdam, pp 207–220.
76.14 Shah, S P, and Naaman, A E. Mechanical properties of glass and steel fiber reinforced mortar, *J Am Concr Inst* **73**, 50–54.
76.15 Spooner, D C, Pomeroy, C D, and Dougill, J W. Damage and energy dissipation in cement pastes in compression, *Mag Concr Res* **28**(94), 21–29.
1977
77.1 Andenaes, F, Gerstle, K, and Ko, H Y. Response of mortar and concrete to triaxial compression, *J Eng Mech ASCE* **103**(4), 515–526.
77.2 Bažant, Z P, and Ohtsubo, H. Stability conditions for propagation of a system of cracks in a brittle solid, *Mech Res Commun* **4**(5), 353–366.
77.3 Building Code Requirements for Reinforced Concrete (ACI Standard 318-377), Am Concr Inst, Detroit MI.
77.4 Burt, W J, and Dougill, J W. Progressive failure in a model of heterogeneous medium, *J Eng Mech ASCE* **103**(3), 365–376.
77.5 Buyukozturk, O. Nonlinear analysis of reinforced concrete structures, *J Comput Struct* **7**, 149–156.
77.6 Cedolin, L, Crutzen, Y R J, and deiPoli, S. Triaxial stress-strain relationship for concrete, *J Eng Mech ASCE* **103**(3), 423–439.
77.7 Cedolin, L, and deiPoli, S. Finite element studies of shear-critical R/C beams, *J Eng Mech* **103**, 395–410.
77.8 Gjørv, O E, Sørensen, S I, and Arnesen, A. Notch sensitivity and fracture toughness of concrete, *Cement Concr Res* **7**, 333–344.
77.9 Janson, J, and Hult, J. Fracture mechanics and damage mechanics, a combined approach, *J Méc Appl* **1**(1), 69–84.
77.10 Kfouri, A P, and Rice, J R. Elastic-plastic separation energy rate for crack advance in finite growth steps, in *Fracture 1977*, Proc 4th Int Conf on Fracture, Waterloo, Ontario, Jun 1977, D M R Taplin, Ed, Univ of Waterloo, Waterloo ON, Canada, vol 1, pp 43–59.
77.11 Kotsovos, M D, and Newman, J B. Behavior of concrete under multiaxial stress, *J Am Concr Inst* **74**, 443–446.
77.12 Marchertas, A, Bažant, Z P, Belytschko, T, and Fistedis, S H. Extension of HCDA safety analysis of large PCRV containment structures, in *Preprints*, 4th int conf on struct mech in reactor tech, San Francisco, Paper E4/1.
77.13 Mihashi, H, and Izumi, M. A stochastic theory for concrete fracture, *Cement Concr Res* **7**, 411–421.
77.14 Mindess, S, Lawrence, F V, and Kesler, C E. The J-integral as a fracture criterion for fiber reinforced concrete, *Cement Concr Res* **7**, 731–742.
77.15 Ottosen, N S. A failure criterion for concrete, *J Eng Mech ASCE* **103**, 527–535.
77.16 Willis, J R. Bounds and self-consistent estimates for the overall properties of anisotropic composites, *J Mech Phys Solids* **25**, 185–202.
77.17 Zaitsev, Y W, and Wittmann, F H. Crack propagation in a two-phase material such as concrete, in *Fracture 1977*, Proc 4th Int Conf on Fracture, Univ of Waterloo Press, Waterloo ON, Canada, vol 3, pp 1197–1203.
77.18 Zienkiewicz, O C, and Pande, G N. Time-dependent multi-laminate model of rocks—a numerical study of deformation and failure of rock masses, *Int J Numer Anal Methods Geomech* **1**, 219–247.
1978
78.1 Batdorf, S B. and Heinisch, M L. Weakest link reformulation of arbitrary fracture criterion, *J Am Ceramic Soc* **61**, 355–358.
78.2 Bažant, Z P, and Panula, L. Statistical stability effects in concrete failure, *J Eng Mech ASCE* **104**(5), 1195–1212.
78.3 CEB-FIP Model Code for Concrete Structures, CEB Bull No 124/125-E, Comité eurointernational du béton, Paris.
78.4 Cleary, M P. Elastic and dynamic response regimes of fluid impregnated solids with diverse microstructures, *Int J Solids Struct* **14**, 795–819.
78.5 Gerstle, K H et al. Strength of concrete under multiaxial stress states, Douglas McHenry Int Symp on Concr and Concr Struc, Publ Sp55-5, Am Concr Inst, Detroit MI, pp 103–131.
78.6 Hoenig, A. The behavior of a flat elliptical crack in an anisotropic elastic body, *Int J Solids Struct* **14**, 925–934.
78.7 Kotsovos, M D, and Newman, J B. Generalized stress-strain relations for concrete, *J Eng Mech ASCE* **104**(4), 845–856.
78.8 Lemaitre, J, and Chaboche, J-L. Aspect phenomenologique de la rupture par endommagement, *J Méc Appl* **2**, 317–365.
78.9 Lowe, P G. Deformation and fracture of plain concrete, *Mag Concr Res* **30**(105), 200–204.
78.10 Marchertas, A H, Fistedis, S H, Bažant, Z P, and Belytschko, T. Analysis and application of prestressed concrete reactor vessels for LMFBR containment, *Nucl Eng Des* **49**, 155–173.
78.11 Nemat-Nasser, S, Keer, L M, and Parihar, K S. Unstable response of thermally induced interacting cracks in brittle solids, *Int J Solids Struct* **14**, 409–430.
78.12 Sture, S, and Ko, H Y. Strain-softening of brittle geologic materials, *Int J Numer Anal Methods Geomech* **2**, 237–253.
78.13 Swartz, S E, Hu, K K, and Jones, G L. Compliance monitoring of crack growth in concrete, *J Eng Mech ASCE* **104**(4), 412–417.
78.14 Walraven, J C. The influence of depth on the shear strength of

lightweight concrete beams without shear reinforcement, Stevin Lab Rep No 5-78-4, Delft Univ of Technology, Netherlands.

1979

79.1 Bažant, Z P, and Cedolin, L. Blunt crack band propagation in finite element analysis, *J Eng Mech ASCE* **105**(2), 297–315.

79.2 Bažant, Z P, and Kim, S S. Plastic fracturing theory for concrete, *J Eng Mech ASCE* **105**(3), 407–428.

79.3 Bažant, Z P, Ohtsubo, H, and Aoh, K. Stability and post-critical growth of a system of cooling or shrinkage cracks, *Int J Fract* **15**(5), 443–456.

79.4 Bažant, Z P, and Panula, L. *Practical prediction of time-dependent deformations of concrete materials and structures*, RILEM, Paris, vol 11, pp 307–328, 415–434 (1978), vol 12, pp 169–183 (1979).

79.5 Bažant, Z P, and Wahab, A B. Instability and spacing of cooling or shrinkage cracks, *J Eng Mech ASCE* **105**(5), 873–889.

79.6 Buyukozturk, O. A constitutive model for concrete in compression, in *Proc 3rd ASCE Eng Mech Div Specialty Conf*, Austin, Sep 1979.

79.7 Cedolin, L, and Bažant, Z. P. Effect of finite element choice in blunt crack band analysis, report, Northwestern Univ (see also Ref. 80.10).

79.8 Dragon, A, and Mróz, Z. A continuum model for plastic-brittle behavior of rock and concrete, *Int J Eng Sci* **17**, 137.

79.9 Elwi, A A, and Murray, D W. A 3D hypoelastic concrete constitutive relationship, *J Eng Mech ASCE* **105**(4), 623–641.

79.10 Grudemo, A. Microcracks, fracture mechanism, and strength of the cement paste matrix, *Cement Concr Res* **9**, 19–34.

79.11 Hoenig, A. Elastic moduli of a non-randomly cracked body, *Int J Solids Struct* **15**, 137–154.

79.12 Kotsovos, M D. Effect of stress path on the behavior of concrete under triaxial stress states, *J Am Concr Inst* **76**, 213–223.

79.13 Marchertas, A H, Belytschko, T B, and Bažant, Z P. Transient analysis of LMFBR reinforced/prestressed concrete containment, in *Transactions, 5th international conference on structural mechanics in reactor technology*, vol H, Paper H4/1, W Berlin, W Germany, T A Jaeger and B A Boley, Eds, North-Holland, Amsterdam.

79.14 Ottosen, N S. Constitutive model for short time loading of concrete, *J Eng Mech ASCE* **105**(1), 127–141.

79.15 Pariseau, W G. A finite element approach to strain softening and size effects in rock mechanics, in *Proceedings, 3rd international conference on numerical methods in geomechanics*, Aachen, W Germany, Apr.

79.16 Sok, C, Baron, J, and François, D. Mécanique de la rupture appliquée au béton hydraulique, *Cement Concr Res* **9**, 641–648.

79.17 Stroeven, P. Geometric probability approach to the examination of micro-cracking in plain concrete, *J Mat Sci* **14**, 1141–1151.

79.18 Van Greunen, T. Nonlinear geometric, material and time dependent analysis of reinforced and prestressed concrete slabs and panels, UC-SEM Rep No 79-3, Univ of California, Berkeley.

1980

80.1 Bažant, Z P, Instability of parallel thermal cracks and its consequences for geothermal energy, Proc int conf on thermal stresses in severe environments VPI, Blacksburg, Mar 1980, pp 169–181.

80.2 Bažant, Z P, and Cedolin, L. Fracture mechanics of reinforced concrete, *J Eng Mech ASCE* **106**(6), 1287–1306; discussion, **108**, 464–471 (1982).

80.3 Bažant, Z P, and Gambarova, P. Rough cracks in reinforced concrete, *J Struct Div ASCE* **106**, 819–842; discussion, 2579–2581.

80.4 Bažant, Z P, and Shieh, C-L. Hysteretic fracturing endochronic theory for concrete, *J Eng Mech ASCE* **106**(5), 929–950.

80.5 Bažant, Z P, and Tsubaki, T. Slip-dilatancy model for cracked reinforced concrete, *J Struct Eng ASCE* **106**(9), 1947–1966.

80.6 Bažant, Z P, and Tsubaki, T. Total strain theory and path dependence of concrete, *J Eng Mech ASCE* **106**(6), 1151–1173.

80.7 Bažant, Z P, Tsubaki, T, and Belytschko, T B. Concrete reinforcing net: safe design, *J Struct Eng ASCE* **106**(9), 1899–1906.

80.8 Bažant, Z P, and Wahab, A B. Stability of parallel cracks in solids reinforced by bars, *Int J Solids Struct* **16**, 97–105.

80.9 Carpinteri, A. Static and energetic fracture parameters for rocks and concretes, report, Istituto di Scienza delle Costruzioni-Ingegneria, Univ of Bologna, Italy.

80.10 Cedolin, L. and Bažant, Z P. Effect of finite element choice in blunt crack band analysis, *Comput Methods Appl Mech Eng* **24**(3), 305–316.

80.11 Cotterell, B, and Rice, J R. Slightly curved or kinked cracks, *Int J Fract* **16**, 155–169.

80.12 Crisfield, M A. Incremental/iterative solution procedures for nonlinear structural analysis, in *Numerical methods for non-linear problems*, C Taylor, E Hinton, and D R J Owen, Eds, Pineridge, Swansea, UK, vol 1, pp 261–290.

80.13 Dougill, J W, and Rida, M A M. Further consideration of progressively fracturing solids, *J Eng Mech ASCE* **106**(5), 1021–1038.

80.14 Gerstle, K H et al. Behavior of concrete under multiaxial stress states, *J Eng Mech ASCE* **106**(6), 1383–1403.

80.15 Gottesman, T, Hashin, Z, and Brull, M A. Effective elastic moduli of cracked fiber composites, in *Advances in composite materials*, Proc ICCM3, A R Bunsell et al, Eds, Pergamon, Oxford, pp 749–758.

80.16 Hillerborg, A. Analysis of fracture by means of the fictitious crack model, particularly for fibre reinforced concrete, *Int J Cement Compos* **2**(4), 177–184.

80.17 Kachanov, M. Continuum model of medium with cracks, *J Eng Mech Div ASCE* **106**, 1039–1051.

80.18 Keenan, J H, et al. Principles of thermodynamics, in *Encyclopedia Britannica*, 15th ed, vol 18, p 301 (Fig. 6).

80.19 Løland, K E. Continuous damage model for load-response estimation of concrete, *Cement Concr Res* **10**, 395–402.

80.20 Maher, A, and Darwin, D. Mortar constituent of concrete under cyclic compression, SM Rep No 5, Univ of Kansas, Center for Research Inc, Oct.

80.21 Mihashi, H, and Wittmann, F H. Stochastic approach to study the influence of rate of loading on strength of concrete, *Heron* **25**(3).

80.22 Mindess, S, and Diamond, S. A preliminary SEM study of crack propagation in mortar, *Cement Concr Res* **10**, 509–519.

80.23 Petersson, E. Fracture energy of concrete: method of determination, *Cement Concr Res* **10**, 78–79; Fracture energy of concrete, practical performance and experimental results, *Cem Concr Res* **10**, 91–101.

80.24 Piau, M. Crack induced anisotropy and scattering in stressed rocks: effective moduli and attenuation, *Int J Eng Sci* **18**, 549–568.

80.25 Terrien, M. Emission acoustique et comportement mécanique post-critique d'un béton sollicité en traction, *Bull Liaison Ponts Chausées* **105**, 65–72.

80.26 Wastiels, J. *A softening plasticity model for concrete*, Numerical methods for nonlinear problems, Proc int conf held at Univ College of Swansea, Sep 2-5, Pineridge Press, Swansea, UK, C Taylor, E Hinton, and D R J Owen, Eds, pp 481–498.

80.27 Wecharatana, M, and Shah, S P. Double torsion tests for studying slow crack growth of Portland cement mortar, *Cement Concr Res* **10**, 833–844.

80.28 Wecharatana, M, and Shah, S P. Resistance to crack growth in Portland cement composites, report, Dept of Mat Eng, Univ of Illinois, Chicago.

80.29 Ziegeldorf, S, Muller, H S, and Hilsdorf, H K. A model law for the notch sensitivity of brittle materials, *Cement Concr Res* **10**(5).

1981

81.1 Bažant, Z P, and Tsubaki, T. Concrete reinforcing net: optimum slip-free limit design, *J Struct Eng ASCE* **105**(2), 327–346; discussion and closure, 1375–1383.

81.2 Bažant, Z P, and Gambarova, P. Rough cracks in reinforced concrete, *J Struct Eng ASCE* **106**(4), 819–842; discussions, 2579–2581, 1377–1388.

81.3 Carpinteri, A. Experimental determination of fracture toughness parameters K_{IC} and J_{IC} for aggregative materials, in *Advances in fracture research*, Proc 5th int conf on fracture, Cannes, D François, Ed, vol 4, pp 1491–1498.

81.4 Carpinteri, A. Static and energetic fracture parameters for rock and concrete, *Mat Construct (RILEM, Paris)* **14**(81).

81.5 Carrasquillo, R L, Nilson, A H, and Slate, F O. Properties of high strength concrete subject to short term loads, *J Am Concr Inst* **78**, 171–178.

81.6 Carrasquillo, R L, Slate, F O, and Nilson, A H. Micro-cracking and behavior of high strength concrete subject to short term loading, *J Am Concr Inst* **78**, 179–186.

81.7 Cedolin, L, and Bažant, Z P. Fracture mechanics of crack bands in concrete, in *Fracture mechanic methods for ceramics, rocks and concrete*, S W Freiman and E P Fuller, Eds, STP745, Am Soc for Testing and Mat, Philadelphia, pp 221–236.

81.8 Flanagan, D P, and Belytschko, T. A uniform strain hexahedron and quadrilateral with orthogonal hourglass control, *Int J Numer Methods Eng* **17**, 679–706.

81.9 Fonseka, G K, and Krajcinovic, D. The continuous damage theory of brittle materials, part 2: Uniaxial and plane response modes, *J Appl Mech, Trans ASME* **48**, 816–824.

81.10 Gerstle, K H. Simple formulation of biaxial concrete behaviour, *J Am Concr Inst* **78**(1), 62–68; Simple formulation of triaxial concrete behaviour, **78**(Sep).

81.11 Huang, C M J. Finite element and experimental studies of stress intensity factor for concrete beams, PhD thesis, Kansas State Univ.

81.12 Krajcinovic, D, and Fonseka, G U. The continuous damage theory of brittle materials, part 1: General theory, *ASME J Appl Mech* **48**, 809–815.

81.13 Kupfer, H, and Gerstle, K. Simple formulation of biaxial concrete behaviour, *J Am Concr Inst* **78**(1), 62–68.

81.14 Mazars, J. Mechanical damage and fracture of concrete structures, in *Advances in fracture research*, Proc 5th int conf fracture, Cannes, D François, Ed, vol 4, pp 1499–1506.

81.15 Ottosen, N S. Nonlinear finite element analysis of pullout test, *J Struct Div ASCE* **107**(4), 591–603.

81.16 Parker, A P. *The mechanics of fracture and fatigue*, E&F N Spon, Ltd, Methuen, London.

81.17 Petersson, P E. Crack growth and development of fracture zones in plain concrete and similar materials, doctoral dissertation, Lund Inst of Tech, Lund, Sweden.

81.18 Pietruszczak, St, and Mróz, Z. Finite element analysis of deformation of strain-softening materials, *Int J Numer Methods Eng* **17**, 327–334.

81.19 Reinhardt, H W, Masstabeinfluss bei Schubversuchen im Licht der Bruchmechanik (Size effect in shear tests in the light of fracture mechanics), *Beton und Stahlbetonbau* **7**(1), 19–21.

81.20 Reinhardt, H W. Similitude of brittle fracture of structural concrete,

in *Proceedings, IABSE colloquium on advances in mechanics of reinforced concrete*, Delft, Netherlands, Jun, pp 201–210.
81.21 Rep TVBM-1006, Division of Building Materials, Univ of Lund, Sweden.
81.22 Saouma, V E, and Ingraffea, A R. Fracture mechanics analysis of discrete cracking, in *Proceedings IABSE conference on advances in mechanics of reinforced concrete*, Delft, Netherlands, Jun, pp 393–416.
81.23 Swartz, S E, Hu, K K, Fartash, M, and Huang, C M J. Stress intensity factors for plain concrete in bending—prenotched versus precracked beams, report, Dept of Civil Eng, Kansas State Univ.
81.24 Task Committee on Concrete and Masonry Structures, ASCE. State of the art report on finite element analysis of reinforced concrete, ASCE, New York.
81.25 Walraven, J C, and Reinhardt, H W. Concrete mechanics, Part A: Theory and experiments on the mechanical behaviour of cracks in plain and reinforced concrete subjected to shear loading, *Heron* **26**(1A).
81.26 Wittmann, F H. Mechanics and mechanisms of fracture of concrete, in *Advances in fracture research*, Preprints 5th int conf on fracture, Cannes, Mar, Pergamon, Paris, vol 4, pp 1467–1487.
81.27 Zaitsev, J B, and Wittmann, F H. Simulation of crack propagation and failure of concrete, *RILEM, Mat Construct* **14**(83), 357–365.
1982
82.1 Ahmad, S H, and Shah, S P. Complete triaxial stress-strain curves for concrete, *J Struct Eng ASCE* **108**(4), 728–742.
82.2 Arrea, M, and Ingraffea, A R. Mixed-mode crack propagation in mortar and concrete, Rep 81-13, Dept of Struct Eng, Cornell Univ, Ithaca NY.
82.3 Bažant, Z P. Crack band model for fracture of geomaterials, Proc 4th int conf on numer methods in geomech, Edmonton, AB, Canada, Jun, Z Eisenstein, Ed, vol 3 (invited lectures), pp 1137–1152.
82.4 Bažant, Z P. Mathematical models for creep and shrinkage of concrete, in *Creep and shrinkage in concrete structures*, Z P Bažant and F H Wittmann, Eds, Wiley, London, pp 163–286.
82.5 Bažant, Z P, and Cedolin, L. Fracture mechanics of reinforced concrete, *J Eng Mech ASCE* **106**(6), 1287–1306; discussion and closure, **108**, 464–471.
82.6 Bažant, Z P, and Oh, B H. Efficient numerical integration on the surface of a sphere, Report, Center for Concr and Geomat, Northwestern Univ, Evanston, IL.
82.7 Bažant, Z P, and Oh, B H. Rock fracture via stress-strain relations, Center for Concr and Geomat, Rep No 82-11/665r, Northwestern Univ, Evanston, IL; also, *J Eng Mech ASCE* **110**, 1015–1035 (1984).
82.8 Bažant, Z P, and Raftshol, W J. Effect of cracking in drying and shrinkage specimens, *Cement Concr Res* **12**, 209–226.
82.9 Carpinteri, A. Notch-sensitivity and fracture testing of aggregate materials, *Eng Fract Mech* **16**(14), 467–481.
82.10 Chen, W F, and Saleeb, A T. *Constitutive equations for engineering materials, vol 1, Elasticity and modelling*, Wiley, New York.
82.11 Chudnovsky, A. On the law of fatigue crack layer propagation in polymers, *Polym Eng Sci* **22**(15), 922–927.
82.12 Crisfield, M A. Local instabilities in the non-linear analysis of reinforced concrete beams and slabs, *Proc Inst Civil Eng Part 2* **73**, 135–145.
82.13 Crisfield, M A. Accelerated solution techniques and concrete cracking, *Comput Methods Appl Mech Eng* **33**, 585–607.
82.14 Drescher, A, and Vardoulakis, I. Geometric softening in triaxial tests on granular material, *Geotechnique* **32**(4), 291.
82.15 Kachanov, M L. A microcrack model of rock inelasticity, *Mechanics of materials*, North-Holland, Amsterdam, vol 1, pp 19–41.
82.16 Kotsovos, M D. A fundamental explanation of the behaviour of reinforced concrete beams in flexure based on the properties of concrete under multiaxial stress, *Mat Struct RILEM* **15**(90), 529–537.
82.17 Krajcinovic, D, and Silva, M A G. Statistical aspects of the continuous damage theory, *Int J Solids Struct* **18**, 531–562.
82.18 Maher, A, and Darwin, D. Mortar constituent of concrete in compression, *J Am Concr Inst* **79**, 100–109.
82.19 Marchertas, A H, Kulak, R F, and Pan, Y C. Performance of blunt crack approach within a general purpose code, in *Nonlinear numerical analysis of reinforced concrete*, L E Schwer, Ed, presented at ASME Winter Annual Meeting, Phoenix, ASME, New York, pp 107–123.
82.20 Finite element analysis of reinforced concrete, ASCE State-of-the-Art Rep prepared by a Task Committee chaired by A Nilson, ASCE, New York.
82.21 Ortiz, M, and Popov, E P. Plain concrete as a composite material, *Mech Mat* **1**, 139–150.
82.22 Ottosen, N S. 2-D finite element analysis of massive r.c. structures, *J Struct Eng ASCE* **108**(8), 1874–1893.
82.23 Pande, G N, and Sharma, K G. Multi-laminate model of clays—a numerical evaluation of the influence of rotation of the principal stress axes, Report, Dept of Civil Eng, Univ College of Swansea, UK; also in *Proceedings, symposium on implementation of computer procedures and stress-strain laws in geotechnical engineering*, C S Desai and S K Saxena, Eds, Chicago, Acorn Press, Durham, NC, pp 575–590.
82.24 Pande, G N, and Xiong, W. An improved multi-laminate model of jointed rock masses, in *Proceedings international symposium on numerical models in geomechanics*, R Dungar, G N Pande, and G A Studer, Eds, Zürich, Balkema Publishers, Rotterdam, pp 218–226.
82.25 Phillips, D C, and Wells, G M. The stability of transverse cracks in fibre composites, *J Mat Sci Lett* **1**.
82.26 Reinhardt, H W, and Walraven, J C. Cracks in concrete subject to shear, *J Struct Eng ASCE* **108**(1), 207–224.
82.27 Seaman, L, Curran, D R, and Shockey, D A. Computational models for ductile and brittle fracture, *J Appl Phys* **47**(11), 4814–4826; also L Seaman, in *Proceedings NSF workshop on damage and fracture*, Stone Mountain, Nov, A Atluri, Ed, Georgia Inst of Tech, Atlanta.
82.28 Swartz, S E, Hu, K K, and Huang, C M J. Stress intensity factor for plain concrete in bending—prenotched versus precracked beams, *Exp Mech* (Nov), 412–417.
82.29 Thompson, J M T. *Instabilities and catastrophes in science and engineering*, Wiley, Chichester and New York.
82.30 Vecchio, F, and Collins, M P. The response of reinforced concrete to in-plane shear and normal stresses, Res rep, Dept of Civil Eng, Univ of Toronto, Mar.
82.31 Wecharatana, M, and Shah, S P. Prediction of nonlinear fracture process zone in concrete, *J Eng Mech ASCE* **108**(Jun), 1100–1113.
82.32 Wecharatana, M, and Shah, S P. Slow crack growth in cement composites, *J Struct Eng ASCE* **108**(6), 1400–1413.
82.33 Wittmann, F H. Creep and shrinkage mechanisms, in *Creep and shrinkage in concrete structures*, Z P Bažant and F H Wittmann, Eds, Wiley, chap 6.
1983
83.1 Aifantis, E C, and Serrin, J B. Equilibrium solutions in the micromechanical theory of fluid microstructure, *J Colloid Interface Sci* **96**, 530–547.
83.2 Bažant, Z P. Comment on orthotropic models for concrete and geomaterials, *J Eng Mech ASCE* **109**, 849–865.
83.3 Bažant, Z P. Fracture in concrete and reinforced concrete, in *Mechanics of geomaterials: Rocks, concretes, soils*, Proc IUTAM W Prager Symp, Northwestern Univ, Sep Wiley, Chichester and New York, pp 259–304.
83.4 Bažant, Z P. Imbricate continuum: variational formulation, Rep No 83-11/428i, Center for Concr and Geomat, Northwestern Univ, Evanston IL; also *J Eng Mech ASCE* **110**(10), (1984).
83.5 Bažant, Z P. Size effect in brittle failure of concrete structures, Rep No 83-2/665s, Center for Concr and Geomat, Northwestern Univ, Evanston, IL; also *J Eng Mech ASCE* **110**, 518–535 (1984).
83.6 Bažant, Z P, and Belytschko, T B. Wave propagation in a strain-softening bar: exact solution, Rep No 83-10/401w, Center for Concr and Geomat, Northwestern Univ, Evanston IL; also *J Eng Mech ASCE* **111**(3), (1985).
83.7 Bažant, Z P, and Cedolin, L. Finite element modeling of crack band propagation, *J Struct Eng ASCE* **109**(2), 69–92.
83.8 Bažant, Z P, Chang, T P, and Belytschko, T B. Continuum theory for strain softening, Rep No 83-11/428c, Center for Concr and Geomat, Northwestern Univ, Evanston IL; also *J Eng Mech* **110**(12), 1666–1692 (1984).
83.9 Bažant, Z P, and Oh, B H. Crack band theory for fracture of concrete, *Mat Construct* **16**(93), 155–177.
83.10 Bažant, Z P, and Oh, B H. Microplane model for fracture analysis of concrete structures, in *Proceedings, symposium on the interaction of nonnuclear munitions with structures*, US Air Force Academy, Colorado Springs, CO, C A Ross, Ed, McGregor and Werner, Washington DC.
83.11 Bažant, Z P, and Oh, B H. Model of weak planes for progressive fracture of concrete and rock, Rep No 83-2/448m, Center for Concr and Geomat, Northwestern Univ, Evanston IL.
83.12 Bažant, Z P, and Oh, B H. Spacing of cracks in reinforced concrete, *J Struct Eng ASCE* **109**, 2066–2085.
83.13 Bažant, Z P, Pfeiffer, P, and Marchertas, A H. Blunt crack band propagation in finite element analysis for concrete structures, in *Transactions, 7th international conference on structural mechanics in reactor technology*, Chicago, Aug, Paper H5/2, pp 227–234.
83.14 Cedolin, L, DeiPoli, S, and Iori, L. Experimental determination of the stress-strain curve and fracture zone for concrete in tension, in *Proceedings, international conference on constitutive laws for engineering materials*, C Desai, Ed, Univ of Arizona, Tucson, Jan.
83.15 Cedolin, L, DeiPoli, S, and Iori, I. Experimental determination of the fracture process zone in concrete, *Cement Concr Res* **13**, 557–567.
83.16 Chudnovsky, A, Moet, A, Bankert, R J, and Takemori, M. Effect of damage dissemination on crack propagation in polypropylene, *J Appl Phys* **54**(10), 5562–5567.
83.17 Cleary, M P. Modeling and development of hydraulic fracturing technology, in *Rock fracture mechanics*, H P Rossmanith, Ed, Centre Internationale des Sciences Mécaniques (Udine), Springer-Verlag, Berlin, pp 383–475.
83.18 Collins, M P, Vecchio, F, and Mehlhorn, G. An international competition to predict the response of reinfored concrete panels, in *Festschrift Prof D Bruno Thürlimann zum 60 Geburtstag*, ETH, Zürich, pp 471–491.
83.19 Costin, L S. A microcrack damage model for brittle rock, Sandia Rep SAND 83-1590.
83.20 Costin, L S. A microcrack model for the deformation and failure of brittle rock, *J Geophys Res* **88**, 9485.
83.21 Costin, L S, and Holcomb, D J. A continuum model of inelastically deformed rock based on the mechanics of microcracks, in *Proceedings, international conference on constitutive laws for engineering materials*, C S

Desai and R H Gallagher, Eds, Univ of Ariz, Tucson AZ.
83.22 Crisfield, M A. An arc-length method including line searchers and accelerations, *Int J Numer Methods Eng* **19**, 1269–1289.
83.23 Dougill, J W. Constitutive relations for concrete and rocks: Applications and extensions of elasticity and plasticity theory, in *Preprints, Wm Prager symposium on mechanics of geomat: Rocks, concretes, soils*, Z P Bažant, Ed, Northwestern Univ, Evanston IL, pp 17–54.
83.24 Eringen, A C, and Ari, N. Nonlocal stress field at Griffith crack, *Cryst Latt Def Amorph Mat* **10**, 33–38.
83.25 Fardis, M N, Alibe, B, and Tassoulas, J L. Monotonic and cyclic constitutive law for concrete, *J Eng Mech ASCE* **109**(2), 516–536.
83.26 Gerstle, K et al. Behaviour of concrete under multiaxial stress states, *J Eng Mech ASCE* **106**(6), 1383–1403.
83.27 Gylltoft, K. Fracture mechanics models for fatigue in concrete structures, doctoral thesis, 1983:25D, Div of Struct Eng, Lulea Univ of Tech, Lulea, Sweden.
83.28 Hanant, D J, Hughes, D C, and Kelly, A. Toughening of cement and of other brittle solids with fibers, *Phil Trans Roy Soc London* **A310**, 175–190.
83.29 Hashin, Z. Analysis of composite materials—a survey, *ASME J Appl Mech* **50**(Sep), 481–505.
83.30 Haugeneder, E. A note on finite element analysis of blunt crack band propagation, in *Proceedings, International Conference on Constitutive Equations for Engineering Materials*, C Desai, Ed, Univ of Arizona, Tucson AZ, pp 561–564.
83.31 Hillerborg, A. Examples of practical results achieved by means of the fictitious crack model, in *Preprints, Wm Prager symposium on mechanics of geomat: rocks, concretes, soils*, Z P Bažant, Ed, Northwestern Univ, Sep, pp 611–614.
83.32 Ichikawa, Y et al. Brittle-ductile fracture of a tuffaceous rock and plasticity theory, in *Constitutive laws for engineering materials*, C S Desai and G H Gallagher, Eds, Tucson AZ, Jan, pp 349–355.
83.33 Ingraffea, A R. Fracture propagation in rock, in *Preprints, Wm Prager symposium on mechanics of geomat: Rock, concretes, soils*, Z P Bažant, Ed, Northwestern Univ, Sep, pp 227–280.
83.34 Körmeling, H A, and Reinhardt, H W. Determination of the fracture energy of normal concrete and epoxy modified concrete, Report 5-83-18, Stevin Lab, Delft Univ of Tech, Netherlands.
83.35 Kotsovos, M D. Effect of testing techniques on the post-ultimate behaviour of concrete in compression, *Mat Struct RILEM* **16**(91), 3–12.
83.36 Krajcinovic, D. Constitutive equations for damaging materials, *J Appl Mech* **50**, 355–360.
83.37 Lamon, J, and Evans, A G. Statistical analysis of bending strengths for brittle solids: A multiaxial fracture problem, *J Am Ceramic Soc* **66**, 177–182.
83.38 Laws, N, Dvorak, G J, and Hejazi, M. Stiffness changes in unidirectional composites caused by crack systems, *Mech Mat* **2**, 123–137.
83.39 Lorrain, M, and Løland, K E. Damage theory applied to concrete, in *Fracture mechanics of concrete*, F H Wittmann, Ed, Elsevier, Amsterdam, Chap 4.4, pp 341–369.
83.40 Margolin, L G. Numerical simulation of fracture, in *Proceedings, International Conference on Constitutive Relations for Engineering Mechanics*, C Desai, Ed, Univ of Arizona, Tucson AZ, pp 567–572.
83.41 Mihashi, H. A stochastic theory for fracture of concrete, in *Fracture mechanics of concrete*, F H Wittmann, Ed, Elsevier, Amsterdam, pp 301–339.
83.42 Mindess, S. The application of fracture mechanics to cement and concrete: a historical review, in *State-of-the-Art Report of RILEM Tech Committee 50-FMC on Fracture Mechanics of Concrete*, F H Wittmann, Ed, Elsevier, Amsterdam.
83.43 Owen, D R J, Figueiras, J A, and Damjanić, F. Finite element analysis of reinforced and prestressed concrete structures including thermal loading, *Comput Methods Appl Mech Eng* **41**, 323–366.
83.44 Pan, Y C, Marchertas, A H, and Kennedy, J M. Finite element analysis of blunt crack propagation, a modified *J*-integral approach, in *Transactions, 7th international conference on structural mechanics in reactor technology*, Paper H5/3, North-Holland, Amsterdam, pp 235–292.
83.45 Wecharatana, M, and Shah, S P. A model for predicting fracture resistance of fiber reinforced concrete, *Cement Concr Res* **13**, 819–829.
83.46 Wecharatana, M, and Shah, S P. Predictions of nonlinear fracture process zone in concrete, *J Eng Mech ASCE* **109**(5), 1231–1246.
83.47 Wittmann, F H. Structure of concrete with respect to crack formation, in *Fracture mechanics of concrete*, F H Wittmann, Ed, Elsevier, Amsterdam, pp 321–324.
83.48 Zubelewicz, A, and Mróz, Z. Numerical simulation of rock-burst processes treated as problems of dynamic instability, *Rock Mech* **16**, 253–274.
83.49 Zubelewicz, A. Proposal of a new structural model of concrete (in Polish), *Arch Inz Ladowej* **29**(4), 417–429.

1984

84.1 Aifantis, E C. On the microstructural origin of certain inelastic models, *J Eng Mat Tech* **106**, 326–330.
84.2 Ballarini, R, Shah, S P, and Keer, L M. Crack growth in cement based composites, *Eng Fract Mech* **20**(3).
84.3 Bažant, Z P. Imbricate continuum and its variational derivation, *J Eng Mech* **110**(12), 1693–1712.
84.4 Bažant, Z P. Mechanics of fracture and progressive cracking in concrete structures, in *Fracture mechanics applied to concrete structures*, G C Sih, Ed, Martinus Nijhoff, The Hague.
84.5 Bažant, Z P. Size effect in blunt fracture: Concrete, rock, metal, *J Eng Mech ASCE* **110**, 518–535.
84.6 Bažant, Z P, Belytschko, T B, and Chang, T-P. Continuum theory for strain softening, *J Eng Mech* **110**, 1666–1692.
84.7 Bažant, Z P, and Cedolin, L. Approximate linear analysis of concrete fracture by *R*-curves, Rep No 83-7/679a, Center for Concr and Geomat, Tech Inst. Northwestern Univ, Evanston IL; also *J Struct Eng* **110**, 1336–1355.
84.8 Bažant, Z P, and Gambarova, R G. Crack shear in concrete: crack band microplane model, *J Eng Mech ASCE* **110**, 2015–2035.
84.9 Bažant, Z P, and Kim, J K. Size effect in shear failure of longitudinally reinforced beams, *J Am Concr Inst* **81**(5), 456–468; discussions **82**(4), 579–583.
84.10 Bažant, Z P, Kim, J K, and Pfeiffer, P. Determination of nonlinear fracture parameters from size effect tests, in *Proceedings of NATO advanced workshop on application of fracture mechanics to cementitious composites*, S P Shah, Ed, NATO-ARW, Northwestern Univ, Evanston IL [extension: *J Struct Div ASCE* **112**(Feb), (1986)].
84.11 Bažant, Z P, and Oh, B H. Deflections of cracked reinforced concrete beams, *J Am Concr Inst* **81**,
84.12 Bažant, Z P, and Oh, B H. Rock fracture via stress-strain relations, concrete and geomaterials, Rep No 82-11/665r, Northwestern Univ, Evanston IL; *J Eng Mech ASCE* **110**.
84.13 Bažant, Z P. Microplane model for strain-controlled inelastic behavior, in *Mechanics of engineering materials*, C S Desai and R H Gallagher, Eds, Wiley, Chichester and New York, chap 4, pp 45–59.
84.14 Brumer, R K, and Rorke, A J. Mining-induced fracturing around deep gold mine slopes, Res Rep No 38/84, Project No GR3F01, Chamber of Mines of South Africa, Johannesburg, Jul.
84.15 Crisfield, M A. Difficulties with current numerical models for reinforced concrete and some tentative solutions, *Proceedings, international conference on computer aided analysis and design of concrete structures*, Split, Yugoslavia, Sep, F Damjanić, E Hinton, et al, Eds, Pineridge Press, Swansea, UK, pp 331–358.
84.16 Crisfield, M A. Overcoming limit points with material softening and strain localization, in *Numerical methods for non-linear problems*, C Taylor et al, Eds, Pineridge, Swansea, UK, vol 2, pp 244–277.
84.17 Carpinteri, A, and Ingraffea, A R, Eds. Fracture mechanics of concrete: Material characterization and testing, Martinus Nijhoff, The Hague.
84.18 De Borst, R, Kusters G M A, Nauta, P, and Witte, F C de. DIANA —A comprehensive, but flexible finite element system, in *Finite element systems handbook*, 3rd ed, Springer-Verlag, New York.
84.19 De Borst, R, and Nauta, P. Smeared crack analysis of reinforced concrete beams and slabs failing in shear, in *Proceedings, international conference on computer-aided analysis and design of concrete structures*, Split, Yugoslavia.
84.20 De Borst, R, Kusters, G M A, Nauta, P, and De Witte, F C. DIANA: A three-dimensional, nonlinear finite element package on a microcomputer, in *Engineering software for micro-computers*, B A Schrefler, R W Lewis, and S A Odonizzi, Eds, Pineridge, Swansea, UK, p 435.
84.21 De Borst, R. Application of advanced solution techniques to concrete cracking and non-associated plasticity, in *Numerical methods for non-linear problems*, C Taylor et al, Eds, Pineridge Press, Swansea, UK, vol 2, pp 314–325.
84.22 Diamond, S, and Bentur, A. On the cracking in concrete and fiber-reinforced cements, in *Application of fracture mechanics to cementitious composites*, S P Shah, Ed, NATO Workshop, Northwestern Univ, Sep.
84.23 Dilger, W H, Koch, R, and Kowalczyk, R. Ductility of plain and confined concrete under different strain rates, *J Am Concr Inst* (Jan/Feb), 73.
84.24 Dvorak, G J, and Laws, N. Analysis of matrix cracking in composite laminates: Theory and experiment, in *1984 advances in aerospace sciences and engineering*, AD-08, by V Yuceoglu and R Hesser, Eds, ASME Book No G00276, ASME, New York.
84.25 Gopalaratnam, V S, and Shah, S P. Softening response of concrete in direct tension, *J Am Concr Res* **81**, ms 5252.
84.26 Hellan, K. *Introduction to fracture mechanics*, McGraw-Hill, New York, 302 pp.
84.27 Hillerborg, A. Numerical methods to simulate softening and fracture of concrete, in *Fracture mechanics applied to concrete structures*, G C Sih, Ed, Martinus Nijhoff, The Hague.
84.28 Ingraffea, A. In *Fracture mechanics applied to concrete structures*, G C Sih and A Carpinteri, Eds, Martinus Nijhoff, The Hague.
84.29 Jamet, P, Millard, A, and Nahas, G. Triaxial behaviour of micro-concrete complete stress-strain curves for confining pressures ranging from 0 to 100 MPa, in *RILEM-CEB symposium on concrete under multiaxial conditions*, INSA Toulouse, session 4, experimental results, vol 1, pp 133–140.
84.30 Jenq, Y S, and Shah, S P. Nonlinear fracture parameters for cement based composites: Theory and experiments, in *Proceedings of NATO advanced workshop on application of fracture mechanics to cementitious composites*, S P Shah, Ed, pp 213–253.
84.31 Jenq, Y S, and Shah, S P. A fracture toughness criterion for concrete,

Eng Fracture Mech.
84.32 Kobayashi, A S, Hawkins, N M, and Barker, D B. Fracture process zone of concrete, in *Proceedings of NATO advanced workshop on application of fracture mechanics to cementitious composites*, S P Shah, Ed, pp 24–47.
84.33 Mazars, J. Description of the multiaxial behavior of concrete with an elastic damaging model, in *Proceedings, RILEM symposium on concrete under multiaxial conditions*, INSA-OPS Toulouse, May, pp 190–203.
84.34 Mazars, J. Application de la mécanique de l'endommagement au comportement non-linéaire et a la rupture du béton de structures, thèse de Doctorat d'Etat, Université de Paris 6.
84.35 Mier, J G M van. Complete stress-strain behaviour and damaging status of concrete under multiaxial conditions, in *RILEM-CEB symposium on concrete under multiaxial conditions*, INSA Toulouse, session 3, experimental results, vol 1, pp 75–85.
84.36 Mihashi, H., Stochastic approach to study the fracture and fatigue of concrete, in *IUTAM Weibull symposium*, Stockholm, Jun.
84.37 Ortiz, M. A constitutive theory for the inelastic behavior of concrete, Brown Univ Report, Nov (to appear in *Mech Mat*).
84.38 Ottosen, N S. Evaluation of concrete cylinder tests using finite elements, *J Eng Mech* **110** (3), 465–481.
84.39 Pan, Y C, Marchertas, A H, Pfeiffer, P A, and Kennedy, J M. Concrete cracking simulations for nuclear applications, *Theor Appl Fract Mech* **2** (1), 27–38.
84.40 Read, H E, and Hegemier, G A. Strain softening of rock, soil, and concrete—a review article, *Mech Mat*.
84.41 Reinhardt, H W. Fracture mechanics of an elastic softening material for concrete, *Heron* **29** (2).
84.42 Reinhardt, H W, and Cornelissen, H A W. Post-peak cyclic behaviour of concrete in uniaxial tensile and alternating tensile and compressive loading, *Cement Concr Res* **14** (2), 263–270.
84.43 Resende, L, and Martin, J B. A progressive damage 'continuum' model for granular materials, *Comput Methods Appl Mech Eng* **42**, 1–18.
84.44 Rice, J R. Conserved integrals and energetic forces, in *Fundamentals of deformation and fracture*, Proc of IUTAM-ICF-ICM Eshelby Memorial Symp, Apr, Sheffield, K J Miller, Ed, Cambridge Univ Press.
84.45 Rots, J G, Kusters, G M A, and Blaauwendraad, J. The need for fracture mechanics options in finite element models for concrete structures, in *Proceedings, international conference on computer aided analysis and design of concrete structures*, Split, Yugoslavia, Sep, F Damjanić, E Hinton, et al, Eds, Pineridge Press, Swansea, UK, pp 19–32.
84.46 Sandler, I S. Strain softening for static and dynamic problems, in *Proceedings of symposium on constitutive equations: Micro, macro, and computational aspects*, ASME Winter Annual Meeting, New Orleans, Dec, K Willam, Ed, ASME, New York, pp 217–231.
84.47 Schreyer, H L, and Chen, Z, The effect of localization on the softening behavior of structural members, in *Proceedings of symposium on constitutive equations: Micro, macro, and computational aspects*, ASME Winter Annual Meeting, New Orleans, Dec, K Willam, Ed, ASME, New York, pp 193–203.
84.48 Shah, S P. Dependence of concrete fracture toughness on specimen geometry and on composition, in *Fracture mechanics of concrete: Material characterization and testing*, A Carpinteri and A R Ingraffea, Eds, Martinus Nijhoff, The Hague.
84.49 Shah, S P. In *Fracture mechanics applied to concrete structures*, G C Sih and A Carpinteri, Eds, Martinus Nijhoff, The Hague.
84.50 Suaris, W, and Shah, S P. Rate sensitive damage theory for brittle solids, *J Eng Mech ASCE* **110** (6), 985–997.
84.51 Valanis, K C. On the uniqueness of solution of the initial value problem in strain softening materials, Univ of Cincinnati, Cincinnati OH, to appear *J Appl Mech*.
84.52 Van Mier, J G M. Strain-softening of concrete under multiaxial loading conditions, Ph D dissertation, Univ of Eindhoven, Netherlands.
84.53 Willam, K J. Experimental and computational aspects of concrete fracture, in *Proceedings, international conference on computer aided analysis and design of concrete structures*, Split, Yugoslavia, Sep, F Damjanić, E Hinton, et al, Eds, Pineridge Press, Swansea, UK.
84.54 Willam, K J, Bicanić, N, and Sture, S. Constitutive and computational aspects of strain-softening and localization in solids, in *Proceedings of symposium on constitutive equations: Micro, macro and computational aspects*, ASME Winter Annual Meeting, New Orleans, Dec, K J Willam, Ed, ASME, New York.
84.55 Wittmann, F H, and Gheorghita, I. Fracture toughness of autoclaved aerated concrete, *Cement Concr Res* **14**, 369–374.
84.56 Wittmann, F H, Roelfstra, P E, and Sadouki, H. Simulation and analysis of composite structures, *Mat Sci Eng* **68**, 239–248.
84.57 Wium, D J W, Buyukozturk, O, and Li, V C. *J Eng Mech ASCE* **111** (Aug), 1211–1229.
84.58 Wu, F H, and Freund, L B. Deformation trapping due to thermoplastic instability in one-dimensional wave propagation, *J Mech Phys Solids* **21** (2), 119.

1985

85.1 Barker, D B, Hawkins, N M, Jeang, F L, Cho, K Z, and Kobayashi, A S. Concrete fracture in CLWL specimen, *J Eng Mech ASCE* **111**, 623–638.
85.2 Bažant, Z P. Comment on Hillerborg's comparison of size effect law with fictitious crack model, in *Dei Poli anniversary volume*, L Cedolin, Ed, Politecnico di Milano, Oct.
85.3 Bažant, Z P. Distributed cracking and nonlocal continuum, in *Preprints, Europe-US symposium on finite element methods for nonlinear problems*, P Bergan, Ed, Norwegian Inst of Tech, Trondheim, Aug, pp II.2-1–II.2-25.
85.4 Bažant, Z P. Mechanics of fracture and progressive cracking in concrete structures, in *Fracture mechanics applied to concrete structures*, G C Sih, Ed, Martinus Nijhoff, The Hague, chap 1.
85.5 Bažant, Z P, and Belytschko, T B. Wave propagation in a strain-softening bar: exact solution, *J Eng Mech ASCE* **111** (3).
85.6 Bažant, Z P, and Cao, Z. Size effect in punching shear failure of slabs, Rep No 85-8/4285, Center for Concr and Geomat, Northwestern Univ, Evanston IL, May.
85.7 Bažant, Z P, and Chang, T P. Imbricate finite element analysis of strain-softening solids, Rep No 85-8/428, Center for Concr and Geomat, Northwestern Univ, Evanston IL, Aug, *J Eng Mech ASCE*, in press.
85.8 Bažant, Z P, and Chern, J C. Strain-softening with creep and exponential algorithm, *J Eng Mech* **111**, 381–390.
85.9 Bažant, Z P, and Oh, B H. Microplane model for progressive fracture of concrete and rock, *J Eng Mech ASCE* **111**, 559–582.
85.10 Bažant, Z P, and Pfeiffer, P D. Tests of shear fracture and strain-softening in concrete, in *Proceedings, 2nd symposium on the interaction of non-nuclear munitions with structures*, Panama City Beach FL, Apr, pp 254–264; further extension in *Mat Construct (RILEM, Paris)*, in press.
85.11 Bažant, Z P, Ed. *Mechanics of geomaterials: Rocks, concretes, soils*, Wiley, Chichester and New York, 1985. (Proc, IUTAM Prager Symp, Northwestern Univ, Sep 1983).
85.12 Bažant, Z P. Fracture in concrete and reinforced concrete, in Ref. 85.11, pp 259–303.
85.13 Bažant, Z P, Fracture mechanics and strain-softening of concrete, in *Proceedings, US-Japan seminar on finite element analysis of reinforced concrete structures*, Tokyo, May 1985, ASME, New York, 1986.
85.14 Carpinteri, A, and Sih, G C. Damage accumulation and crack growth in bilinear material with softening: application of strain energy density theory, *J Theor Appl Fracture Mech* **2** (2).
85.15 Carpinteri, A. Scale effects in fracture of plain and reinforced concrete structures, in *Fracture mechanics of concrete: Structural application and numerical calculation*, G C Sih and A DiTomasso, Eds, Martinus Nijhoff, Dordrecht and Boston, chap 2, pp 95–138.
85.16 Chen, E S, and Buyukozturk, O. Constitutive model for concrete in cyclic compression, *J Eng Mech ASCE* **111**, 797–816.
85.17 Cho, K Z, Kobayashi, A S, Hawkins, N M, Barker, D B, Fure, L J. Fracture process zone of concrete cracks, *J Eng Mech ASCE* **111**, 1185–1210.
85.18 Cornelissen, H A W, Hordijk, D A, and Reinhardt, H W. Experiments and theory for the application of fracture mechanics to normal and lightweight concrete, *Proceedings, international conference on fracture mechanics of concrete*, F H Wittmann, Ed, Elsevier, Amsterdam.
85.19 Darwin, D. Crack propagation in concrete—study of model parameters, in *Proceedings, seminar on finite element analysis of reinforced concrete structures*, Tokyo.
85.20 De Borst, R, and Nauta, P. Non-orthogonal cracks in a smeared finite element model, *Eng Comput* **2**, 35–46.
85.21 Determination of the fracture energy of mortar and concrete by means of three-point bend tests on notched beams, RILEM recommendation, *Mat Construct (RILEM, Paris)* **18** (106), 43–48.
85.22 Dougill, J W. Constitutive relations for concrete and rock: Applications and extensions of elasticity and plasticity theory, in Ref. 85.11, chap 3, pp 21–46.
85.23 Dvorak, G J, and Teply, J L. Periodic hexagonal array models for plasticity analysis of composite materials, in *Plasticity today: Modelling, methods and applications*, W Olszak Memorial Vol, A Sawczuk and V Bianchi, Eds, Elsevier, Amsterdam, pp 623–642.
85.24 Dvorak, G J, Laws, N, and Hejazi, M. Analysis of progressive matrix cracking in composite laminates I. Thermoelastic properties of a ply with cracks, *J Compos Mat* **19**, 216–230.
85.25 Dvorak, G J, and Laws, N. Analysis of progressive matrix cracking in composite laminates II. First ply failure, Report, RPI, Jun.
85.26 Dvorak, G J. Thermal expansion of elastic plastic composite materials, Tech Rep No 1 to ONR (Contract N00014-85-K-0247), Dept of Civil Eng, RPI, Oct.
85.27 Ehrlacher, A. Behaviour of solids with a system of cracks, in Ref. 85.11, chap 8, pp 157–165.
85.28 Gopalaratnam, V S, and Shah, S P. Softening response of plain concrete in direct tension, *J Am Concr Inst* **82** (May–Jun).
85.29 Hawkins, N M. The role of fracture mechanics in conventional reinforced concrete design, in *Application of fracture mechanics to cementitious composites*, S P Shah, Ed, Martinus Nijhoff, Dordrecht and Boston, pp 639–666.
85.30 Hillerborg, A. Results of three comparative test series for determining the fracture energy G_f of concrete, *Mat Construct (RILEM, Paris)* **18** (106), 43–48.
85.31 Hillerborg, A. The theoretical basis of a method to determine the fracture energy G_f of concrete, *Mat Construct (RILEM, Paris)* **18** (106), 25–30.
85.32 Hilsdorf, H K, and Brameshuber, W. Size effects in the experimental determination of fracture mechanics parameters, in *Application of fracture mechanics to cementitious composites*, S P Shah, Ed, Martinus Nijhoff,

Dordrecht and Boston, pp 361–398.
85.33 Hu, X Z, Cotterell, B, and Mai, Y W. Computer simulation models of fracture in concrete, in *Proceedings, RILEM international symposium on fracture of concrete*, Lausanne, Oct, F H Wittmann, Ed, RILEM, Paris.
85.34 Ingraffea, A R. Fracture propagation in rock, in *Mechanics of geomaterials: Rocks, concretes, soils*, Z P Bažant, Ed, Wiley, Chichester and New York, pp 219–258.
85.35 Ingraffea, A R, and Panthaki, M J. In *Proceedings of the US-Japan seminar on finite element analysis of reinforced concrete structures*, Tokyo, May, ASME, New York.
85.36 Krajcinovic, D. Mechanics of solids with a progressively deteriorating structure, in *Application of fracture mechanics to cementitious composites*, S P Shah, Ed, Martinus Nijhoff, Dordrecht and Boston, pp 453–479.
85.37 Laws, N and Dvorak, G J. The loss of stiffness of cracked laminates, in *Fundamentals of deformation and fracture*, Eshelby Memorial Symposium, B A Bilby et al, Ed, Cambridge Univ Press, Cambridge, pp 119–127.
85.38 Marshall, D B, and Evans, A G. Failure mechanisms in ceramic-fiber/ceramic-matrix composites, *J Am Ceramic Soc* **68** (5), 225–231.
85.39 Mazars, J, and Lemaitre, J. Application of continuous damage mechanics to strain and fracture behavior of concrete, in *Application of fracture mechanics to cementitious composites*, S P Shah, Ed, Martinus Nijhoff, Dordrecht and Boston, pp 507–520.
85.40 Mróz, Z. Current problems and new directions in mechanics of geomaterials, in Ref. 85.11, chap 24, pp 539–566.
85.41 Ouchterlony, D F. Summary of discussions on fracture propagation and fracture energy, in Ref. 85.11, pp 577–580.
85.42 Pijaudier-Cabot, G. Caracterisation et modelisation du comportement du béton par un essai multiaxial automatique, thèse de doctorat de 3ème cycle, Lab de Mécanique et Tech, ENSET (Ecole Normale Supérieure), Paris-Cachan.
85.43 Planas, J, and Elices, M. In *Proceedings, RILEM international symposium on fracture of concrete*, Lausanne, Oct, F H Wittmann, Ed, RILEM, Paris.
85.44 Rots, J G. Strain softening analysis of concrete fracture specimens, in *Proceedings, RILEM international symposium on fracture mechanics of concrete*, Lausanne, Oct, F H Wittmann, Ed.
85.45 Rots, J G, Nauta, P, Kusters, G M A, and Blauwenraad, J. Smeared crack approach and fracture localization in concrete, *Heron* **30** (1).
85.46 Rots, J G. Strain-softening analysis of concrete fracture specimens, in *Proceedings, RILEM international conference on fracture mechanics of concrete*, F H Wittmann, Ed, Elsevier, Amsterdam.
85.47 Schreyer, H L. A third-invariant plasticity theory for low-strength concrete, *J Eng Mech ASCE* **111**, 545–558.
85.48 Stout, P B. Failure analysis and microcrack dependent discontinuum mechanics, in *ASME conference on fatigue, corrosion cracking, fracture mechanics and failure analysis*, Salt Lake City, ASME, New York.
85.49 Willam, K J, Hurlbut, B, and Sture, S. Experimental, constitutive and computational aspects of concrete failure, in *Preprints, US-Japan seminar on finite element analysis of reinforced concretes*, Tokyo, May, pp 149–172.
85.50 Wittmann, F H. Deformation of concrete at variable moisture content, in Ref. 85.11, chap 19, pp 425–460.
85.51 Yamaguchi, H, and Nomura, S. Inelastic analysis of reinforced concrete members based on plastic-fracturing theory, in *Preprints, US-Japan seminar on finite element analysis of R. C. structures*, Tokyo, May, vol 2, pp 207–216.
85.52 Yang, B L, Dafalias, Y F, and Herrmann, L R. A bounding surface plasticity model for concrete, *J Eng Mech ASCE* **111** (Mar), 359–380.
85.53 Zaitsev, Yu V. Inelastic properties with random cracks, in Ref. 85.11, chap 6, pp 89–128.
85.54 Zaitsev, Yu V, and Kovler, K L. Notch sensitivity of concrete and size effect, *Cement Concr Res*, **15**, 979–987 and **16**, 7–16.
85.55 Zubelewicz, A, and Bažant, Z P. Contact element modeling of fracture in aggregate composites, Rep 85-11/428c, Cener for Concrete and Geomat, Northwestern Univ, Evanston IL, Nov 1985.

1986

86.1 Bažant, Z P, and Cao, Z. Size effect in brittle failure of unreinforced pipes, *J Am Concr Inst* **83** (3).
86.2 Bažant, Z P, and Cao, Z. Size effect in shear failure of prestressed concrete beams, *J Am Concr Inst* **83** (2).
86.3 Bažant, Z P, and Oh, B H. Efficient numerical integration on the surface of a sphere, *Z Angew Math Mech (ZAMM)* **66**, 37.
86.4 Bažant, Z P, Kim, J-K, and Pfeiffer, P. Nonlinear fracture properties from size effect tests, *J Struct Eng ASCE* **112**, 289–307.
86.5 Belytschko, T B, Bažant, Z P, Hyun, V V, and Chang, T P. Strain-softening materials and finite element solutions, *Comput Struct*, in press.
86.6 De Borst, R. Computational aspects of smeared crack analysis, in *State-of-the-art text on constitutive modeling of concrete structures*, Pineridge Press, Swansea, UK.
86.7 Gopalaratnam, V S, and Shah, S P. Softening response of plain concrete in direct tension, *J Am Concr Inst* (MS 5652), in press.
86.8 Horii, H, and Nemat-Nasser, S. Compression-induced microcrack growth in brittle solids: axial splitting and shear failure, *J Geophys Res*, to appear.
86.9 Reinhardt, H. The role of fracture mechanics in rational rules for concrete design, IABSE Survey S-34/86, IABSE Periodica No 1, pp 1–15.

Zdeněk P Bažant *was born and educated in Prague, obtaining a Civil Engineer degree from Czech Technical University in 1960 and a PhD in mechanics from the Czechoslovak Academy of Sciences in 1963. He moved to University of Toronto in 1967, then to UC Berkeley in 1968, and in 1969 joined the faculty of Northwestern University where he has been Professor of Civil Engineering since 1973, Structural Engineering Coordinator from 1974 to 1978, and Director of the Center for Concrete and Geomaterials since 1981. He is a Registered Structural Engineer in Illinois, a consultant to Argonne National Laboratory and other firms, and is on the editorial boards of a number of journals. Dr. Bažant is active as a fellow in ASCE, ACI, and RILEM, serving currently as chairman of the ACI Committee 446 on Fracture Mechanics, of the RILEM International Committee TC69 on Concrete Creep, and of IASMiRT Division H, Concrete Structures, and recently as chairman of the ASCE-EMD Committee on Properties of Materials. He is a member of the ASCE Committee on Probabilistic Methods, the ACI Safety Committee, and the ASTM Committee on Skiing. The distinguished nature of his research contributions has been recognized by the conferral of the RILEM Medal, the ASCE Huber Prize, the ASCE Lin Award, the IR-100 Award, Guggenheim and Ford Foundation Fellowships, the French Government ASTEF Fellowship, and his election as Fellow of the American Academy of Mechanics.*